Title
Synaptic and network alterations in the medial prefrontal cortex of the CNTNAP2 mouse model of autism

Author
Lazaro, Maria T.

Publication Date
2016

Peer reviewed|Thesis/dissertation

UNIVERSITY OF CALIFORNIA

Los Angeles

Synaptic and network alterations in the medial prefrontal cortex of the *CNTNAP2* mouse model of autism

A dissertation submitted in partial satisfaction of the

requirements for the degree of Doctor of Philosophy

in Neuroscience

by

María Teresa Lázaro

2016

ABSTRACT OF THE DISSERTATION

Synaptic and network abnormalities in the medial prefrontal cortex of the *CNTNAP2* mouse model of autism

by

María Teresa Lázaro

Doctor of Philosophy in Neuroscience

University of California, Los Angeles, 2016

Professor Daniel H. Geschwind, Chair

Autism Spectrum Disorders (ASDs) are highly prevalent developmental disorders that affect 1 in every 68 individuals. Due to the high phenotypic heterogeneity in ASDs, both the identification of causative factors and the development of successful therapeutic interventions has been challenging. Thus, understanding convergent pathophysiological mechanisms by which defined etiologies result in ASDs can serve as an invaluable starting point towards the development of successful therapeutic treatments. Here, I investigate how alterations in *CNTNAP2*, an autism-susceptibility gene, can lead to ASD-related deficits in neuronal function. Recessive truncating mutations in *CNTNAP2* cause Cortical Dysplasia Focal Epilepsy (CDFE), a syndromic form of ASD in humans. Remarkably, *Cntnap2* knock-out (KO) mice, which have been genetically engineered to

lack *Cntnap2* expression, recapitulate the core behavioral deficits of the disorder, including impairments in social interactions and communication, repetitive and restrictive behaviors, seizures, decreased neuronal synchrony, and neuronal migration deficits. Here, I take advantage of this invaluable research tool to dissect the synaptic, cellular, and neuronal microcircuit activity changes associated with loss of *Cntnap2* in the KO mouse. I use electrophysiology and histological studies to assess these alterations within the medial prefrontal cortex (mPFC), an area associated with social behavior. I observe that although there are no significant alterations in the intrinsic excitability of pyramidal neurons or parvalbumin-positive interneurons in the KO, excitatory cells show a significant decrease in both excitatory and inhibitory inputs. These changes are accompanied by a decrease in dendritic spine density, and suggest a reduction in the total number of functional synapses within mPFC. These in vitro findings are concurrent with a notable reduction in local field potential (LFP) power in vivo, and likely reflect an overall decrease in excitatory drive, likely to be underlie some of the behavioral deficits observed in the mouse. Finally, I describe the collaborative development of a novel social interaction task that can be used to assess changes in neuronal activity in vivo, both at baseline, in a social behavioral context, and in response to potential pharmacological interventions. The findings delineated here serve as a roadmap for neurophysiological characterization of a rodent model of ASD, and provide initial mechanistic insights into how loss of *Cntnap2* alters mPFC microcircuitry. This work therefore serves as a starting point to finding convergent molecular, biological and physiological pathways that can contribute to our understanding and treatment of the ever so complex ASDs.

The dissertation of María Teresa Lázaro is approved.

Peyman Golshani

Kelsey Martin

Thomas Otis

Daniel H. Geschwind, Committee Chair

Univeristy of California, Los Angeles

2016

Dedication

To my parents, Goguie and Tuti

and to my siblings, Jorge and Chabe.

Thank you for being the light of my universe

and illuminating my thoughts and actions

with righteousness, joy, and love.

TABLE OF CONTENTS

LIST OF FIGURES

LIST OF TABLES

ACKNOWLEDGEMENTS

Chapter 1 is a version of "The utility of rodent models of autism spectrum disorders", published April 2015 in *Current Opinion in Neurology*, Volume 28, Issue 2 p 103-109. DOI: 10.1097/WCO.0000000000000183. Wolters Kluwer Health Lippincott Williams & Wilkins©. This work was co-authored by Peyman Golshani, principal investigator, co-advisor, and committee member, who has agreed to the publication of this review in this dissertation.

Chapters 2-4 contains work co-authored by María T. Lazaro, Olga Peñagarikano, Iris Bachmutsky, Taruna Ikrar, Rommel Santos, Tristan Shuman, Apoorva Myalavarapu, Swasty Chandra, Hongmei Dong, Xiangmin Xu, Daniel H. Geschwind, and Peyman Golshani. Results obtained from these investigations are part of a manuscript in preparation, titled "Synaptic and network abnormalities in the Cntnap2 mouse model of autism." María T. Lázaro, Olga Peñagarikano, Daniel H. Geschwind, and Peyman Golshani conceived of experimental design and contributed to data analysis, interpretation of the study, and manuscript text. María T. Lázaro performed all in vitro electrophysiology experiments, including data acquisition, analysis, and interpretation. Additional analysis tools were contributed by Peyman Golshani, Jiannis Taxidis, Tristan Shuman, and Michael Einstein. Taruna Ikrar, Rommel Santos, and Xiangmin Xu contributed to the design, data acquisition, analysis, and manuscript text of the cortical input mapping experiments. Iris Bachmutsky, Apoorva Myalavarapu and Swasty Chandra contributed to data acquisition and analysis for histological and anatomical studies of dendritic morphology, spine density, and immunolabeling of synaptic markers.

Tristan Shuman and Iris Bachmutsky contributed to experimental design, data acquisition, and analysis of all in vitro electrophysiology experiments and design of the novel social behavior task. Hongmei Dong helped with mouse colony management and genotyping. All co-authors have agreed to the publication of this study on this dissertation.

Chapter 3 contains a version of "The autism related protein contactin-associated protein-like 2 (*CNTNAP2*) stabilizes new spines: an *in vivo* mouse study", published May 7, 2015 in *PLoS ONE*, Volume 10, Issue 5, p 1-7. DOI: 10.1371/journal.pone.0125633. This work was co-authored by Amos Gdalyahu, Maria Lazaro, Olga Penagarikano, Peyman Golshani, Joshua T. Trachtenberg, and Daniel H. Geschwind. Experiments were conceived and designed by Amos Gdalyahu, Olga Peñagarikano, and Daniel H. Geschwind. Experiments were performed by Amos Gdalyahu and Olga Peñagarikano. Data was analyzed by Amos Gdalyahu. Joshua T. Trachtenberg contributed with reagents, materials, and analysis tools. The manuscript was written by Amos Gdalyahu, Maria Lazaro, Olga Penagarikano, Peyman Golshani, Joshua T. Trachtenberg, and Daniel H. Geschwind. All co-authors have agreed to the re-publication of this study on this dissertation.

Chapter 4 is based on content derived from "Exogenous and evoked oxytocin restores social behavior in the *Cntnap2* mouse model of autism", published January 21, 2015 in *Science translational medicine*, Volume 7, Issue 271, p 271-8. DOI: 10.1126/scitranslmed.3010257. This work was co-authored by Olga Peñagarikano, María T. Lázaro, Xiao-Hong Lu, Aaron Gordon, Hongmei Dong, Hoa A. Lam, Elior Peles, Nigel T. Maidment, Niall P. Murphy, X. William Yang, Peyman Golshani, and Daniel H.

Geschwind. Olga Peñagarikano and Daniel H. Geschwind designed the overall study. The portions of this paper displayed in this dissertation include histological and behavioral experiments performed by Olga Peñagarikano. Hongmei Dong engineered DREADD construct and helped with mouse histological analysis, as well as behavioral testing. Peyman Golshani designed and María T. Lázaro performed electrophysiology experiments. This publication also includes work not presented in this dissertation with work performed by the following: X. William Yang and Xiao-Hong Lu designed stereology experiments. Nigel T. Maidment and Niall P. Murphy designed and Hoa A. Lam performed radioimmunoassay experiments experiments. Elior Peles designed and Aaron Gordon performed LacZ staining experiments. All co-authors have agreed to the re-publication of this study in this dissertation.

I also gratefully acknowledge the sources of financial support for this work. Studies presented in this dissertation were supported by NIH/National Institute of Mental Health (NIMH) R01 MH081754-02R, NIH Autism Centers of Excellence (ACE) 1P50-HD055784-01 (Project II), network grant 5R01-MH081754-04, and the Simons Foundation Autism Research Initiative, granted to Daniel H. Geschwind and NIMHRO1MH101198–1 and Circuit Dynamics Grant from the Simons Foundation, granted to Peyman Golshani. María T. Lázaro was funded by the UCLA Eugene Cota-Robles Fellowship, NSF-GRFP DGE-0707424, the NIMH T32MH073526 UCLA Neurobehavioral Genetics Training Grant, and the UCLA Dissertation Year Fellowship.

VITA

María Teresa Lázaro

Education:

Bachelor of Science in Biology, 2010

University of Puerto Rico, Río Piedras Campus, San Juan, PR

Selected publications:

2016 **Lázaro, M.T**., Peñagarikano, O., Bachmutsky, I., Ikrar, T., Santos, R., Shuman, T., Myalavarapu, A., Chandra, S., Dong, H., Xu, X., Geschwind, D.H., & Golshani, P. Synaptic and Network Abnormalities in the CNTNAP2 Mouse Model of Autism. *In prep.*

2016 Cantero, G., Liu, X.-B., Mervis, R. F., **Lazaro, M. T.**, et al. (2016). Rescue of the Functional Alterations of Motor Cortical Circuits in Arginase Deficiency by Neonatal Gene Therapy. *The Journal of Neuroscience : The Official Journal of the Society for Neuroscience*, *36*(25), 6680–90.

2015 Gdalyahu, A., **Lazaro, M.**, Penagarikano, O., Golshani, P., Trachtenberg, J. T., & Gescwind, D. H. (2015). The autism related protein contactin-associated protein-like 2 (CNTNAP2) stabilizes new spines: An in vivo mouse study. *PLoS ONE*, *10*(5), 1–7.

2015 Jalbrzikowski, M., **Lazaro, M. T.**, Gao, F., Huang, A., Chow, C., Geschwind, D. H., Bearden, C. E. (2015). Transcriptome profiling of peripheral blood in 22q11.2 deletion syndrome reveals functional pathways related to psychosis and autism spectrum disorder. *PLoS ONE*, *10*(7), 1–22.

2015 **Lázaro, M. T.**, & Golshani, P. (2015). The utility of rodent models of autism spectrum disorders. *Current Opinion in Neurology*, *28*(2), 103–9.

2015 Peñagarikano, O., **Lázaro, M. T.**, Lu, X.-H., Gordon, A., Dong, H., Lam, H. A., Geschwind, D. H. (2015). Exogenous and evoked oxytocin restores social behavior in the Cntnap2 mouse model of autism. *Science Translational Medicine*, *7*(271), 271ra8.

2013 Garcia-Junco-Clemente, P., Chow, D. K., Tring, E., **Lazaro, M. T.**, Trachtenberg, J. T., & Golshani, P. (2013). Overexpression of calcium-activated potassium channels underlies cortical dysfunction in a model of PTEN-associated autism. *Proceedings of the National Academy of Sciences*, *110*(45), 18297–18302.

2013 Schreiner, M. J., **Lazaro, M. T.**, Jalbrzikowski, M., & Bearden, C. E. (2013). Converging levels of analysis on a genomic hotspot for psychosis: Insights from 22q11.2 Deletion Syndrome. *Neuropharmacology*, *68*, 157–173.

2012 Voineagu, I., Huang, L., Winden, K., **Lazaro, M.**, Haan, E., Nelson, J., … Geschwind, D. (2011). CCDC22: a novel candidate gene for syndromic X-linked intellectual disability. *Molecular Psychiatry*, *17*(1), 4–7.

Grants awarded:

2014-2016 Pre-doctoral Training Program in Neurobehavioral Genetics from NIMH, T32MH073526 (University of California, Los Angeles)

2015-2016 Dissertation Year Fellowship (University of California, Los Angeles)

2011-2014 Graduate Research Fellowship Program from the National Science Foundation, DGE-0707424 (University of California, Los Angeles)

2010-2011 Eugene Cota-Robles Fellowship (University of California, Los Angeles)

Chapter 1:

An introduction to autism spectrum disorders

and

the utility of mouse models

1.1: History of Autism Spectrum Disorders

The first clinical description of Autism Spectrum Disorders (ASDs) dates back to 1943, when Leo Kanner described it as an "autistic disturbance of affective contact" (Kanner, 1943). Since then, our conception of autism and criteria used for diagnosis has been sporadically modified in order to obtain a sharper definition out of such a heterogeneous spectrum (Baker, 2013). The DSMV now defines autism as disorders characterized by deficits in social communication and language, as well as repetitive or restrictive behaviors (APA, 2013). It also now includes four disorders from the previous manual, including: autistic disorder, Asperger's disorder, childhood disintegrative disorder, and pervasive developmental disorder not otherwise specified (APA, 2013). In addition to these traits, ASDs are often accompanied by detrimental comorbidities, including intellectual disability, sensorimotor abnormalities, hyperactivity, gastrointestinal issues, and epileptic seizures (Geschwind, 2009; de la Torre-Ubieta et al., 2016). Thus, autism is clearly not a single condition, and is often a devastating and debilitating disorder, that not only affects patients, but also their families.

Current estimates reveal that ASDs affect 1 in every 68 individuals, thus making it a highly prevalent developmental disorder (Developmental Disabilities Monitoring Network, 2014). To this date, no successful cure for autism has been developed. Pharmacological treatments often target the comorbid symptoms, such as hyperactivity and epilepsy, but none of them has proven completely effective in ameliorating the deficits as a whole (Mehta and Golshani, 2013; Jacquemont et al., 2014). Likewise, non-pharmacological therapies have also been developed, including behavioral interventions, language therapy, and sensorimotor therapies (Ospina et al., 2008; Schreibman et al.,

2015). Recent advances in our ability to diagnose autism at an early age have made early intervention possible, often providing best results in the long term (Pickles et al., 2016). Yet, the great heterogeneity and interpatient variability have made the development of successful interventions quite challenging (Jacquemont et al., 2014; de la Torre-Ubieta et al., 2016). It is therefore necessary to understand the cause(s) of autism and find convergent pathways that can help define etiological subgroups and fine-tune therapeutic targets.

1.2: ASD etiology

The cause of ASDs is complex and has been attributed to genetic factors as well as to poorly understood non-genetic or environmental causes (Mehta and Golshani, 2013; Chen et al., 2015). Large-scale next-generation sequencing studies from large cohorts of ASD patients and controls have found highly validated de-novo and inherited genetic alterations. These have identified dozens of susceptibility genes contributing to the manifestation of the disorders, and have stressed the contribution of rare variants to its etiology (Zhao et al., 2007; Bodmer and Bonilla, 2008; O'Roak et al., 2012; De Rubeis et al., 2014; Iossifov et al. 2014; Krimm et al., 2014). Over time, the size and depth of these sequencing studies has increased, as has the list of validated causative gene mutations, which is expected to include at least several hundred additional genes (Rubeis et al., 2014). Indeed, ASDs are highly heritable disorders, as we have learned from twin, sibling, and family studies, which have found large concordance rates that correlate with genetic similarity (Rosenberg et al., 2009; Ozonoff et al., 2011; Hallmayer et al., 2011). However, identification of causative genetic alterations is only the first essential step for understanding how each one of these etiologies alters downstream molecular cascades,

perturbs brain development and function, and ultimately leads to autism-related phenotypes and behaviors.

Recent advances in genetics have increased our understanding of ASDs, both by promoting the discovery of autism susceptibility genes and by elucidating convergent molecular pathways that are impacted by gene mutations. This knowledge is incredibly important, as it can eventually be used to cluster specific ASD subtypes and lead to the development of targeted therapeutics. Deleterious genetic mutations, such as rare genetic disruptions in the form of copy number variants (CNVs) and single-nucleotide variants (SNVs) account for as many as 60% of reported ASD cases (de la Torre-Ubieta et al., 2016). Such alterations are often predicted to result in truncation, nullification, or disruption of gene protein products, and can interfere with important biological functions, such as brain development and function (Berg and Geschwind, 2012). Indeed, the ontology many of these identified genes has been repeatedly associated with synaptic function, neuron-glia signaling, and immune responses (Voineagu et al., 2011; Chen et al., 2015). More recently, chromatin structure processes have also been implicated in ASD (De Rubeis et al., 2014). The study of these genes and their function, as well as the impact of ASD-associated alterations on molecular pathways, cellular function, brain microcircuit activity, and then behavior, therefore provide a comprehensive venue for understanding and treating ASDs.

1.3: Utility of mouse models of ASD

Until recently, our study of psychiatric disorders, including autism, solely relied on clinical, behavioral, psychophysical, and low resolution (mostly non-invasive) human

electrophysiology or functional studies. The sequencing of both the human and mouse genome, was the first step towards delving into deeper mechanistic studies of therapeutic value (Austin et al., 2004). Technological advances, nonetheless, have allowed us to delve deeper into the biological and physiological mechanisms that lead to ASD. In this current age and time, rodent models incorporating this growing list of genetic changes are one of the prime methods used to dissect the effects of mutations on neuronal anatomy, connectivity, physiology, and behavior. Below I describe some of the more recent advances made in the field using mouse models of ASDs and discuss ways these models could be used to study ASD pathogenesis and find new treatments (Table 1.1).

1.4: What are mouse models and why should we use them?

"*We are unlikely to ever know everything about every organism. Therefore, we should agree on some convenient organism(s) to study in great depth, so that we can use the experience of the past (in that organism) to build on in the future. This will lead to a body of knowledge in that 'model system' that allows us to design appropriate studies of non-model systems to answer important questions about their biology."*

-Thomas Henry Huxley (1869)

Model systems have long been used to provide mechanistic insights into biological processes and the cause of disease. Model organisms are typically species that are easily maintained in a laboratory setting and can be easily experimentally manipulated with the goal of uncovering the mechanistic foundation of a given biological question or function (Nestler and Hyman, 2010). Our main goal in both the basic and the

biomedical sciences, is to be able to dissect a biological process or cellular component, and understand the mechanism leading to the resulting consequences. Even though model systems such as rodents are fundamentally different from humans, as they are 60 million years apart in evolution, shared similarities can provide substantial information about our own biology. For example, Miller et al., 2010 showed that, despite interspecies divergence in expression of cell type-specific genes, global gene transcription patterns are conserved between mice and humans. These overlapping similarities provide a substrate for performing research in models in a way that can be directly translated to humans, with the caveat of species-specific differences, which could also be informative with regards to human-specific disease pathogenesis (Miller et al., 2010). In light of this, we as researchers must set the goal of achieving predictive validity, taking advantage of robust interspecific similarities in a way that allows for reliable prediction of drug effectiveness in humans, from testing them in rodents, for example. Rodents and other model animals thus provide an effective route for generating treatments as quickly as possible.

Although there are indeed some disadvantages that accompany the use of these model systems, one if which is that they are often too simple and reductionist, they have indeed been pivotal in the creation of knowledge. These invaluable research tools, have allowed us to dissect biological organs and systems in a way that would otherwise be impossible or otherwise too harmful to humans (Austin et al., 2004). Model systems allow us to break down the discovery of molecular targets and pharmacologic therapies for human illness and, as described below, have elucidated invaluable clues into the pathological mechanisms that lead to disorders such as ASD. I must state, nonetheless, that it is immensely crucial for us scientists to never let go of the notion that these model

organisms too are sentient creatures, and should be therefore always treated with measure and outmost respect. Although it may be hard sometimes to experiment with animals, we do so with the hope and intention of benefiting society and bettering humanity. I am forever thankful to the universe and all the lives of mice that were sacrificed in the formation of this thesis and I hope that the findings that I here describe can be useful in solving the autism puzzle.

Because of their close evolutionary relationship, mice and humans share great preservation of genes, biological processes, brain circuits and, to some extent, behaviors (Austin et al., 2004) Although uniquely human disorders, many of the core deficits of autism can be paralleled in mice through close behavioral investigation (Peñagarikano et al., 2011; Kas et al., 2014). This evolutionary conservation, together with our ability to employ experimental manipulations through genetic engineering and other cutting-edge technologies like CRISPR and optogenetics (Boyden et al., 2005; Platt et al., 2014), have not only helped us probe the underlying mechanism of the disorder, but have also paved the way towards the development of targeted and effective therapeutic approaches.

Rodent models of ASDs have been useful in a number of mutually reinforcing ways. First, they present a relevant and tractable biological system for understanding the complex relationship between a specific genetic mutation and the resultant downstream consequences, especially with regards to molecular and biological pathways. Second, these models can be used to define the anatomical and physiological changes in precisely defined microcircuits. Our ability to examine these alterations across multiple models, each one representing specific genetic mutations in distinct molecular pathways, can then help identify fundamental or overarching changes in neuronal circuitry and their effects

on relevant behavioral phenotypes. Third, these discrete alterations can, in some cases, be interpreted as biomarkers which can be paralleled in humans, and therefore have the potential of being used to gauge the effect of treatments and predict therapeutic outcomes. These models are therefore useful for screening therapeutic effects of behavioral and pharmacological interventions. With this intention, a battery of behavioral tests have been developed in order to provide careful assessment of relevant deficits in these models (Nestler and Hyman, 2010; Silverman et al., 2010; Kas et al., 2014).

In addition, increasing knowledge of genetics and the recent technological advances have amplified our ability to easily manipulate specific genes in a temporally-precise and even cell type-specific manner; what we refer to as conditional "knock-ins" or "knock-outs". These elegant experimental manipulations have helped us define critical developmental windows, brain regions, and functionally-distinct neuronal types and their contribution to specific ASD-related traits (Guy et al., 2007; Cobb et al., 2010; Robinson et al., 2012; Rabeneda et al., 2014). Moreover, many of these genetic changes may not only alter brain development but could also directly and indirectly affect the function of fully mature brain circuits (Enhinger et al., 2008). Thus, these conditional genetic manipulation techniques hold the potential for effective dissection of involved molecular pathways and circuits, which will be crucial for effective treatment of both children and adults with certain forms of ASD. Finally, the use of these genetically-defined models will help us, sometime in the future, assess and understand the complex interplay of gene-environment interactions and their role in the development of ASDs and associated comorbidities.

1.5: Search for convergence: molecular pathways

To better understand the core pathological mechanisms that lead to ASD, it is critical for us to comprehend the function and ontology of any given implicated gene, its protein product, its cellular purpose, and its role in molecular cascades. Moreover, uncovering convergent pathways that connect the already identified autism susceptibility genes can bring us one step closer to understanding the underpinnings of such an etiologically complex disorder.

One of the most well-known and well-characterized signaling pathways implicated in ASD is the *PI3K*-mammalian target of rapamycin (*mTOR*) molecular cascade (Wetmore et al., 2010). Over the years, many genes that have been strongly linked to syndromic forms of ASD, including mutations in Tuberous Sclerosis Complex 1 and 2 (*TSC2*, *TSC2*), and Neurofibromatosis 1 (*NF1*) and *PTEN*, have been found to be involved in the *mTOR* pathway (Chow et al., 2009; Ehninger et al., 2008; Zhou et al., 2009; Tsai et al., 2012; Sato et al., 2012; Cambiaghi et al., 2013). The study of these genetic alterations in rodents has been crucial for obtaining useful convergent clues and treatment development. Multiple studies in these mouse models have shown the beneficial effects of the *mTOR* inhibitor rapamycin, for instance, in ameliorating anatomical, physiological, and behavioral deficits in these mice. Moreover, parallel studies in mice and humans have shown that other seemingly unrelated ASD-associated proteins are in fact connected to the canonical *mTOR* pathway. One such example is loss of *FMR1*, which causes Fragile X syndrome; lack of *FMR1* increases *mTOR* activation, and leads to elevated cap-dependent translation and impaired plasticity in Fragile X mice (Sharma et al., 2010). Additional genes, such as *CYFIP1* and *JAKMIP1*, also play an

important role in protein translation and participate in the *mTOR* pathway, have also been associated with ASD (Oguro-Ando et al., 2014; Wang et al., 2015; Berg et al., 2015). These findings suggest that *mTOR*-dependent translation could act as a unifying common pathway for a number of ASD- related molecular cascades. Thus, pharmacological downregulation of *mTOR* using rapamycin could be beneficial not only for the traditional *mTOR*-related disorders but also for a wide range of other ASD syndromes. Mouse models can help us determine which syndromes are likely to respond to particular treatments, such as therapies targeting the *mTOR* pathway. Instances like these can therefore serve as guides for treatment of specific clinical subpopulations and can help tailor clinical trials towards identified patients that are more likely to respond and benefit from specific therapies.

To this date, unfortunately, potential drug treatments that have been thoroughly studied and proven to improve a variety of autism-related phenotypes in mice, have failed to function as successful therapeutic interventions in humans. Such is the case of treatment with *mGlu5* antagonists, which had shown a promising reversal of ASD-related molecular, cellular, and behavioral impairments in both *Fmr1* knock-out flies and mice, revealed no significant benefit in human clinical trials (Berry-Kravis et al., 2016). This highlights how the aforementioned evolutionary divergence between humans and model systems can often be a limiting, as parallel biological processes do not always translate according to what is predicted. This thus warrants incredibly high scrutiny when selecting molecules and pathways as potential drug targets and stresses the importance of fine-tuning points of translational convergence.

1.6 Search for convergence: macro and microcircuits

Mouse models have also been extremely useful in helping us discover autism-related changes in cortical circuit connectivity during brain development (Table 1). Tang et al., 2014 made an important advance in our understanding of cortical connectivity by showing that the developmental pruning of cortical dendritic spines is defective in *TSC2* knockout mice. In addition, they were able to further dissect the cause of this pruning impairment by mating their knockout animals to mice with impaired autophagy, including social impairments, in these animals. Interestingly, rapamycin could no longer rescue the pruning deficits in the *TSC2* knockout mice when they were bred with mice with impaired autophagy. Together, these findings suggest that blockade of autophagy mediates the observed phenotypes in the *TSC2* model. This discovery pathway, downstream of *mTOR*, which links changes in cortical connectivity with impaired social behavior, highlights the benefit of creatively using genetic mouse models to uncover novel and otherwise overlooked molecular mechanism (Tang et al., 2014).

Similar to findings in the *TSC2* model, electrophysiological studies in the *FMR1* model of Fragile X syndrome show a developmental deficit in the pruning of connections between L5A cortical neurons, suggesting that deficits in developmental pruning may extend across multiple models of ASD (Patel et al., 2014). Similar deficits in pruning caused by loss of chemokine receptor *Cx3cr1* in microglia also induce deficits in social interactions and an increase in repetitive behaviors, providing convergent evidence that indeed these deficits are likely contribute to abnormal autism-related behaviors (Zhan et al., 2014). In support of this notion, excessive dendritic spine pruning in adult cortical neurons also strongly correlates with onset of behavioral abnormalities, as seen in the

MECP2 duplication syndrome mouse (Jiang et al., 2013). This therefore indicates that spine density needs to be precisely controlled for proper motor, cognitive, and social function. Furthermore, this impaired developmental pruning is not limited to cortical pyramidal neurons in autism models, as it has also been observed at the climbing fiber-Purkinje cell synapse in the 15q11 – 13 duplication model, suggesting that impaired developmental pruning of connections may extend to other circuits across the brain and that genetic mutations could result in such global deficits (Piochon et al., 2014). It is important to keep in mind, nonetheless, that any disruption in the *mGluR* pathway is likely to result in spine alterations, as has been observed in numerous mouse models, both knock-outs and knock-ins of related genes (Wang et al., 2015; Peter et al., 2016; Piochon et al., 2016). Therefore, searching and finding specificity within these pathways should be of primary importance when modeling ASD.

In addition to identifying novel molecular mechanisms leading to changes in neuronal connectivity, mouse models of ASD have also been effective in mapping of precise circuits involved in specific behavioral alterations. A prime example of this was a recent study by Rothwell et al. (2014), who showed that cell type-specific deletions of the autism-related *NLGN3* gene in dopamine (*D1*) receptor-positive nucleus accumbens (NAc) neurons (*Drd1þ* neurons) [but not in *D2* receptor positive neurons (*Drd2þ* neurons) or cerebellar neurons] was sufficient to induce a motor phenotype (Rothwell et al., 2014). Furthermore, this study showed that such deletion led to impaired inhibition in Drd1þ medium spiny neurons (MSNs) of NAc, further suggesting that ASD-related genetic changes can result in highly specific alterations, that vary based on distinct microcircuit elements within specific subcortical structures. Another study in the mouse

model of 16p11.2 deletion syndrome used single-cell transcriptomics to discover an increase in the number of striatal *Drd2þ* neurons, and a decrease in the number of *Drd1þ* neurons in the deep cortical layers. In this model, excitatory input onto striatal MSN in the NAc showed decreased NMDA/AMPA ratios and decreased probability of synaptic vesicle release, as assayed by paired pulse ratios. Behaviorally, these mice showed hyperactivity, circling, deficits in movement control, and a lack of habituation (Portmann et al., 2014). Together, both studies highlight the importance of striatal reward circuits in understanding repetitive behaviors and motor control in autism.

Interestingly, these findings are somewhat at odds with the tuberosclerosis literature, as studies here have found that cerebellar dysfunction plays a *central* role in all ASD-related behaviors in the *TSC1* rodent model. Specifically, deletion of *TSC1* in cerebellar Purkinje cells results in abnormal social interactions, repetitive behaviors, and abnormal vocalizations (Ehninger et al., 2008; Tsai et al., 2012). This evidence supports earlier histological work implicating the cerebellum in autism (Courchesne et al., 1994; Jones et al., 2002; Fatemi et al., 2002). In support of this, one of the mouse models for 15q11–13 duplication syndrome, which in humans causes autism, intellectual disability, and seizures, also shows profound changes in cerebellar physiology, as well as both motor and social behaviors, providing convergent evidence of cerebellar disorder in autism (Piochon et al., 2014). This evidence highlights the importance of unbiased screens in searching for ASD-relevant circuits. Consequently, further studies in multiple models are needed to understand the complex interactions and disruptions within the multiple cortical, cerebellar, and subcortical regions and their influence on abnormal motor and non-motor behaviors (Tsai et al., 2012).

In addition to the contingent glutamatergic, cortical, and subcortical changes, loss of inhibition seems to be a prevalent and convergent theme among many ASD models. There is a specific loss of inhibition in the hippocampus of *TSC1* mice (Bateup et al., 2013), and a massive loss of parvalbumin neuron-specific inhibition in the hippocampus of *Nlgn3* R451C mice (Földy et al., 2013). Inhibition by cholecystokinin-positive (CCKþ) basket cells was strongly increased, which was mediated by loss of tonic endocannabanoid signaling. This example demonstrated how highly discrete and cell-specific changes in perisomatic inhibition causes some of the major ASD-related phenotypes in the *Nlgn3* R451C model (Földy et al., 2013). In contrast, in the *FMR1* knockout mouse, there is a delayed developmental switch of chloride reversal potential, which naturally drives GABAergic neurotransmission from excitatory to inhibitory (He et al., 2014); this was also concurrent with a reduction in overall excitation onto fast-spiking cortical interneurons, which ultimately reduced their inhibitory output (Patel et al., 2013). These alterations correlate with delayed developmental desynchronization of network activity in the Fragile X mouse model, suggesting that alterations in synaptic connectivity directly impact network synchrony and potentially activity-dependent circuit development (Gonçalves et al, 2013). Moreover, in the BTBR model of autism, an inbred mouse strain with severe social deficits and repetitive behaviors, loss of inhibition leads to abnormal multisensory integration in the insular cortex (Gogolla et al., 2014). Remarkably, in both the BTBR and Fragile X models, there is diminished oxytocin-dependent decrease of intracellular chloride at birth, leading to aberrant excitatory GABAergic responses. Treatment of pregnant females with bumetanide, a blocker of the Na-Cl-K co-transporter *NKCC1*, prevented these pathological changes and improved

autism-related behaviors by normalizing intracellular chloride concentrations and therefore the driving force for GABAergic transmission (Tyzio et al., 2014). This study highlights the long-lasting effects of altered inhibition in early development. In support of these findings, bumetanide administration to a small group of children with autism resulted in some improvements in autism-related behaviors; these findings will need to be replicated in larger studies (Lemonnier et al., 2012).

These changes in inhibition will likely not only impact basal synaptic transmission, but will also alter synaptic plasticity. For example, the *TSC1* (Bateup et al., 2013) and *PTEN* models (Takeuchi et al., 2013) show a loss of metabotropic receptor-dependent long-term depression (LTD) in CA1 and dentate gyrus of the hippocampus, respectively, whereas the *FMR1* model of Fragile X and the Ube3a knockout model of Angelman syndrome both show an enhancement of *mGluR*-dependent LTD (Huber et al., 2002; Bear et al., 2004; Pignatelli et al., 2014). In the *FMR1* model, *mGluR*-dependent LTD pathologically persists in absence of protein synthesis (Nosyreva et al., 2006). This suggests that either diminished or excessive plasticity could result in abnormal circuit function. Such findings posited the hypothesis that many of the physiological and behavioral deficits in Fragile X could arise from increased mGluR signaling (Bear et al., 2004). This provocative notion inspired several studies that indeed demonstrated how blocking mGluR5 rescued many of the Fragile X-associated phenotypes, including cognitive deficits, auditory hypersensitivity, aberrant dendritic spine density, overactive ERK, and mTOR signaling (Michalon et al., 2012; Michalon et al., 2014) or social behavioral deficits (Gantois et al., 2013) in FMR1 knockout mice. Unfortunately, these findings have not translated successfully to treatment of individuals with Fragile X in

clinical trials (Berry-Kravis et al., 2016). This highlights the unique complexity of the human phenotype, even with highly defined genetic classifiers, and warrants more careful selection of treatments, patients, and outcome measures (Jacquemont et al., 2014; Jeste and Geschwind, 2016).

Many of these genetically-defined ASD etiologies have been linked to changes in brain functional connectivity, which is often a manifestation of the inability of neurons to adequately communicate, process and transfer information (Chen et al., 2015). Such phenotypes can be attributed to synaptic disruptions, as described above, as well as to alterations in neuronal excitability. In the *PTEN* model of autism, for instance, a single copy deletion in adulthood results in diminished intrinsic excitability of L2/3 visual cortical neurons in mice (García-Junco-Clemente et al., 2013). It was shown that these changes directly resulted from up-regulated calcium-activated small conductance (SK-type) potassium channels and were associated with decreased cortical responses to visual stimuli in visual cortex (García-Junco-Clemente et al., 2013). Conversely, in the *FMR1* model of Fragile X, there is decreased expression of dendritic BK-type calcium-activated potassium channels, which in turn increases dendritic excitability and heightens sensitivity to incoming somatosensory inputs (Zhang et al., 2014). Therefore, autism-related mutations can lead to intrinsic excitability changes that can dramatically alter the processing of sensory information, either by increasing or decreasing sensitivity to external stimuli. Indeed, understanding how specific genetic etiologies alter processing of the various sensory modalities can give us insights into which specific treatments should be catered to autistic individuals (García-Junco-Clemente et al., 2013; Zhang et al., 2014).

A more profound understanding of the specific circuit elements that drive social and nonsocial behaviors has come to life in virtue of innovative tools such as optogenetics and Designer Receptors Exclusively Activated by Designer Drugs (DREADDs) (Lee et al., 2013; Deisseroth et al., 2015). Technologies such as these have allowed us to manipulate brain circuits in wild-type mice in order to produce behaviors reminiscent of autistic phenotypes, thus giving us clues about which functional alterations might be involved in human ASDs. For instance, increasing excitatory activity in the medial amygdala inhibits aggression and mating behaviors, whereas increasing inhibition promotes social interactions and decreases repetitive self-grooming (Hong et al., 2014). Similar effects have been observed when activating or inhibiting amygdala projections within the ventral hippocampus, thus highlighting the potential contribution of this structure to autism-related phenotypes (Felix-Ortiz et al., 2014). Future studies can therefore make use of these findings and focus on dissecting microcircuit changes in such brain regions, or determine whether pharmacological or cell-specific treatments and manipulations can be used to treat social impairments or other behavioral dysfunctions associated with ASD.

1.7: A new generation of treatments

Mouse models are also an invaluable vessel for testing an entirely new generation of rationally designed treatments. One such remarkable example is comes from a recent study in a Ube3a overexpression mouse, which models Angelman syndrome, a condition that is highly comorbid with ASD (Williams et al., 2007). In this study, researchers used antisense oligonucleotides (ASOs) to silence the overexpressed and nuclear-localized

long noncoding RNA, *UBE3A* antisense transcript (*UBE3A*-ATS), which typically inhibits expression of the paternal copy of *UBE3A* itself. This treatment astonishingly resulted in sustained unsilencing of paternal *UBE3A*, both in vitro and in vivo, and improved cognitive deficits in the mouse model of the disorder (Meng et al., 2015). Although many details remain to be worked out in terms of timing treatment and mode of delivery, experiments such as these provide hope towards novel human therapeutics and prove rodent models as an essential intermediate step for the development of novel human therapeutics.

Table 1.1: Summary of most recent advances in the study of mouse models of ASD

Model	ASD-related behaviors	Functional disruptions	Treatment	Reference
15q11-13dup	Decreased sociability	Spine pruning deficits in Purkinje neurons	None	Piochon et al., 2014
	Increased vocalizations in pups	Enhanced LTD		
	Reduced vocalizations in adults			
	Behavioral inflexibility			
	Increased grooming			
	Hyperactivity			
16p11.2del	Reduced sociability	Alterations in dopaminergic pathways in MSNs	None	Portmann et al., 2014
	Repetitive behaviors	Decreased striatal and nucleus acumbens volume	Decreased sensitivity to risperidone	
	Hyperactivity			
BTBR	Reduced sociability	Decreased inhibition	Diazapam	Gogolla et al., 2014
	Repetitive grooming	Alterations in multisensory integration		
	Increased vocalizations in pups			
	Altered vocalizations in adults			
FMR1	Altered social behavior	Spine pruning deficits	mGluR antagonists	Bear et al., 2004
	Increased vocalizations	Delayed inhibitory maturation and inhibitory function	BK-Ca channel openers	Patel et al., 2014
	Stereoypies	Altered developmental synchrony	Prenatal bumetanide	Parel et al., 2013
	Repetitive behaviors	Enhanced LTD		Goncalves et al., 2013
	Anxiety	Increased dendritic and cortical excitability (BK channels)		Tyzio et al., 2014
	Hyperactivity			
	Cognitive defects			
Mecp2	Altered sociability	Excessive spine pruning	Levodopa	Jiang et al., 2013
	Decreased vocalizations	Altered inhibition	Dopa-decarboxylase inhibitors	
	Increased grooming		IGF1	
Nlgn3	Altered sociability	Alterations in dopaminergic pathways (Nucleus accumbens)	None	Rothwell et al., 2014
	Repetitive behaviors	Impaired inhibition onto MSNs		
	Inflexibility	Decreased perisomatic inhibition		
PTEN	Decreased sociability	Decreased LTD	None	Takeuchi et al., 2013
	Increased grooming	Decreased intrinsic excitability (SK channels)		García-Junco-Clemente et al., 2013
TSC1	Decreased sociability	Cerebellar abnormalities	Rapamycin/mTOR	Bateup et al., 2013
	Inflexibility	Decreased inhibition		
	Increased grooming	DecreasedLTD		
	Increased pup calls			
TSC2	Decreased sociability	Deficits in developmental spine pruning and autophagy	Rapamycin/mTOR	Tang et al., 2014
	Increased grooming			
Ube3a	Decreased sociability	Decreased synaptic pruning	ASOs	Meng et al., 2014
	Decreased vocalizations	Decreased excitatory neurotransmission		Piochon et al., 2014
	Repetitive behaviors			

1.8: The CNTNAP2 autism susceptibility gene

Recessive, truncating mutations in the *CNTNAP2* gene cause cortical dysplasia focal epilepsy (CDFE), a syndromic form of autism. It has been reported that 70% of homozygous mutations carriers display autism-related deficits, in addition to the characteristic language and cognitive impairments, hyperactivity, and epilepsy observed in CDFE (Strauss et al., 2006). Other variants, including point mutations in *CNTNAP2*, have also been shown to correlate with ASD-related alterations, including non-specific language impairments, attention deficit disorders, schizophrenia, and disruptions in frontal lobe connectivity (Scott Van-Zeeland et al., 2010; Peñagarikano and Geschwind, 2012; Rodenas-Cuadrado et al., 2014).

CNTNAP2 encodes a neuronal transmembrane protein, contactin-associated-like protein 2 (Caspr2), which is a member of the neurexin superfamily (Poliak et al., 1999). It mediates neuron-glia interactions by binding to Tag-1 (*CNTN2*), a neuroligin, and is crucial for the clustering of Kv1 potassium channels in the juxtaparanodal region of myelinated axons (Poliak et al., 2003). More recently, it has been demonstrated that Caspr2 in fact localizes at the synapse and has a role in the formation and stabilization of excitatory synapses (Anderson et al., 2012; Gdalyahu et al., 2015; Varea et al. 2015). The protein is also expressed in multiple sensory systems in rodents, thus suggesting that alterations in its normal function could underlie some of the sensory processing manifestations observed in ASD (Gordon et al., 2016).

Importantly, Caspr2 is also strongly brain-expressed in embryonic stages, enriched in areas such as the medial ganglionic eminence, well before the onset of myelination and is thought to play an important role for proper neuronal migration

(Abrahams et al., 2007). This fact is of high importance when considering pathological mechanisms of ASDs, as they are indeed developmental disorders. The role of Caspr2 in development has not only been evidenced by altered cortical lamination in brain samples from epileptic of CDFE patients (Strauss et al., 2006), it has also been supported by the neuronal migration abnormalities observed in *Cntnap2* KO mouse, as described in the next section (Peñagarikano et al., 2011).

1.9: The *CNTNAP2* mouse model of autism

In this current era of research, mouse models have become a critical tool for understanding physiological and pathological deficits involved in neurological disease. Our lab published the initial characterization of the *Cntnap2* KO mouse (Peñagarikano et al., 2011). Remarkably, these mice recapitulated core features of autism, including reduced vocalizations, impaired social interactions, and repetitive or restrictive behaviors (Figure 1.1). In addition, *Cntnap2* KO mice showed CDFE traits, such as neuronal migration abnormalities, reduced number of inhibitory neurons, decreased neural synchronization, and epilepsy. When treated with Risperidone, an atypical antipsychotic, and the only FDA-approved drug for treatment of irritability and aggression in ASD, the repetitive and hyperactive behaviors in *Cntnap2* KO mice were ameliorated. More recently, we showed that both acute and early postnatal treatment of *Cntnap2* KO mice with oxytocin improved its social behavior (Peñagarikano et al., 2015). These studies highlighted the

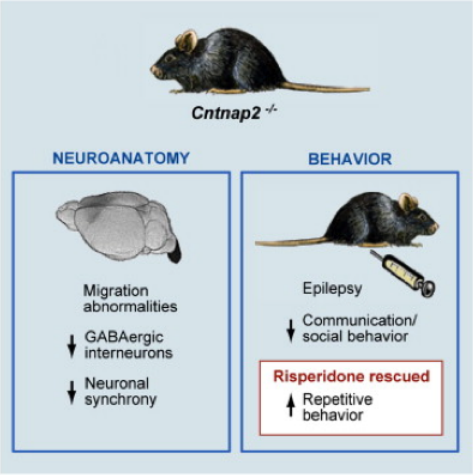

Figure 1.1: *Cntnap2* KO mice recapitulate behavioral and pathological deficits of ASDs (Peñagarikano et al., 2011).

value of our model as an accurate research tool, as it fulfilled the main standard criteria of construct validity, face validity, and predictive validity (Chadman et al., 2009; Nestler and Hyman, 2010).

1.10: Conclusions

The utility of rodent models of autism will increase nonlinearly with improvements in genetic engineering and genome editing, high-throughput electrophysiology and cellular functional imaging, and activity modulation techniques (Prakash et al., 2012; Platt et al., 2014; Rickgauer et al., 2014). By genetically manipulating specific neuronal subpopulations and modulating specific activity patterns, we will finally be able to understand the functional changes that cause but also rescue the deficits characteristic of ASD (Ziv et al., 2013). Mouse models will also continue to complement results obtained in other in-vitro models such as those from induced pluripotent stem cells (Shcheglovitov et al., 2013). Most importantly, understanding of basic neuron circuit function at the most fundamental level will likely yield the most impact for understanding ASDs in the long run. Rodent models serve as a starting point for assessing adequate therapeutic interventions for ASD, keeping in mind that it could necessitate further validation in closer evolutionary relatives (like primates) and humans.

Chapter 2:

In vitro assessment of intrinsic neuronal excitability, synaptic neurotransmission, cortical inputs, and microcircuit connectivity in the mPFC of *Cntnap2* KO mice

2.1: Abstract

Recessive truncating mutations in *CNTNAP2* cause Cortical Dysplasia Focal Epilepsy (CDFE), a syndromic form of Autism Spectrum Disorder (ASD). *CNTNAP2* encodes for contactin-associated protein-like 2 (Caspr2), a neurexin family protein that mediates neuron-glia interactions and the clustering of K^+ channels in axons. *Cntnap2* knock-out (KO) mice recapitulate core deficits of ASD, including impairments in social interactions and communication, repetitive/restrictive behaviors, seizures, decreased neuronal synchrony, and neuronal migration deficits. Here, I investigate whether loss of Caspr2 alters intrinsic excitability, synaptic neurotransmission, or synaptic connectivity between identified excitatory and inhibitory neurons. I perform *in vitro* whole-cell patch-clamp recordings in acute slices of medial prefrontal cortex (mPFC), an area that is implicated in social behavior and autism. By performing these whole-cell recordings and laser scanning photostimulation mapping via glutamate uncaging, in *Cntnap2* KO mice and wild-type (WT) controls, I find that our autism model displays a dramatic decrease in both excitatory and inhibitory synaptic inputs to L2/3 mPFC excitatory neurons. Miniature excitatory postsynaptic current (mEPSC) frequency and amplitude, as well as evoked EPSCs, were decreased in excitatory neurons, but short term plasticity and intrinsic excitability were not altered. These findings support emerging evidence suggesting that Caspr2 has a role in synaptic neurotransmission and that loss of *Cntnap2* results in the reduction of the total number of functional synapses.

2.2: Background

Previous studies have shown that adequate membrane localization of Caspr2 is crucial for clustering of potassium channels in the juxtaparanodes of axons (Poliak et al., 2001; Poliak and Peles 2003; Poliak et al., 2003). Such biological function could be important for efficient action potential firing via modulation of intrinsic neuronal properties (Aranciba and Atwell, 2014). These alterations in E/I ratio can emerge in many ways, including disturbances in tonic GABAergic and glutamatergic neurotransmission, changes in microcircuit connectivity and neural weights, or disruptions in the firing patterns or excitability of excitatory and inhibitory cells (Gogolla et al., 2009; Yizhar et al., 2011; Berg and Geschwind, 2012; D'amour and Froemke, 2015; Nelson and Valakh, 2015).

Pyramidal (Pyr) excitatory neurons in the mPFC primarily function in assemblies that carry information to and from connected brain regions (Buzsáki and Watson, 2012). In doing so, they contribute to modulation of executive functions, emotions, and indeed social behaviors (Yizhar et al., 2016). Parvalbumin-positive (PV) inhibitory neurons, on the other hand, are responsible for pacing and entraining Pyr neurons in synchronous activity, contribute to gain modulation, and promote transmission of a coherent message that results in a cohesive and appropriate behavioral output (Einstein et al., 2016). Alterations in the excitability of Pyr and/or PV neurons might explain some of the previously observed pathologies of *Cntnap2* KO mice, including seizures and decreased neuronal synchrony (Peñagarikano et al., 2011).

2.3: Intrinsic excitability of L2/3 pyramidal (Pyr) neurons and parvalbumin-positive (PV+) inhibitory neurons in *Cntnap2* WT and KO mice.

Caspr2 has a known role in the clustering of potassium channels in the juxtaparanodes of axons (Poliak et al., 2001; Poliak and Peles 2003; Poliak et al., 2003). This, together with the fact that *Cntnap2* KO mice display epileptic seizures and decreased neuronal synchrony in vivo, suggests that alterations in neuronal excitability might be at play in producing these phenotypes. I therefore hypothesized that *Cntnap2* KO mice would display alterations in the excitability and membrane properties of Pyr neurons and PV inhibitory neurons of the mPFC. I expected either an increase in pyramidal neuron excitability or a decrease in inhibitory neuron excitability, consistent with our previous pathological findings.

To test these hypotheses, we performed whole-cell current-clamp recordings on L2/3 Pyr neurons and PV inhibitory neurons of mPFC in *Cntnap2* KO and wild-type (WT) controls. Input-output curves showing average number of action potentials elicited by increasing current injections for pyramidal neurons (WT n = 28, KO n = 21; p = 0.7057, Two-way ANOVA) and parvalbumin-positive inhibitory neurons (WT n = 27, KO n = 42; p = 0.30, Two-way ANOVA) revealed no statistically significant alterations in action potential firing rate (Figure 2.1). Action potential (AP) features, such as threshold, amplitude, half-width, afterhyperpolarization (AHP) potential, or time from peak to AHP were also not significantly different between WT and KO. Similarly, passive membrane properties such as resting membrane potential (RMP), input resistance (Rin), cell membrane capacitance (Cm), or membrane time constant (Tau) were also not significantly different (Table 2.1 and 2.2). This suggests that loss of *Cntnap2* likely does

not materially affect the intrinsic excitability of L2/3 neurons of mFPC, contrary to what was expected.

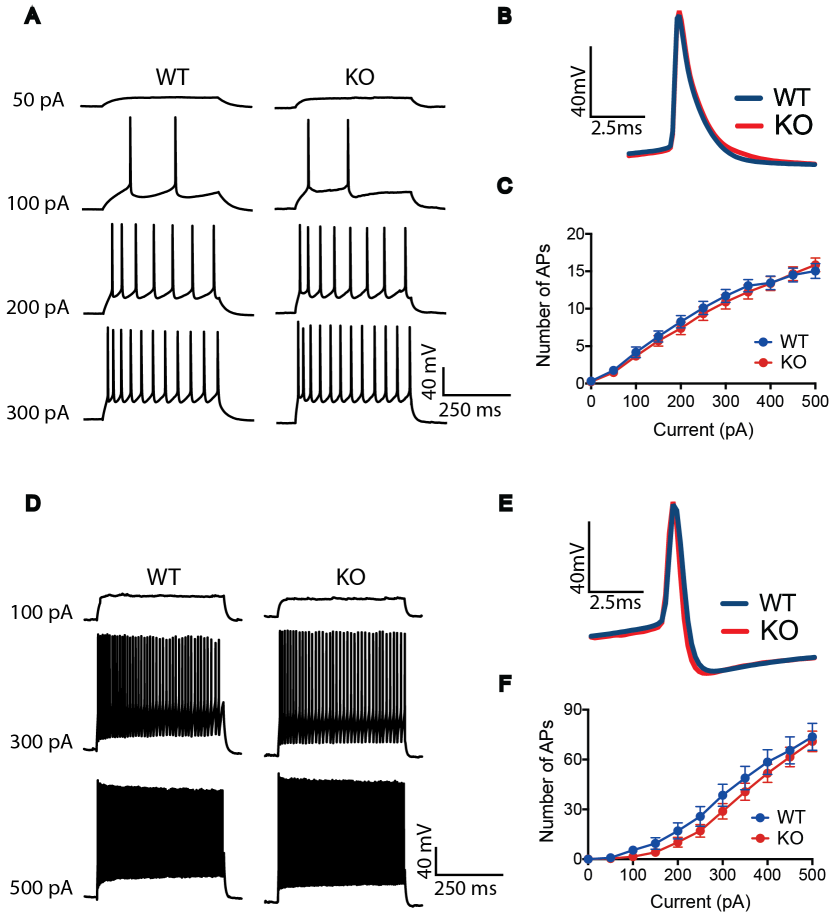

Figure 2.1 Intrinsic excitability of L2/3 pyramidal (Pyr) neurons and parvalbumin-positive (PV+) inhibitory neurons in *Cntnap2* WT and KO mice. (A, D) Representative action potential traces from L2/3 WT and KO pyramidal and PV+ neurons, showing responses to various current injections and (B, E) corresponding average action potential waveforms. (C, F) Input-output curves showing average number of action potentials elicited by increasing current injections for pyramidal neurons (WT n = 28, KO n = 21; p = 0.71, Two-way ANOVA) and parvalbumin-positive inhibitory neurons (WT n = 27, KO n = 42; p = 0.30, Two-way ANOVA). Data obtained from

current-clamp recordings of neuronal spikes elicited by stimulating with 50 pA step increments, cells clamped at -70mV.

Table 2.1 and 2.2. Summary of passive membrane properties and action potential features for pyramidal neurons and parvalbumin-positive inhibitory neurons in *Cntnap2* WT and KO mice.

Table 2.1 Pyramidal neurons

Passive Membrane Properties	WT	KO
RMP (mV)	-73.2 ± 2.0	-68.7 ± 2.3
Rin (mOhms)	174.1 ± 18.7	173.5 ± 21.7
Cm (pF)	96.1 ± 8.1	106.8 ± 12.3
Tau (ms)	14.7 ± 1.0	16.6 ± 0.9
Action Potential Features		
Amplitude (mV)	84.9 ± 1.7	82.1 ± 1.9
Half-width (ms)	1.0 ± 0.1	1.1 ± 0.1
AHP Amplitude (mV)	-4.5 ± 1.2	-4.0 ± 1.7
Peak to AHP (ms)	3.8 ± 0.5	3.1 ± 0.5
Threshold (mV)	-39.3 ± 1.0	-37.0 ± 0.9

Table 2.2 Parvalbumin-positive inhibitory neurons

Passive Membrane Properties	WT	KO
RMP (mV)	-80.6 ± 1.2	-78.0 ± 0.8
Rin (mOhms)	93.2 ± 6.3	85.1 ± 4.2
Cm (pF)	69.8 ± 4.2	80.5 ± 4.5
Tau (ms)	6.2 ± 0.2	6.4 ± 0.2
Action Potential Features		
Amplitude (mV)	62.0 ± 2.3	64.5 ± 1.7
Half-width (ms)	0.3 ± 0.0	0.3 ± 0.0
AHP Amplitude (mV)	-24.0 ± 0.7	-22.1 ± 0.6
Peak to AHP (ms)	0.8 ± 0.1	0.8 ± 0.0
Threshold (mV)	-39.7 ± 1.0	-41.0 ± 0.9

2.4: Quantification of excitatory and inhibitory synaptic inputs

Given that no major excitability changes in Pyr or PV neurons were observed, I next tested whether alterations in synaptic transmission could underlie some of the previously reported physiological deficits in *Cntnap2* KO mice (Peñagarikano et al., 2011). This was especially salient given recent data that *Cntnap2* plays an important role in the formation and stabilization of synapses (Anderson et al., 2012; Gdalyahu et al., 2015). I hypothesized that functional excitatory and inhibitory synaptic transmission would be altered in *Cntnap2* KO mice. To test this hypothesis, I performed in vitro whole-cell voltage-clamp recordings of L2/3 mPFC Pyr and PV neurons and recorded miniature excitatory and inhibitory postsynaptic currents (mEPSCs and mIPSCs, respectively) in acute slices.

Remarkably, I observed a two-fold decrease in the frequency of mEPSCs (Figure 2.2 B) and a nominal, non-statistically significant decrease in mIPSCs (Figure 2.2 E) on Pyr neurons. I also observed a small, but significant decrease in the average amplitude of mEPSCs in *Cntnap2* KO pyramidal neurons (Figure 2.2 C), but not mIPSCs (Figure 2 F). These findings point towards a reduction in both excitation and inhibition in pyramidal neurons in the mPFC of *Cntnap2* KO mice. Thus, rather than a shift in the balance of excitation/inhibition in L2/3 of mPFC (Figure 2.3), *Cntnap2* KO mice display an overall reduction in the total number of functional synapses.

I also performed the same analyses of excitatory and inhibitory inputs on PV+ inhibitory neurons. In contrast to my observations in pyramidal cells, I observed no statistically significant alterations in frequency or amplitude of mEPSCs (Figure 2.1 G-I) or mIPSCs (Figure 2 J-L) in PV neurons. This indicates that loss of *Cntnap2* results in

reduced excitatory synaptic transmission that primarily affects pyramidal neurons in the mPFC.

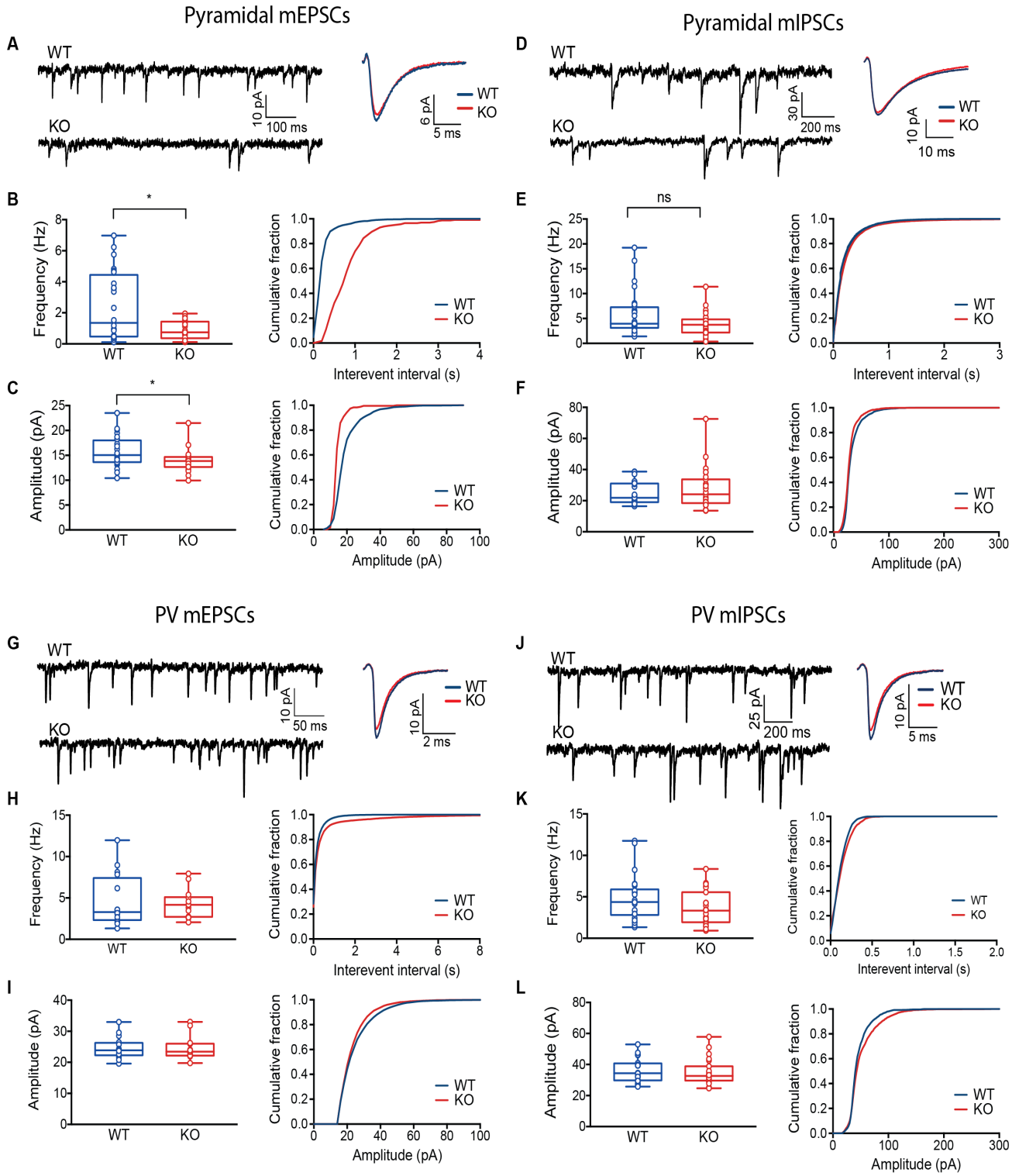

Figure 2.2: *Cntnap2* KO pyramidal neurons display a two-fold decrease in the frequency of miniature excitatory postsynaptic currents (mEPSCs). (A,D) Representative traces from recorded mEPSCs and mIPSCs in *Cntnap2* WT and KO pyramidal cells, voltage-clamped at -70 mV, with corresponding average unitary events. (B,E) Frequency of mEPSCs (WT 2.42 ± 0.45 Hz, n = 24 cells; KO 0.89 ± 0.1 Hz, n = 24 cells; p = 0.002, Unpaired t test with Welch's correction) is decreased in KO mice, while mIPSCs show a non-statistically significant decrease in frequency, compared to WT (WT 5.8 ± 0.8 Hz, n = 28; KO 3.9 ± 0.4 Hz, n = 27; p = 0.141, Mann-Whitney test). (C,F) Amplitude of mEPSCs (WT 15.7 ± 0.6 pA, n = 24; KO 13.9 ± 0.5 pA, n = 24; p = 0.017, Mann-Whitney test), but not mIPSCs (WT 24.4 ± 1.3 pA, n = 28; KO 27.2 ± 2.5 pA, n = 27; p = 0.8740, Mann-Whitney test) is decreased in KO mice. (G-L) Frequency (WT 4.5 ± 0.8 Hz, KO 4.3 ± 0.5 Hz; p = 0.990, Unpaired t test) and amplitude (WT, 24.5 ± 0.9 pA, KO 24.6 pA ± 1.0; p = 0.597, Mann-Whitney test) of mEPSCs (WT n = 17, KO n = 15) and frequency (WT 4.7 ± 0.5 Hz, KO 3.6 ± 0.4 Hz; p = 0.407, Mann-Whitney test) and amplitude (WT 36.0 ± 1.9 pA, KO 37.6 ± 2.5 pA; p = 0.824, Mann-Whitney test) of mIPSCs (WT n = 28, KO n = 25) recorded from parvalbumin-positive (PV) inhibitory neurons are not statistically different between *Cntnap2* KO and WT mice. Distribution of data is represented as box and whiskers plots with mean ± SEM. Individual cells are represented as open circles. Statistical significance is represented by * for Mann Whitney test $p<0.05$.

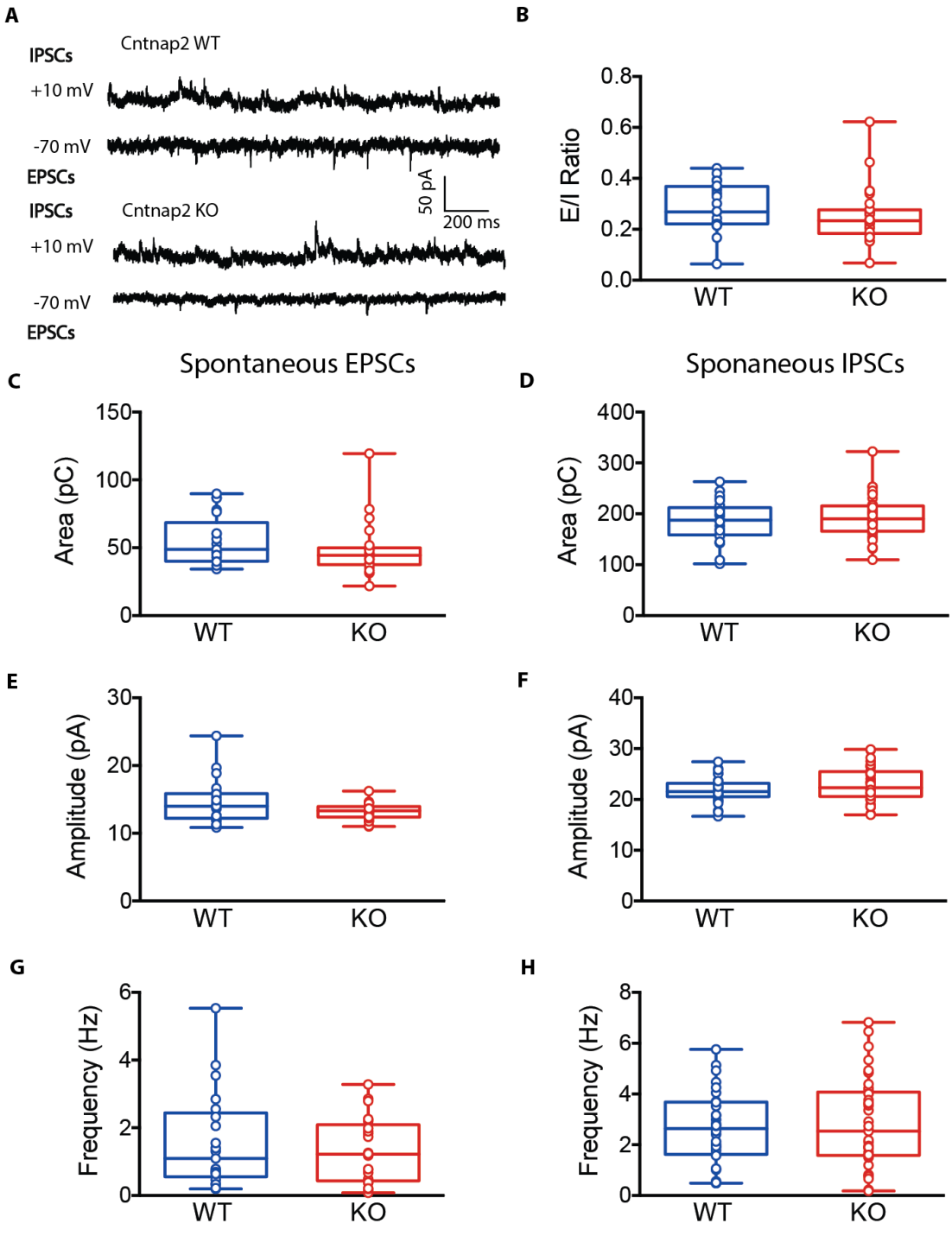
A
Cntnap2 WT
IPSCs
+10 mV
-70 mV
EPSCs
50 pA
200 ms
IPSCs
Cntnap2 KO
+10 mV
-70 mV
EPSCs
B
E/I Ratio
0.8
0.6
0.4
0.2
0.0
WT
KO
C
Spontaneous EPSCs
Area (pC)
150
100
50
0
WT
KO
D
Sponaneous IPSCs
Area (pC)
400
300
200
100
0
WT
KO
E
Amplitude (pA)
30
20
10
0
WT
KO
F
Amplitude (pA)
40
30
20
10
0
WT
KO
G
Frequency (Hz)
6
4
2
0
WT
KO
H
Frequency (Hz)
8
6
4
2
0
WT
KO

Figure 2.3: Excitatory/inhibitory ratio in pyramidal neurons of *Cntnap2* KO mice. (A) Representative traces from recorded spontaneous excitatory and inhibitory postsynaptic currents (sEPSCs and sIPSCs), respectively. Both of these were recorded from the same cell by clamping at -70 mV for sEPSCs were recorded by clamping the cells at -70 mV and at +10 mV for sIPSCs. (B) Average excitatory/inhibitory ratios calculated by dividing the average charge, calculated as the area under the curve in picocoulombs (pC) of sEPSCs and sIPSCs per cell (WT 0.3 $\pm$ 0.0, n = 23, KO 0.3 $\pm$ 0.0, n = 28; p = 0.153, Mann-Whitney test). (C-H) Average area (WT 54.9 $\pm$ 4.0 pC, KO 48.2 $\pm$ 4.0 pC; p = 0.169, Mann-Whitney test), amplitude (WT 14.6 $\pm$ 0.7 pA, KO 13.3 $\pm$ 0.2 pA; p =0.164, Mann-Whitney test) and frequency (WT 1.6 $\pm$ 0.3 Hz, KO 1.3 $\pm$ 0.2 Hz; p = 0.760, Mann-Whitney test) of sEPSCs (WT n = 21, KO n = 24) and average area (WT 186.7 $\pm$ 7.2 pC, KO 193.3 $\pm$ 6.8 pC; p = 0.510), amplitude (WT 21.87 $\pm$ 0.4 pA, KO 23.0 $\pm$ 0.5 pA; p = 0.189, Mann-Whitney test), and frequency (WT 2.6 $\pm$ 0.3 Hz, KO 2.8 $\pm$ 0.3 Hz; p = 0.657, Unpaired t test) for sIPSCs (WT n = 29, KO n = 27). Distribution of data is represented as box and whiskers plots with mean $\pm$ SEM. Individual cells are represented as open circles. No statistically significant differences were observed between genotypes for any of these measures.

2.5: Synaptic vesicle release and AMPA/NMDA ratios

The observed decrease in mEPSC frequency on pyramidal neurons could be caused by either a disruption in 1) the probability of synaptic vesicle release and/or 2) a reduction in the total number of functional or mature synapses (Malinow and Malenka, 2002; Burrone et al., 2002; Golshani et al., 2005). To address this first possibility, I

stimulated long-range axonal projections to mPFC in slices, and measured evoked excitatory currents elicited in L2/3 pyramidal cells (Figure 2.4 A). I found no significant difference in paired-pulse ratios of evoked currents between WT and KO mice (Figure 3B-C). Thus, the observed decrease in mEPSC frequency in the KO is likely not due to alterations short-term plasticity or deficits in synaptic vesicle release probability.

Using the same experimental approach, I tested whether the reduction in mEPSCs was due to an increase in the proportion of immature or silent synapses, characterized by a decreased the ratio of AMPA/NMDA receptors (Malinow and Malenka, 2002; Golshani et al., 2005; González-Burgos et al., 2008). I recorded evoked AMPA and NMDA currents by holding the cells at -70 mV and at +40 mV in voltage-clamp, respectively, and found no significant difference in the ratio when comparing *Cntnap2* WT and KO mice (Figure 2.4 F). Interestingly, input-output curves revealed a decrease in the amplitude of current responses in the KO at higher stimulation intensities (Figure 2.4 B). This finding supports the notion that indeed there is a decrease in excitatory neurotransmission in the mPFC of *Cntnap2* KO mice. Thus, although loss of Caspr2 does not seem to affect synaptic vesicle release and maturation of already stabilized synapses, we find an overall decreased excitatory inputs in the KO's local mPFC microcircuit.

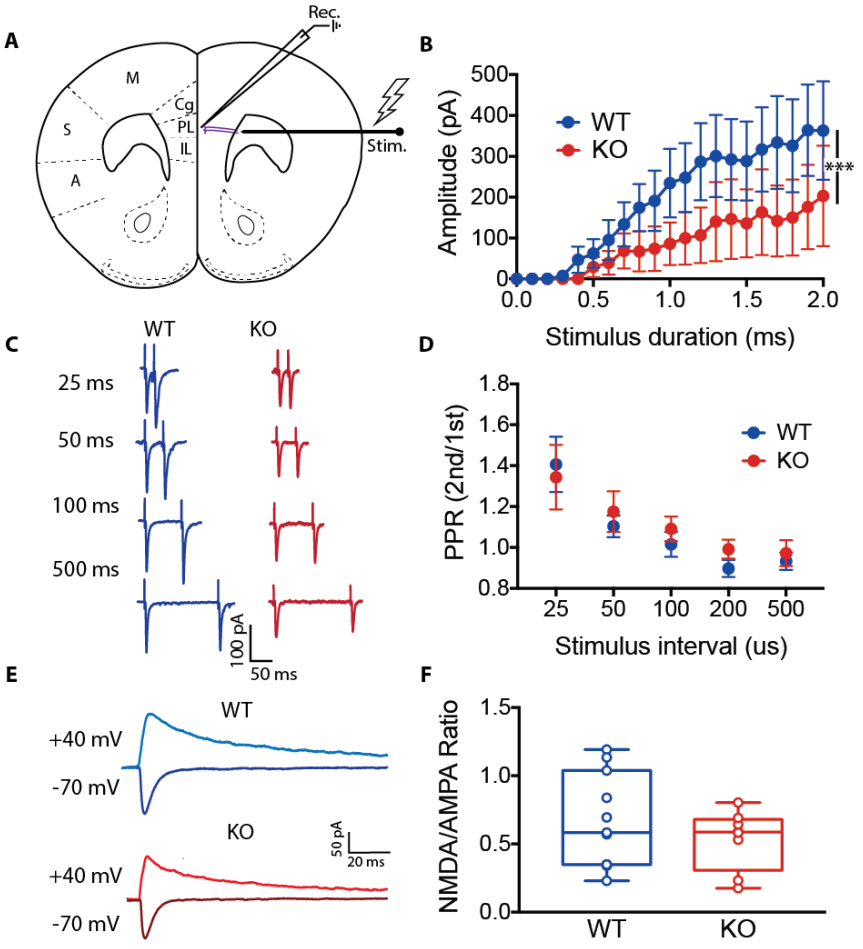

Figure 2.4: Evoked synaptic responses reveal decreased long range excitatory inputs in *Cntnap2* KO mice. (A) Monopolar tungsten electrode was used to stimulate long-range axons (purple), which extend from the anterior forceps of the corpus callosum and project onto a patched excitatory neuron in L2/3 mPFC. (B) Input-output curves of unitary excitatory responses resulting from a range of increasing stimulus intensities in *Cntnap2* WT and KO mice (WT n = 7 cells, KO n = 9 cells; $p < 0.0001$, Two-way ANOVA). (C) Representative current responses from paired-pulses given at various inter-stimulus intervals (ISIs) in WT and KO mice. (D) Ratio of 2nd/1st evoked synaptic

response to paired-pulse stimulation at increasing ISIs suggests no significant deficits in the probability of synaptic vesicle release in *Cntnap2* KO mice (WT n = 10 cells, KO n = 8 cells; p = 0.893, Two-way ANOVA). (E) Evoked AMPA (cells voltage-clamped at -70mV) and NMDA (cells voltage-clamped at +40mV) currents in WT and KO mice. Stimulus artifact was blanked for clarity. (F) AMPA/NMDA ratios of *Cntnap2* KO mice were not significantly altered, compared to WT mice, suggesting no significant changes in synaptic maturity (WT 0.7 $\pm$ 0.1, n = 11 cells; KO 0.5 $\pm$ 0.1, n = 8 cells; p = 0.347, Unpaired t test).

2.6: Cortical mapping of excitatory and inhibitory synaptic inputs using local scanning photostimulation (LSPS) and glutamate uncaging

To garner further evidence for the decrease in synaptic inputs suggested by the physiological data, I next used laser scanning photostimulation (LSPS) via glutamate uncaging to map local circuit inputs of patched pyramidal neurons, in collaboration with the laboratory of Dr. Xiangmin Xu at UC Irvine. We reasoned that if synaptic inputs were in fact reduced, as suggested by our initial findings, the input currents would be weaker in the KO (Callaway and Katz, 1993; Xu and Callaway, 2009; Xu et al., 2010; Ikrar et al., 2011). In order to test this, we quantified and mapped input strengths on patched L2/3 Pyr neurons (Figure 2.5). We quantified and mapped excitatory and inhibitory input strengths by holding the pyramidal neuron near the reversal potential for inhibitory (-70 mV) and excitatory (+10 mV) conductances in voltage clamp mode, while uncaging glutamate and activating small clusters of surrounding neurons (Figure 2.6) and observed that similar to WT neurons, KO neurons receive most of their excitatory and inhibitory

synaptic inputs from L2/3 and L5 in mPFC (Figure 5B-C). We observed that, similar to WT neurons, KO neurons receive most of their circuit inputs from L2/3 and L5 in mPFC (Figure 2.6 B-C). However, compared to WT, we found that L2/3 excitatory neurons in Cntnap2 KO mice display a dramatic reduction in both excitatory and inhibitory local synaptic inputs (Figure 2.6 E-I). This decrease in synaptic connections does not appear to be due to lower neuronal responsiveness to glutamate uncaging in KO mice, because both KO and WT neurons show large responses to glutamate uncaging in perisomatic regions (Figure 2.5). Whereas KO neurons have decreased EPSC and IPSC inputs from local mPFC circuits, the balance of the total IPSC/ total EPSC inputs to individual neurons is not significantly altered, as the average ratio of IPSC/EPSC is not significantly different between genotypes (Figure 2.6 G). Thus, this more refined experimental approach extends and confirms the mEPSCs and stimulating electrode findings, demonstrating that there is a robust reduction of both excitatory and inhibitory synaptic inputs on layer 2/3 pyramidal cells in the mPFC of KO mice.

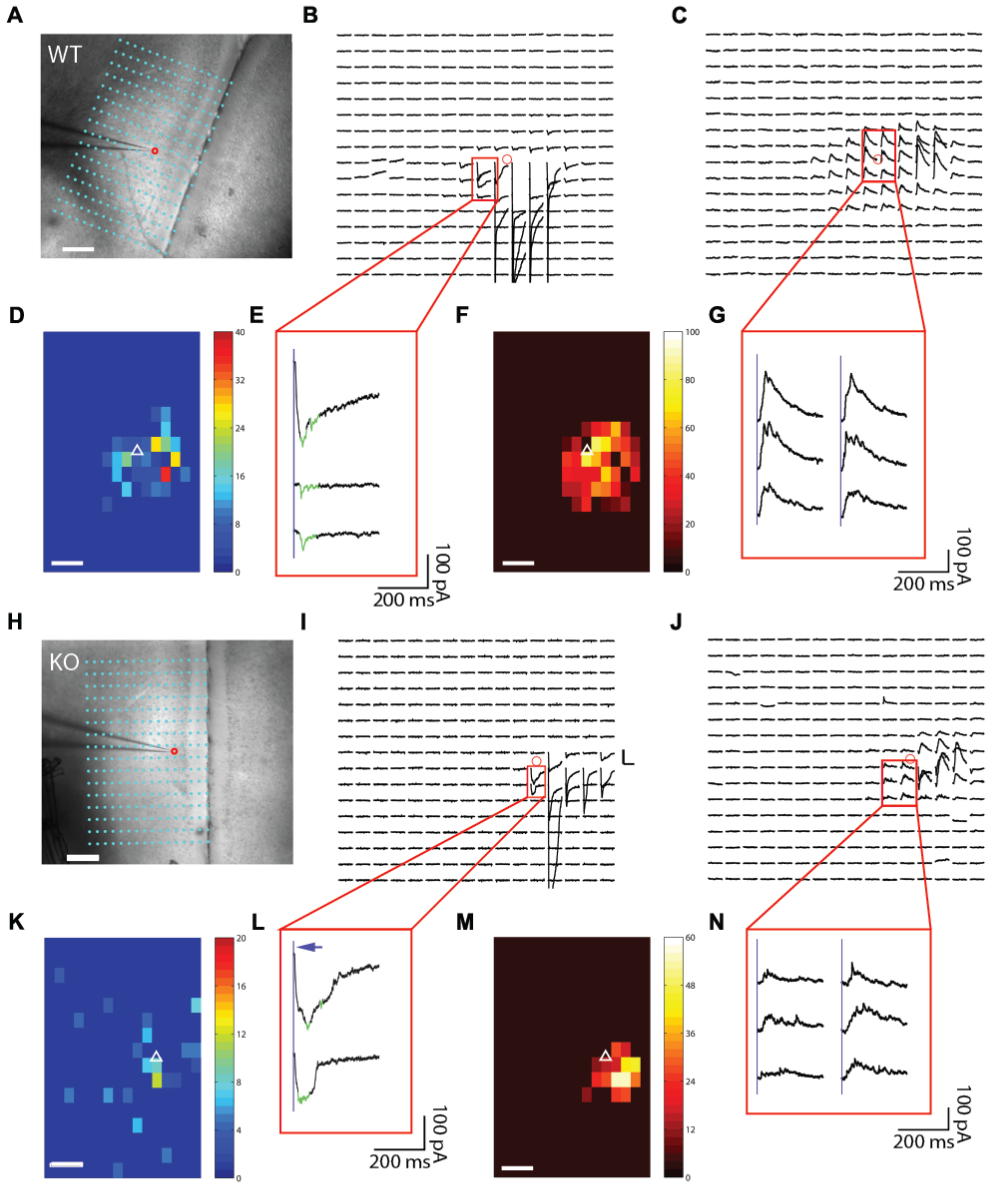

Figure 2.5: Example cortical input map data for *Cntnap2* WT and KO L2/3 mPFC excitatory neurons. (A,H) Differential interference contrast (DIC) image of mPFC, superimposed with photostimulation sites (cyan dots), spaced at 100 µm x 60 µm, for WT and KO mice. The tip of the patch pipette (recording electrode) and the cell body location of a recorded L2/3 neuron is indicated by a red circle. (B, C, I, J) Photostimulation-

evoked response traces plotted according to their corresponding photostimulation sites, as shown in (A,H). Traces depict currents recorded 250 ms after stimulation (1.5 ms, 15 mW) onset. Cells were voltage-clamped at −70 mV to detect inward excitatory postsynaptic currents (EPSCs), depicted in (B) and (I), and at +5 mV to detect inhibitory postsynaptic currents (IPSCs), depicted in (C and J). Excitatory (D, K) and inhibitory (F, M) input maps of average integrated stimulation responses for datasets shown in (B, I) and (C, J), respectively. Somatic location of the recorded neuron is represented by a white triangle. (E, L) and (G, N) show enlarged insets of selected responses in (B, I) and (C, J), respectively. Green overlays mark over-riding synaptic responses. Average input amplitudes were calculated as mean integrated amplitudes of EPSCs or IPSCs elicited within the 250 ms post-stimulus onset timeframe. White scale bars represent 250 µm.

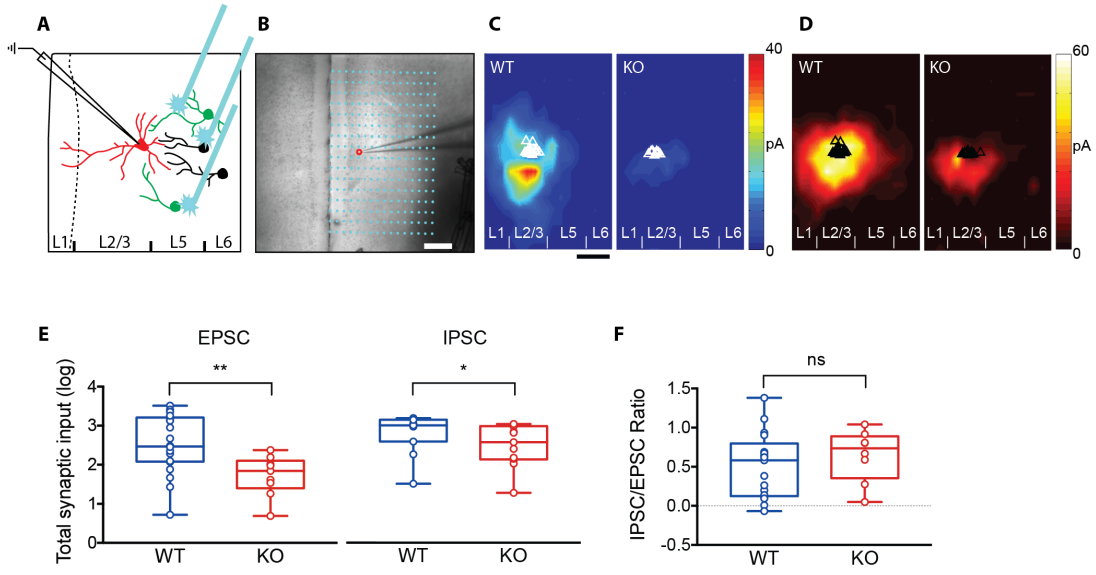

Figure 2.6: Excitatory neurons in the mPFC of *Cntnap2* KO mice show reduced local synaptic inputs. (A) Schematic of laser scanning photostimulation (LSPS) via

glutamate uncaging in acute slices of the medial prefrontal cortex (mPFC), combined with whole cell recordings to map of local synaptic connections to individually recorded excitatory pyramidal neurons. (B) Differential interference contrast (DIC) visualization of mPFC slice with superimposed photostimulation sites (cyan dots), spaced within a 100 μm x 60 μm grid. Red circle indicates the location of recorded glutamatergic neuron in L2/3, approached by the patch pipette (electrode). Scale bar represents 250 μm. (C) Group-averaged, excitatory input maps of L2/3 excitatory cells for WT (n = 20 cells) and KO (n = 9 cells). Neurons were clamped at -70 mV for detection of excitatory inputs. White triangles represent location of individually-recorded neurons. The color scale represents excitatory input strength (blue = low, red = high). Scale bar is 200 μm. (D) Group-averaged, inhibitory input maps of L2/3 excitatory cells for WT and KO. Neurons were clamped at +5 mV for detection of inhibitory synaptic inputs. Black triangles represent individual recorded neurons. The color scale represents inhibitory input strength (black = low, white = high). (E) Average total synaptic excitatory and inhibitory input strength (log) measured for L2/3 excitatory cells depicting a robust decrease in the KO (EPSC 1.7 $\pm$ 0.2, n = 9 cells; IPSC 2.5 $\pm$ 0.1, n = 13 cells) compared to WT (EPSC 2.5 $\pm$ 0.2, n = 20 cells; IPSC 2.8 $\pm$ 0.2, n = 11 cells). Data represent mean ± SEM * and ** indicate significance of $p < 0.05$ and $p < 0.005$, respectively, for Mann–Whitney U tests and Student's t test. (F) Average ratios of total excitatory inputs (excitatory postsynaptic currents, EPSC) versus total inhibitory inputs (inhibitory postsynaptic currents, IPSC) from individual cells (WT n = 17 cells; KO, n = 8 cells). There is no significant difference in E/I ratio between WT and KO ($p = 0.43$).

2.7: Assessment of microcircuit connectivity of pyramidal neurons and parvalbumin-positive interneurons using paired recordings

The observed disruptions in synaptic neurotransmission and the reduction in local cortical synaptic currents suggest that there might be disruptions in local microcircuit connectivity within the mPFC of *Cntnap2* KO mice. To further dissect local disruptions in neuronal communication within the mPFC circuit, I used whole-cell quadruple patch-clamp recording. This method is ideal for the evaluation of local synaptic contacts and assessment of the rate of connections between nearby cells (Debanne et al., 2008). Using this method, I stimulated presynaptic neurons by eliciting action potentials by injecting current in a patched cell, while simultaneously recording from one to three nearby neurons, located no further than three cell bodies away, within L2/3 of mPFC. I took advantage of the PVCre x Ai9 x *Cntnap2* mouse line, which allowed for simultaneous recording of both PV and Pyr neurons by labeling PV cells with TdTomato, a red fluorescent marker. This enabled visualization of PV cells under the fluorescent microscope (exciting the fluorophore with green light, 555nm wavelength), such that they could be targeted with the patch pipette. Excitatory neurons were in turn patched based on their pyramidal morphology (Figure 2.7 A,B). Cell-type classification was further verified based on action potential firing properties, as PV cells have a unique, easily-discernible, high firing rate (see Figure 2.1).

I first performed a power analysis to calculate the number of pairs required per group in order to detect an estimated 20% decrease in connectivity. Previous literature estimates that 50% of neighboring PV-Pyr neurons are directly connected and form direct synapses onto each other (Wallace et al., 2012; Lee et al., 2014). Based on these

estimates, I calculated that I needed between 50-60 recorded pairs per group in order to test my hypothesis with reliable (80%) statistical power. Nonetheless, the actual collected data in controls reflected a 22-24% connectivity rate between PV-Pyr pairs in controls. Based on these results, I re-ran the power analysis and found that I would need an approximated 200 pairs per group in order to observe a statistically-significant 20% minimum decrease in PV-Pyr connection probability in the KO, compared to WT, with 80% statistical power. Therefore, as the data collected thus far did not suggest robust alterations in PV-Pyr neuron connection probability in the KO, we decided to withdraw from additional data collection. I conclude then that that the probability of connection between presynaptic Pyr and postsynaptic PV (, presynaptic PV and postsynaptic PV, and presynaptic PV and postsynaptic PV neurons, is not substantially different between WT and KO mice (Figure 2.7 C).

Interestingly, preliminary data from PV-PV paired recordings suggest that there might be a somewhat robust (17%) decrease in connectivity between PV-PV pairs, which warrants additional recordings as a future direction. Moreover, out of the Pyr-Pyr pairs recorded, none were connected in WT (0/14) or KO (0/12). In addition, I also measured the amplitude of the first elicited IPSC or EPSC and my preliminary findings suggests that indeed there might be a decrease in synaptic drive within connected PV-Pyr pairs (Figure 2.5 D), concurrent with our previous findings from the mEPSC and LSPS experiments. Nonetheless, the available dataset for assessment of these measures is currently underpowered and therefore these differences, although robust, are not statistically different. My estimates indicate that, given the current average and standard deviation in WT (x bar = 72.95 pA, σ = 61.92 pA, n = 6 connected pairs) and KO (x bar

= 23.0 pA, σ = 18.81 pA, n = 5 connected pairs) for the amplitude of the 1st IPSC and the 1st EPSC (WT x bar = 59.66 pA, σ = 12.9 pA, n = 3 connected pairs; KO x bar = 12.9 pA, σ = 8.18 pA, n = 3 connected pairs, alterations in the amplitude of the first postsynaptic response warrants further investigation as a future direction.

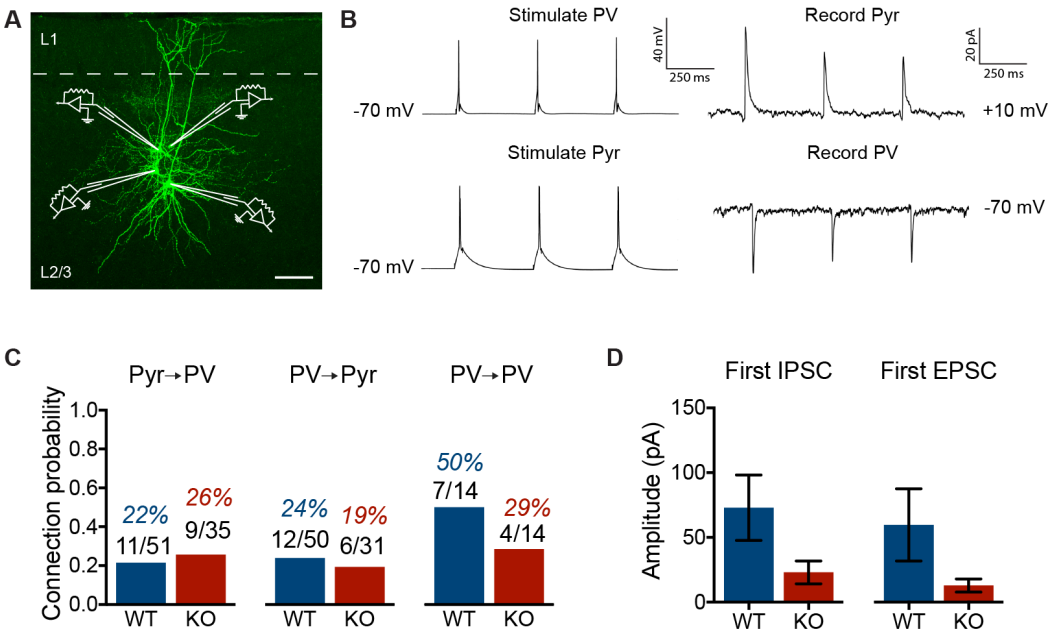

Figure 2.7. Assessment of mPFC microcircuit connectivity of pyramidal neurons and parvalbumin-positive interneurons. (A) Recording configuration represented by a confocal image of four simultaneously patched cells that were filled with Biocytin and visualized with Alexa 488-conjugated Streptavidin. Scale bar represents 100 µm. (B) Representative recordings of presynaptic action potentials evoked and postsynaptic current responses. Average of 10 trials. (C) Connection probability of Pyr neurons to PV neurons ($p = 0.435$, Chi-square test), PV neurons to Pyr neurons ($p = 0.954$, Chi-square test), and PV neurons to PV neurons ($p = 0.299$, Chi-square test). Percent connected and numbers connected/total pairs written above bar columns for each genotype. No Pyr neuron to Pyr neuron connections were observed for either WT or KO mouse (data not shown). (D) Average unitary amplitude for first elicited inhibitory (WT 73.0 $\pm$ 25.3 pA, n = 6 pairs; KO 23.0 $\pm$ 8.9 pA, n = 5 pairs; $p = 0.120$, Unpaired t test) and excitatory (WT 59.7 $\pm$ 27.9 pA, n = 3; KO 12.9 $\pm$ 5.0 pA, n = 3; $p = 0.174$, Unpaired t test) postsynaptic current (IPSC and EPSC, respectively).

2.8: Discussion

Multiple studies have shown that a number of mouse models of ASD display various degrees of disrupted excitatory and inhibitory neurotransmission (Gogolla et al., 2009; Lee et al., 2016) and that a shift in the balance of excitation/inhibition, especially in the medial prefrontal cortex (mPFC), underlie some of the pathologies associated with autism and other psychiatric disorders (Yizhar et al., 2011). Here, I observed a decrease in the frequency and amplitude of mEPSCs on pyramidal neurons of L2/3 mPFC in the KO are in line with previous studies, which found similar phenotypes both in cultured neurons and in vivo (Anderson et al., 2012; Gdalyahu et al., 2015). Indeed, Caspr2 localizes in spines and promotes trafficking of glutamatergic receptors along the dendritic shaft (Varea et al., 2015). Thus, these results strengthen the notion that Caspr2's the biological function expands beyond that of mediating neuron-glia interactions and clustering of potassium channels in the juxtaparanodes of axons (Poliak et al., 1999; Poliak et al., 2003) and has a role in the formation and stabilization of synapses in mPFC.

That we did not observe any statistically significant alterations in the firing properties of either pyramidal neurons or parvalbumin-positive inhibitory neurons, further suggests that Caspr2 likely does not play a role in direct modulation of intrinsic neuronal excitability. This is consistent with previous studies demonstrating that, although absence of Caspr2 does alter clustering of potassium channels along the axon, this does directly impact axon conductance properties (Poliak et al., 2003). This warrants additional research on the mechanistic processes that involve Caspr2 at the excitatory synapse and how it affects neuronal function both in early development and in the mature brain.

Moreover, the role of Caspr2 in inhibition remains unclear. Previous studies have indicated that *Cntnap2* KO mice have decreased number of inhibitory neurons (Peñagarikano et al., 2011) and a recent study found that inhibition is impaired in the hippocampus of *Cntnap2* KO mice (Jurgensen and Castillo, 2015). Here, we show that there is indeed a decrease in inhibitory synaptic inputs onto L2/3 pyramidal neurons in the KO, although this difference is clearly of smaller magnitude, relative to the observed reduction in excitatory inputs. This smaller reduction was not detected by the less-sensitive method of mIPSC quantification, yet was clearly apparent with the use of LSPS and glutamate uncaging. Interestingly, PV+ neurons seem to be spared of significant alterations in either excitatory or inhibitory synaptic currents; again, with the caveat that this is a less sensitive method. Nonetheless, these findings in PV+ neurons are supported by a recent study by Varea et al., (2015), which demonstrated that Caspr2 localizes less closely to inhibitory molecules than excitatory ones in cultured neurons. It is possible the role of Caspr2 in modulating inhibition is restricted to early developmental stages that mediate interneuron migration and differentiation (Peñagarikano et al., 2011). Thus, formation of inhibitory synapses may rely more on other neurexin superfamily proteins, such as *Cntnap4* (Karayannis et al., 2014). These data stress the notion that Caspr2 has cell-type specific roles and is not indispensable for the formation of inhibitory synapses. This therefore requires further study of cell-type specific biological roles of *Cntnap2*, both in early development and in mature neuronal microcircuits. Such studies could elucidate circuit-specific mechanisms that can parse out the cluster of behavioral pathologies in ASD (Geschwind 2008; Banerjee et al., 2012).

2.9: Materials and methods

2.9.a: Animals

Cntnap2 null mice were obtained from E. Peles and backcrossed to the C57BL/6J background for over 12 generations. For targeted electrophysiological recordings of parvalbumin-positive interneurons, *Cntnap2* heterozygous mice were backcrossed to PVCre (Jackson labs number 008069) x Ai9 (Jackson labs number 007909) mice. For spine density analysis, Cntnap2 heterozygous mice were backcrossed with Thy1GFP (Jackson labs x 007788) mice. Experimental mice were obtained from heterozygous crossings and born with the expected Mendelian frequencies; both genders were used. The date of birth was designated at P0 and the three obtained genotypes (wild-type, heterozygous, homozygous knock-out) were house together with three to four mice per same-sex cage. Mice were kept in a 12-hour light/12-hour dark cycle and had ad libitum access to food and water. All procedures involving animals were performed in accordance with the University of California, Los Angeles (UCLA) and the Weizmann Institute of Science animal research committee, and the National Institutes of Health Guide for the Use and Care of Laboratory Animals.

2.9.b: Slice preparation

Acute coronal slices (300um thickness) containing the medial prefrontal cortex were prepared from 4 to 6-wk-old *Cntnap2* knock-out mice and wild-type littermates. Mice were anaesthetized with Isofluorane gas and beheaded after disappearance of toe-pinch reflex. The brain was removed and placed in ice-cold cutting solution consisting of (mM): 222 sucrose, 11 D-glucose, 26 $NaHCO_3$, 1 NaH_2PO_4, 3 KCl, 7 $MgCl_2$, 0.5 $CaCl_2$,

aerated with 95% O_2, 5% CO_2. The brain was cut in a Leica VT1000S Vibratome. Slices were allowed to recover for 30 minutes at 37 °C in standard artificial cerebrospinal fluid (ACSF, in mM): 124 NaCl, 2.5 KCl, 26 $NaHCO_3$, 1.25 NaH_2PO_4, 10 D-glucose, 4 sucrose, 2.5 $CaCl_2$, 2 $MgCl_2$, aerated with 95% O_2, 5% CO_2, and kept at room temperature for at least 40 min until time of recording.

2.9.c: Electrophysiology

Whole-cell patch-clamp recordings of L2/3 neurons were obtained under visual guidance using infrared DIC videomicroscopy and water-immersion 40x objective, with patch pipettes (3-5 MOhms) pulled from borosilicate capillary glass (Sutter) with a Sutter puller. All electrophysiological recordings were performed using Multiclamp 700B (Molecular Devices) patch clamp amplifiers and ACSF was maintained at 33–35 °C. Signals were filtered at 4 kHz using Bessel filter and digitized at 10 kHz with WinWCP and WinEDR electrophysiology software interface (Strathclyde). Series/access resistance was monitored and recordings were discarded if it changed significantly (>20%) or exceeded 25 MOhms.

2.9.d: Current-clamp recordings

For intrinsic excitability experiments, the internal pipette solution contained (in mM): 115 KGluc, 20 KCl, 10 HEPES, 10 phosphocreatine, 4 ATP–Mg^{2+}, 0.3 GTP–Na^+ (pH 7.2, 270-290 mOsm); in some recordings, 0.2% biocytin was added to the solution. Patched pyramidal excitatory neurons were identified and included in the analysis based on their action potential firing characteristics. Parvalbumin-positive interneurons were

identified based on their expression of fluorescent marker TdTomato (from *Cntnap2* x PVCreAi9 mice) and action potential firing properties. Resting membrane potential (V_m) was measured after breaking in to the cell (rupturing the patch) and applying zero current, without taking the junction potential into account. Input resistance (R_{in}) was calculated as the slope of the linear fit of the voltage-current plot, generated from a family of negative and positive 500 ms current injections (-60 pA to +60 pA at 20 pA intervals, for pyramidal cells; -150 pA to +150 pA at 50 pA intervals, for parvalbumin-positive interneurons). The membrane decay constant (τ) was calculated by fitting a single exponential curve to the current-voltage plot that resulted from a -20 pA current injection. Cell membrane capacitance (C_m) was given by $C_m = \tau / R_{in}$. For assessment of intrinsic excitability, cells were clamped at -70 mV and injected a series of increasing current steps at 50 pA intervals. Action potential properties were determined from the first action potential elicited by minimum current injection. The spike adaptation ratio was calculated by dividing the last inter-spike interval to the first inter-spike interval in an action potential train elicited by a 500 ms pulse of 200 pA. All data was analyzed using MATLAB software.

2.9.e: Voltage-clamp recordings

Miniature excitatory postsynaptic currents (mEPSCs) were isolated by applying (in mM): 0.5 tetrodotoxin (TTX) and 10 pictrotoxin to ACSF (described above). Pipette internal solution contained (in mM): 20 KCl, 10 Na-phosphocreatinine, 100 cesium methyl sulfonate, 3 QX-314, 10 HEPES, 4 ATP–Mg^{2+} and 0.3 GTP–Na^{+} (pH 7.2, 270-290 mOsm). Recordings were performed with cells clamped at -70 mV. Miniature

inhibitory postsynaptic currents (mIPSCs) were isolated by applying (in mM): 0.5 tetrodotoxin (TTX), 10 CNQX, and 50 APV to ACSF. A high-chloride pipette internal solution was used, which contained (in mM): 120 KCl, 10 HEPES, 4 ATP-Mg^{2+}, 0.3 GTP–Na^{+} and 10 Na-phosphocreatinine (pH 7.2, 270-290 mOsm). Recordings were performed with cells clamped at -50 mV. Miniature and spontaneous events were recorded for 2 min. Recordings of spontaneous excitatory and inhibitory postsynaptic currents (sEPSCs and sIPSCs, respectively) were performed using standard ACSF conditions and the aforementioned cesium-based pipette internal solution. sEPSCs were recorded by clamping the cell at -70 mV and sIPSCs were recorded by clamping the same cell at +10 mV. MiniAnalysis software (Synaptosoft) was used to automatically identify synaptic events, based on template parameters. Events were then manually examined to exclude false positives. Cell identity was manually verified based on EPSC decay, where cells with decay $\leq$2 ms were considered inhibitory and cells with decay >2ms were considered excitatory (assessed from averages of three individual events per cell. For all cells, events with a decay >1.25 ms were excluded from the analysis, given that we wanted to focus on local (perisomatic inputs) rather than distal inputs, which are of longer decay time, due to the low-pass filtering that occurs as currents travel through dendrites. Events were individually inspected and included in the analysis based on their rise times (the time between 10 and 90% of the maximum amplitude); excluded if it was >1.5ms, since this this temporal dynamic is characteristic of inhibitory interneurons (data not shown). Interevent intervals (event frequency), amplitude, decay, area, rise 10-90, and half-width, were analyzed and comparison between groups was analyzed by Student's T-test. Grouped data are expressed as mean $\pm$ SEM, unless otherwise specified.

2.9.e: External stimulating electrode

A tungsten bipolar stimulating electrode was placed in L5 region of acute sections, to stimulate axon fibers emerging from the anterior forceps of the corpus callosum, which project onto a simultaneously-patched L2/3 pyramidal neuron in PL-mPFC, voltage-clamped at -70 mV. Input-output curves were derived by injecting current steps of increasing stimulus duration (0.01 ms increments) and recording current responses in the patched postsynaptic neurons. Short-term plasticity was assessed by measuring paired-pulse ratios, calculated as the peak amplitudes of 10 averaged episodes at various inter-stimulus intervals. AMPA/NMDA ratios were measured by voltage-clamping the cells at a holding potential of -70 mV for AMPA currents and +40 mV for NMDA currents. Peak amplitude current responses were averaged over 10 episodes. Peak NMDA currents were measured after the offset of AMPA currents within the same cell. Data was analyzed manually using WinEDR software and plotted in MATLAB.

2.9.g: Laser-scanning photostimulation

Coronal sections of medial prefrontal cortex were cut 400 µm thick with a vibratome (VT1200S, Leica Systems) in sucrose-containing artificial cerebrospinal fluid (ACSF) (in mM: 85 NaCl, 75 sucrose, 2.5 KCl, 25 glucose, 1.25 NaH_2PO_4, 4 $MgCl_2$, 0.5 $CaCl_2$, and 24 $NaHCO_3$). Slices were first incubated in sucrose-containing ACSF for 30 min to 1 h at 32°C, and then transferred to recording ACSF (in mM: 126 NaCl, 2.5 KCl, 26 $NaHCO_3$, 2 $CaCl_2$, 2 $MgCl_2$, 1.25 NaH_2PO_4, and 10 glucose) at room temperature. Throughout incubation and recording, the slices were continuously bubbled with 95% O_2-5% CO_2.

The design of our laser scanning photostimulation system has been described previously (Xu et al., 2009). A laser unit (model 3501, DPSS Lasers, Santa Clara, CA) was used to generate a 355 nm UV laser for glutamate uncaging. Various laser stimulation positions were achieved through galvanometer-driven X-Y scanning mirrors (Cambridge Technology, Cambridge, MA), as the mirrors and the back aperture of the objective were in conjugate planes, thereby translating mirror positions into different scanning locations at the objective lens focal plane. Data were acquired with a Multiclamp 700B amplifier (Molecular Devices, Sunnyvale, CA), data acquisition boards (models PCI MIO 16E-4 and 6713, National Instruments, Austin, TX), and custom-modified version of Ephus software (Ephus, available at https://www.ephus.org/). Data were low-pass filtered at 2 kHz using a Bessel filter, digitized at 10 kHz, and stored on a computer.

Cortical slices were visualized with an upright microscope (BW51X, Olympus) with infrared differential interference contrast optics. Electrophysiological recordings, photostimulation, and imaging of the slice preparations were done in a slice perfusion chamber mounted on a motorized stage of the microscope at room temperature. An aliquot of MNI-caged-L-glutamate (4-methoxy-7-nitroindolinyl-caged L-glutamate, Tocris Bioscience, Ellisville, MO) was added to 20–25 ml of circulating ACSF for a concentration of 0.2 mM caged glutamate. To perform whole cell recording, cells were visualized at high magnification (60× objective, 0.9 NA; LUMPlanFl/IR, Olympus). Excitatory neurons were selected based upon their pyramidal somata detected under differential interference contrast (DIC) microscopy. For experiments to assess photo-stimulation evoked spiking profiles of excitatory in mPFC, similar previously

published studies (Olivas et al., 2012; Xu et al., 2016), the patch pipettes (4–6 MΩ resistance) were filled with an K+ internal solution containing (in mM) 126 K-gluconate, 4 KCl, 10 HEPES, 4 ATP-Mg, 0.3 GTP-Na, and 10 phosphocreatine (pH 7.2, 300 mOsm). For the photostimulation experiments to map synaptic inputs, we used a Cs+ internal solution containing (in mM) 6 CsCl, 130 CsOH, 130 D-Gluconic acid, 2 MgCl2, 0.2 EGTA, 10 HEPES, 2.5 ATP-Na, 0.5 GTP-Na, and 10 phosphocreatine-Na2 (pH 7.2, 300 mOsm). Because glutamate uncaging agnostically activates both excitatory and inhibitory neurons, we empirically determined the excitatory and inhibitory reversal potentials in L2/3 pyramidal cells to properly isolate EPSCs and IPSCs. Whole-cell voltage-clamp recordings were made from the recorded postsynaptic neurons with LSPS-evoked EPSCs and IPSCs measured at the holding potential of −70 mV and 5 mV, respectively, across photostimulation sites. The internal solution also contained 0.1% biocytin for cell labeling and morphological identification. The morphology of recorded pyramidal neuron was determined using post-hoc staining with Cy3-conjugated streptavidin (1:500 dilution; Jackson ImmunoResearch). Once stable whole cell recordings were achieved with good access resistance (usually <30 MΩ), the microscope objective was switched from 60× to 4×; laser scanning photostimulation (LSPS) was performed through the 4x objective lens. At low magnification (4× objective lens, 0.16 NA; UplanApo, Olympus), the slice images were acquired by a high-resolution digital CCD camera (Retiga 2000, Q-imaging, Austin, TX) and used for guiding and registering photostimulation sites in cortical slices.

Photostimulation (1.5 ms duration, 15 mW pulses) from a 350nm UV laser generator (DPSS Lasers, Santa Clara, CA) was delivered to the sample, controlled via an

electro-optical modulator and a mechanical shutter. Focal laser spots approximated a Gaussian profile with a diameter of ~50-100 μm. Under our experimental conditions, LSPS evoked action potentials were recorded from stimulation locations within 100 μm of targeted somata of excitatory neurons and occurred within 150 ms post photostimulation. Our calibration analysis indicates that LSPS allows for mapping direct synaptic inputs to recorded neurons. Synaptic currents in patched neurons were detected under voltage clamp. By systematically surveying synaptic inputs from hundreds of different sites across a large cortical region, aggregate synaptic input maps were generated for individual neurons. For our mapping experiments, a standard stimulus grid (16×16 stimulation sites, 100 x 60 μm^2 spacing) was used to tessellate mPFC from pia to white matter. The LSPS site spacing was empirically determined to capture the smallest predicted distance in which photostimulation differentially activates adjacent neurons. Glutamate uncaging was delivered sequentially in a nonraster, nonrandom sequence, following a "shifting-X" pattern designed to avoid revisiting the vicinity of recently stimulated sites.

Photostimulation induces two forms of excitatory responses: (1) those that result from direct activation of the recorded neuron's glutamate receptors, and (2) synaptically mediated responses (EPSCs) resulting from the suprathreshold activation of presynaptic excitatory neurons. Responses that occur within 10 ms of laser pulse onset were considered direct; these responses exhibited a distinct waveform and occurred immediately after glutamate uncaging. Synaptic currents with such short latencies are not possible because they would have to occur before the generation of action potentials in photostimulated neurons. Therefore, direct responses were excluded from local

synaptic input analysis, but they were used to assess glutamate mediated excitability/responsiveness of recorded neurons. At some locations, synaptic responses were over-riding on the relatively small direct responses, and these responses were identified and included in synaptic input analysis. The IPSC input was similarly analyzed as the EPSC input. For data map analysis, we implemented the approach for detection and extraction of photostimulation-evoked postsynaptic current responses described in reference [6]. LSPS evoked EPSCs/IPSCs were quantified across the 16x16 mapping grid for each cell, and 1-2 individual maps were used per recorded cell. The PSC input from each stimulation site was the measurement of the sum of individual PSCs within the analysis window (>10 ms to 160 ms post photostimulation), with the baseline spontaneous response subtracted from the photostimulation response of the same site. The value was normalized with the duration of the analysis window (i.e., 150 ms) and expressed as average integrated amplitudes in picoamperes (pA). The analysis window was chosen because photostimulated neurons fire most of their action potentials during this time. For the color-coded map display, data were plotted as the average integrated PSCs amplitude per pixel location (stimulation site), with the color scale coding input strength. For the group maps obtained across multiple cells, the individual cell maps were first aligned by their slice images using laminar cytoarchitectonic landmarks. Then a new map grid was created to re-sample and average input strength at each site location across cell maps; a smooth version of color-coded map was presented for overall assessments. To further quantitatively compare input strength across cell groups, we measured the total PSC inputs (total synaptic currents) across all map sites (total synaptic input strength) for

individual cells. The total EPSC/IPSC input strength ratios were also measured for the cells when both EPSC and IPSC data were available from the same cells.

As virtually all layer 1 neurons are inhibitory cells, and pyramidal neurons with apical dendritic tufts in layer 1 could fire action potentials when their tufts were stimulated in layer 1(Dantzker et al., 2000), EPSCs detected after photostimulation in layer 1 were not included for analyses. However, because layer 1 neurons can provide inhibition to layer 2/3 neurons, we did analyze IPSCs detected after photostimulation in layer 1.

All data are reported as mean ± standard error of the mean (SEM). When comparing two independent groups, a Mann-Whitney U test was used. Unless specified otherwise, sample size n was defined as cell number. A p value (≤ 0.05) was considered statistically significant.

2.9.h: Paired recordings

Paired recordings were performed by simultaneously patching a combination of two to four pyramidal neurons or PV^+ inhibitory neurons. Patch pipettes contained the same internal solution used in the intrinsic excitability experiments and standard ACSF was used (as described above). The presynaptic neuron was held in current-clamp mode at -70 mV and postsynaptic neurons were held in voltage-clamp mode at -70 mV and +10 mV, for detection of excitatory and inhibitory postsynaptic responses, respectively. Identification of inhibitory and excitatory cell types was determined by action potential firing characteristics or, in the case of PV+ neurons, expression of TdTomato fluorescence. Pairs were categorized as uni-directionally connected if there was a

consistent postsynaptic current response (averaged over 20 trials) to presynaptic neuron stimulation (three to four 5-10 ms pulses given at 30 Hz, each eliciting single action potentials). Chi-square tests were used to calculate statistical significance of connection probabilities. For quantification of 1st EPSC and 1st IPSC amplitudes, elicited responses of the first postsynaptic currents were averaged over 20 trials.

Chapter 3:

Dendritic morphology, spine density, and synaptic markers in *Cntnap2* KO mice

3.1: Abstract

Alterations in brain anatomy, dendritic morphology, and spine density are common abnormalities in human autism brain, as well as in rodent models. *Cntnap2* KO mouse recapitulate some of these neuroanatomical changes. The electrophysiology findings that I describe in Chapter 2 reveal that the total number of synaptic inputs, especially excitatory ones, is decreased in *Cntnap2* KO mice. Here, in Chapter 3, I use immunohistochemical assays to investigate whether *Cntnap2* KO mice display alterations in dendritic complexity or dendritic spine density. I find that, although there are no significant alterations in dendritic morphology of pyramidal neurons in L2/3 of mPFC, these neurons show a stark reduction in the density of both apical and basal dendritic spines. These findings are concurrent with the observed reduction in excitatory inputs and are a tangible substrate that evidences loss of functional synapses in the KO. Furthermore, in search of a potential mechanism by which these phenotypes could arise, I take advantage of unpublished MudPIT data that was kindly shared with us by the laboratory of Elior Peles (The Weizmann Institute of Science, Rehovolt, Israel), which identified a list of putative Caspr2 interactor proteins. One of these, KCC2, was of notable interest given its implications in synaptic development and maturation and regulation by oxytocin, which we have previously shown is impaired in *Cntnap2* KO mice. Using immunohistochemical methods, I also test the hypothesis that KCC2 localization in excitatory neurons is dysregulated in mPFC excitatory neurons of the *Cntnap2* KO. I find that, in fact, KCC2 membrane localization is decreased in *Cntnap2* KO mice, thus providing a potential mechanism by which loss of *Cntnap2* could lead to

developmental pathologies and alterations in neuronal function and thus, consequent behavioral impairments related to ASD.

3.2: Background

Alterations in synaptic neurotransmission, both excitatory and inhibitory, have been common theme in the study of ASDs (Nelson and Valakh, 2015). Furthermore, histological studies in human autism postmortem tissue have revealed that indeed ASD phenotypes reflect fundamental alterations, not only in cortical lamination patterns, but also in neuronal morphology and dendritic spine density (Hustler and Zhang, 2010; Casanova et al., 2014; Stoner et al., 2014; Tang et al., 2014). These findings have been corroborated in various mouse models of autism, representing multiple causes of ASD (Lazaro and Golshani, 2015; de la Torre-Ubieta et al., 2016). Nonetheless, there is currently no predominating phenotype in ASD and some discrepancies have been observed when comparing mouse models, brain regions, or rodents and humans. It is therefore crucial that we obtain a detailed understanding of how each genetic etiology is mechanistically contributing to ASD phenotypes, from physiology, to anatomy, to behavior; gathering sufficient evidence on multiple biological levels in comprehensive studies that dissect biological systems at multiple levels (systems biology approach) can perhaps help us further classify autism based on these specific traits and develop targeted therapeutics. Accordingly, understanding electrophysiological phenotypes and linking them to cellular anatomical and molecular changes can bring us a step closer into finding precise and successful treatments.

The electrophysiology findings that I describe in Chapter 2 reveal that the number of synaptic inputs, especially excitatory ones, is decreased in *Cntnap2* KO mice. Moreover, I show that this decrease is likely not due to alterations in the probability of synaptic vesicle release or significant changes in AMPA/NMDA ratios. Thus, I

hypothesize that this observation is associated with decreased in dendritic complexity or spine density in pyramidal neurons. In fact, recent studies have indicated that Caspr2 likely plays a role in synapse formation and/or stabilization both in vivo (Figure 3.1; Gdalyahu et al., 2015) and in vitro (Anderson et al., 2012; Varea et al., 2015). In vitro knock-down of Cntnap2 in primary neuronal cultures leads to decreased dendritic complexity and alterations in spine morphology (Anderson et al., 2012). Thus, in this chapter I investigate the cellular anatomical and molecular consequences of loss of *Cntnap2* in the mPFC of KO mice.

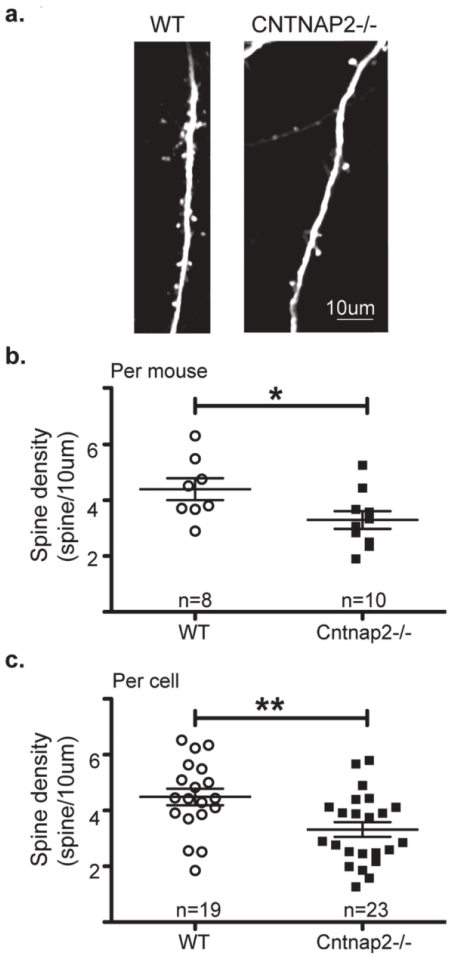

Figure 3.1: Loss of *Cntnap2* decreases spine density *in vivo*. (A) Representative low magnification images of dendrites and spines in a WT (left) and a *Cntnap2* KO mouse (right). (B) Spine density quantification per mouse (WT n = 8 mice, KO n = 10 WT mice). (C) Spine density analysis per cell (Cntnap2 WT n = 18 neurons, KO n = 23 neurons). Error bars indicate standard error (SEM). Statistical significance is indicated by * for $p < 0.05$ and ** for $p < 0.01$, Unpaired t test. (Gdalyahu et al., 2015)

Evidently, neurexins play a crucial role in the formation and stabilization of synapses; they contribute to localization of synaptic scaffolding proteins to the synapse and provide structural stability by binding to extracellular adhesion proteins (Südhof, 2008). Thus, identifying potential protein interactors can provide clues as to which molecular pathways and cellular processes are involved in producing some of the abnormal synaptic phenotypes. A preliminary screening of protein interactions using Multidimmensional Protein Identification Technology (MudPIT) assays form rat brain tissue homogenates provided a preliminary list of putative Caspr2 protein interactors. One of the genes in this list, SLC12A5, was of particular interest (Table 3.1).

Table 3.1: List of putative Caspr2 interactor proteins from MudPIT experiments.*

ACADVL	CLTC	HSPD1	PLP1	SLC2A13
ACAT1	CNP	IDH3B	RAB10	SLC3A2
ACTB	DCD	IDH3G	RAB35	SLC6A1
AGPAT3	DHCR7	IMMT	RAB3B	SLC6A11
AKAP5	DLG1	ITPR1	RAB3C	STXBP1
ARF5	DNM1	LANCL1	RER1	SV2A
ASS1	DNM1L	MPP2	RPN1	TECR
ATP1A1	DNM3	MPP5	RTCD1	TMEM33
ATP1A2	EEF1A1	MPP6	RTN1	TMEM38A
ATP1A3	EEF1A2	MTHFD1	SFXN3	TOMM70A
ATP2A2	EHD3	NDUFS1	**SLC12A5**	TRAP1
ATP2B2	EPB41L3	NORBIN	SLC13A3	TUBA1C
ATP2B3	GAPDH	NSF	SLC16A1	TUBB2A
ATP2B4	GNA13	OPA1	SLC1A3	TUBB2C
ATP5A1	GNAO1	PCBP1	SLC1A4	TUFM
ATP5B	GPRIN1	PCX	SLC25A12	UQCRC2
ATP6V1H	HSP90AB1	PDE2A	SLC25A22	ZG16B
CAND1	HSPA12A	PFKM	SLC25A25	
CDIPT	HSPA5	PFKP	SLC25A3	
CDS2	HSPA9	PIGS	SLC25A6	

*In collaboration with the laboratory of Elior Peles

The *SLC12A5* gene, which is highlighted in Table 3.1, encodes for KCC2, a potassium-chloride co-transporter (Blaesse and Schmidt, 2015). This protein is of particular interest, as it has been shown to play a crucial role in the developmental regulation of both excitatory and inhibitory neurotransmission (Tyzio et al., 2006). Importantly, KCC2 has been shown to be dysregulated in several models of ASD, including the Fragile X model and the valproic acid (VPA) model (Tyzio et al., 2014). Moreover, Tyzio et al., 2014 showed that maternal oxytocin regulates KCC2 expression at birth, which in turn regulates the shift of GABA from excitatory to inhibitory after birth. Moreover, KCC2 expression becomes dysregulated in epilepsy, whereby the amount of membrane-bound (active) protein decreases, relative to the intracellular amount (Kahle et al., 2015). Interestingly, recent studies found that KCC2 also regulates glutamatergic synapses and that disruptions in KCC2 expression and function hinders the formation of mature spines (Li et al., 2007; Gauvain et al., 2011; Blaesse and Schmidt, 2015).

Thus, considering the notion that *Cntnap2* KO mice develop seizures and have disruptions in the oxytocin system (Peñagarikano et al., 2011; Peñagarikano et al., 2015), point towards the possibility that dysregulated KCC2, a putative Caspr2 interactor, could implicated in some of the observed synaptic pathologies. Therefore, I here test whether membrane localization of KCC2 is decreased in Cntnap2 KO mice using immunohistochemistry. This preliminary evidence could point towards a molecular target that can be used as a potential therapeutic avenue.

3.3: Spine density and dendritic morphology in *Cntnap2* KO mice

assess dendritic morphology in *Cntanp2* KO mice, cells were filled with biocytin during in vitro slice recording experiments, imaged, and 3D reconstructed (Methods). Surprisingly, sholl analysis did not reveal any significant changes in total dendritic length or total number of dendritic branches (Figure 4A-B). We then tested whether *Cntnap2* KO neurons display a decrease in dendritic spine density. To do this, we crossed *Cntnap2* heterozygous mice with Thy1-GFP mice, which express GFP in a subset of pyramidal neurons, including L2/3 of mPFC (Figure 3.2 B). Quantification of dendritic spines of *Thy1*-GFP-positive pyramidal neurons in L2/3 of mPFC revealed a significant decrease in the density of spines in both basal (26%; Welch's t test, $p<0.001$) and apical (33%; Student's t test, $p<0.05$) dendritic branches (Figure 3.2 C,D).

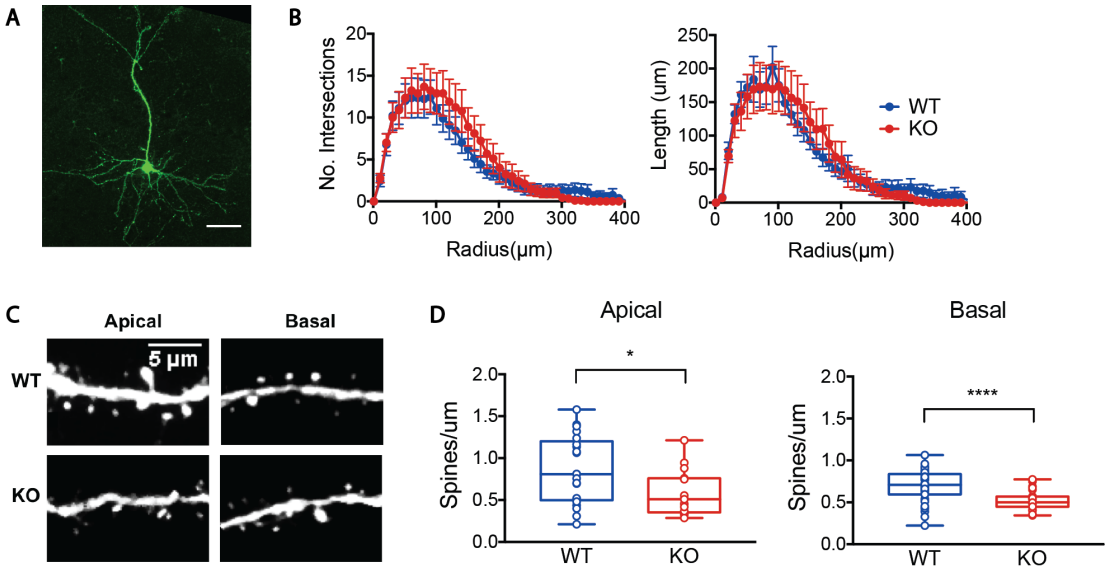

Figure 3.2: Decreased dendritic spine density in *Cntnap2* KO mice. (A) Representative z-stack projection of biocytin-filled L2/3 neuron, visualized with a Streptavidin-Alexa 488

antibody. Scale bar indicates 100 um length. (B) Sholl analysis showing number of intersections (left; p = 0.0632, Two-way ANOVA) and length (right; p = 0.932, Two-way ANOVA) of dendrites is comparable between *Cntnap2* WT (n = 8 cells) and KO (n = 9 cells). (C) Confocal image of L2/3 Thy1-GFP-positive pyramidal neuron in mPFC, demonstrating representative apical and basal dendrites. (D) Summary graphs showing quantification of average spine density in apical (WT 0.9 $\pm$ 0.1 spines/um, n = 21 dendrites; KO 0.6 $\pm$ 0.1 spines/um, n = 15 dendrites) and basal (WT 0.7 $\pm$ 0.0 spines/um, n = 34 dendrites; KO 0.5 $\pm$ n = 24 dendrites) branches. Statistical significance is represented by * for Unpaired t test $p<0.05$ and **** for Unpaired t test with Welch's corrections $p<0.0001$.

3.4: KCC2 dysregulation as a putative mechanism for synaptic deficits

Understanding the proteome of Caspr2 could provide useful insights into the pathological mechanisms that implicate it in ASD. The potassium-chloride cotransporter KCC2 was found to be a putative Caspr2 interactor protein from MudPIT assays (unpuslihed data, Table 3.1). KCC2 dysregulation and cellular mislocalization has been implicated in epilepsy, synaptic disruptions, and autism (Blaesse and Schmidt, 2015). Using immunohistochemistry and confocal imaging, I labeled and quantified KCC2 protein in Cntnap2 KO and WT mice to test whether in fact this protein was dysregulated in our autism model. My results show that KCC2 is downregulated in *Cntnap2* KO mouse mPFC tissue, relative to WT controls (Figure 3.3, Table 3.2). These findings suggest that disrupted Caspr2-KCC2 interactions might underlie some of the synaptic phenotypes observed in *Cntnap2* KO mice.

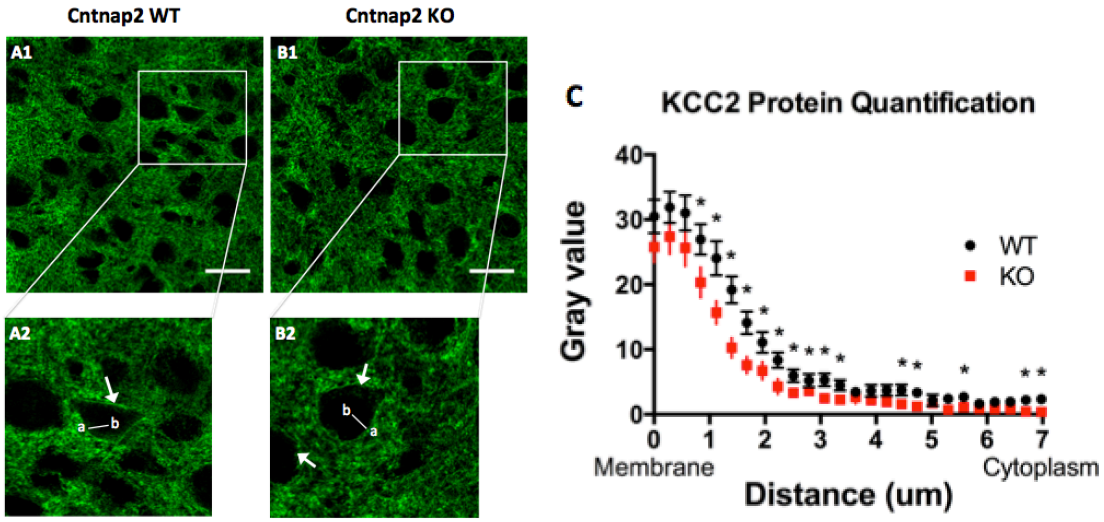

Figure 3.3: KCC2 protein is decreased in *Cntnap2* KO mice. (A, B) Localization of KCC2 immunoreactivity in the mPFC region of control and *Cntnap2* KO mice. (A1, B1) High magnification (63x) confocal images show KCC2 is strongly expressed in both genotypes. Zoomed images depicting cells in control (A2) and KO (B2) neurons. Labeling is concentrated near the cell membrane (arrows) and the cytoplasm is almost devoid of labeling in both genotypes. The line drawn between points "a" (membrane) and "b" (cytoplasm) represent area probed for fluorescence intensity values. Note that both membrane and cytoplasmic labeling are slightly lower in the KO. (C) Graph representing the distribution and quantification of the intensity of fluorescence in mPFC cells (n = 2 mice per genotype, n = 20 cells per animal). Table 3.2 shows intensity and p-values (Student's unpaired T-test) depicted per distance between "a" and "b" in graph. Data presented as mean ± S.E.M. Significance of $p<0.05$ indicated by *.

Table 3.2: Summary of KCC2 quantification in *Cntnap2* KO mice and controls

Distance (um)	WT Mean ± SEM	KO Mean ± SEM	Statistics
0	30.47 ± 2.58	25.79 ± 2.42	n.s.
0.28	31.88 ±2.39	27.37 ± 2.70	n.s.
0.56	31.02 ± 2.70	25.66 ± 2.86	n.s.
0.84	**26.95 ± ±2.33**	**20.31 ± 2.33**	**P<0.05**
1.12	**24.05 ± 2.62**	**15.70 ± 1.77**	**P<0.05**
1.4	**19.20 ± 2.09**	**10.25 ± 1.54**	**P<0.05**
1.67	**14.13 ± 1.77**	**7.58 ± 1.28**	**P<0.05**
1.95	**11.07 ± 1.63**	**6.71 ± 1.38**	**P<0.05**
2.37	**7.88 ± 0.98**	**3.74 ± 1.01**	**P<0.05**
2.51	**5.95 ± 0.96**	**3.32 ± 0.69**	**P<0.05**
2.79	**5.23 ± 1.02**	**3.61 ± 0.72**	**P<0.05**
3.07	**5.33 ± 0.98**	**2.47 ± 0.62**	**P<0.05**
3.35	**4.47 ± 0.80**	**2.27 ± 0.63**	**P<0.05**
3.63	3.44 ± 0.79	2.64 ± 0.96	n.s.
3.91	2.17 ± 0.79	3.65 ± 0.90	n.s.
4.19	1.91 ± 0.61	3.73 ± 0.85	n.s.
4.46	**1.57 ± 0.62**	**3.76 ± 0.85**	**P<0.05**
4.74	**1.23 ± 0.43**	**3.36 ± 0.78**	**P<0.05**
5.02	1.76 ± 0.49	2.18 ± 0.87	n.s.
5.3	**0.73 ± 0.45**	**2.43 ± 0.62**	**P<0.05**
5.58	1.10 ± 0.47	2.69 ± 0.70	n.s.
5.86	0.89 ± 0.37	1.66 ± 0.45	n.s.
6.14	0.82 ± 0.39	1.93 ± 0.45	n.s.
6.42	0.78 ± 0.35	1.94 ± 0.64	n.s.
6.7	**0.44 ± 0.14**	**2.20 ± 0.50**	**P<0.05**
6.98	**0.39 ± 0.18**	**2.35 ± 0.60**	**P<0.05**

3.5: Discussion

The anatomical results described in this chapter point towards a preferential depletion of excitatory synapses. These findings are consistent with the observed decrease in Pyr mEPSCs and are in line with our recent work, in which we found decreased density and stability of dendritic spines in L5 Pyr neurons of somatosensory cortex in the KO (Gdalyahu et al., 2015). This is in agreement with the notion that Caspr2 plays an important role in the formation and/or stabilization of synapses, much like other neurexins (Südhof et al., 2008). Such phenotypes have been observed in other models of ASD and associated syndromes and are therefore not unique to Cntnap2 (Bear et al., 2004; Dani et al., 2005; Arons et al., 2012; Tang et al., 2014). Several other models based on ASD risk genes show phenotypes preferentially involving inhibition rather than excitatory neurotransmission (Wallace et al., 2012; Rothwell et al., 2014; Gogolla et al., 2014; Karayannis et al., 2014; Jurgensen and Castillo, 2015). This suggests that perhaps we can delineate sub-clusters within ASD models (Luongo et al., 2016) that will inform our understanding the contributions of genetic factors to the development of ASD. Finding convergence will facilitate the creation of useful therapeutic interventions and approaches, perhaps even preventative mechanisms (Geschwind 2008; Berg and Geschwind, 2012; Mehta and Golshani, 2013).

Loss of *Cntnap2* thus results in decreased excitatory inputs that are concurrent with decreased dendritic spine density in pyramidal neurons. This strengthens the growing notion that Caspr2 has a role at the synapse and is important for synapse formation, maturation or stabilization. Furthermore, KCC2, a potassium-chloride cotransporter and putative Caspr2 interactor, is mislocalized or decreased in *Cntnap2* KO mice. This provides

a promising molecular target for therapeutic interventions for ASDs. Additional work should be done in order to validate these findings and determine whether drugs that target this pathway in fact rescue some of the behavioral and physiological pathologies in the *Cntnap2* KO.

3.6: Methods

3.6.a: Assessment of dendritic morphology

For assessment of dendritic morphology and complexity, cells were during electrophysiological recordings via passive diffusion of internal pipette solution - containing 0.2% biocytin. After recording for at least 10 min, slices were transferred to a 4% PFA solution for overnight fixation, washed for 10 min (x3) in 0.1 M phosphate buffered saline (PBS), blocked with 10% normal goat serum (NGS) containing 0.3% Triton-X in 0.1 M PBS for 1.5 hrs, and incubated overnight with an Alexa 555 or Alexa 488-conjugated Streptavidin antibody (1:500, Invitrogen) in 0.1M PBS. Sections were finally washed 3x 10 min in 0.1M PBS and mounted on slides using DAPI Fluoromount-G (Invitrogent) for visualization. We assessed dendritic complexity of biocytin-filled cells by imaging at 20x magnification in an LSM520 confocal microscope. Z-stacks of optical sections (1 um) were compiled and images were processed in Neurolucida 10 (MFB Biosciences) for Sholl analysis.

3.6.b: Assessment of dendritic spine density

For quantification of spine density, *Cntnap2* WT and KO mice were crossed with a *Thy1*-GFP mouse line, which sparsely labels pyramidal neurons, including their

dendritic projections and spines. Mice were perfused intracardially with 25 mL 0.1 M PBS, followed by 25 mL of 4% PFA in 0.1 M PBS (at 2 mL/min). The brains were dissected and fixed for at least 24 hrs in the same solution. Brains were then sectioned at a thickness of 100 um, using a Leica vibratome. Sections containing the mPFC were mounted in slides using DAPI Fluoromount-G media. Apical and basal dendrites of GFP-expressing L2/3 mPFC neurons were imaged at high resolution using a 63x oil magnification objective in an LSM-780 confocal microscope. Optical sections of 0.32 um were acquired and maximum intensity projections of dendritic arbors were created in ImageJ. Dendritic segments were chosen using consistent criteria and spines were manually counted. Dendritic density was calculated by dividing the total number of spines over a given length of dendrite (spines/um). Student's t test was used for statistical comparison between the two groups.

3.6.c: Quantification of KCC2 protein

Adult (>P30) *Cntnap2* WT and KO mice were perfused intracardially with 4% paraformaldehyde after deep anesthesia with Pentobarbitol. The brains were cryprotected in sucrose, embedded and frozen in OCT compound and serially cut with a Cryostat (thickness 50 μ m). Selected sections containing the medial prefrontal cortex (mPFC) from control and KO mice were processed, in parallel, for immunohistochemistry under identical conditions. First, sections were washed in Washing Buffer (1X Phosphate Buffered Saline (PBS), 0.1% Triton-X 100), followed by permeabilization in Permeabilization Buffer (1X PBS, 0.3% Triton-X 100). Sections were then incubated for 1 h 30 min at room temperature in Blocking Buffer (10% normal goat serum (NGS) in Washing Buffer). This was followed

by an overnight incubation at 4°C with the rabbit anti-KCC2 antibody (dilution 1:400 in Blocking Buffer; Millipore). The next day, sections were washed in Washing Buffer and incubated with a fluorescent-labeled secondary antibody (1:1000; Alexa Fluor 488 goat anti-rabbit, Invitrogen) for 1 h 30 min at room temperature, protected from light. The sections were washed again with Washing Buffer at room temperature and sections were mounted on slides using DAPI-Fluoromount G and stored at 4°C until further processing.

Adult (>P30) *Cntnap2* WT and KO mice were perfused intracardially with 4% paraformaldehyde after deep anesthesia with Pentobarbitol. The brains were cryprotected in sucrose, embedded and frozen in OCT compound and serially cut with a Cryostat (thickness 50 μ m). Selected sections containing the medial prefrontal cortex (mPFC) from control and KO mice were processed, in parallel, for immunohistochemistry under identical conditions. First, sections were washed in Washing Buffer (1X Phosphate Buffered Saline (PBS), 0.1% Triton-X 100), followed by permeabilization in Permeabilization Buffer (1X PBS, 0.3% Triton-X 100). Sections were then incubated for 1 h 30 min at room temperature in Blocking Buffer (10% normal goat serum (NGS) in Washing Buffer). This was followed by an overnight incubation at 4°C with the rabbit anti-KCC2 antibody (dilution 1:400 in Blocking Buffer; Millipore). The next day, sections were washed in Washing Buffer and incubated with a fluorescent-labeled secondary antibody (1:1000; Alexa Fluor 488 goat anti-rabbit, Invitrogen) for 1 h 30 min at room temperature, protected from light. The sections were washed again with Washing Buffer at room temperature and sections were mounted on slides using DAPI-Fluoromount G and stored at 4°C until further processing.

Images were acquired with a Zeiss LSM-780 laser-scanning confocal microscope. Four sections per mouse for each genotype (KO and WT) were selected for imaging using

an oil-immersed 63x objective (1.4 NA). Images were obtained using identical settings of objective lens, objective aperture, laser power and photomultiplier gain/offset, from areas of fixed size in L2/3 of the mPFC (boundaries of the different cortical layers determined by counterstaining with DAPI).

Quantification of KCC2 intensity was performed blind using ImageJ software (NIH). Regions of Interest (ROIs) were selected for membrane or cytosolic regions and fluorescence intensity was measured for each. Then, Plot Profile values were analyzed by normalizing the fluorescence intensity to the highest intensity of the control condition and calculating the mean for each condition represented on the two curves. Fluorescence intensity values (and distance along neuronal soma) for each cell of both groups (WT and KO) was uploaded into GraphPad Prism Statistical Analysis Software. Mean fluorescence intensities were calculated per group. Differences between WT and KO were then assessed for statistical significance using an unpaired Student's t-test.

Chapter 4:

Network activity changes in the mPFC of *Cntnap2* KO mice

and

Development of a novel method

for assessment of brain network activity and dynamics during social interactions

4.1: Abstract

Here, I use *in vivo* multichannel nanosilicon probes to record local field potentials (LFP) in mPFC. I find a notable reduction in 12-100 Hz local field potential (LFP) oscillations power *in vivo*, which likely reflects an overall decrease in excitatory and inhibitory drive and is concurrent with my findings *in vitro*. These results provide initial mechanistic insights into how loss of *Cntnap2* alters mPFC microcircuit connectivity and function. Furthermore, I develop a novel method that provides a way to detect changes in brain network activity and dynamics in head-fixed mice, during social interactions. This method will be invaluable for increasing our understanding of how brain activity is modulated in a social context or in response to a social stimulus, both in autism mouse models and controls. Furthermore, it is a readily accessible method to for testing the effect of potential therapeutics and their modulation of brain activity biomarkers.

4.2: Background

Functional studies have shown that children with autism have alterations in gamma synchrony (30-90 Hz), which normally contribute to states that involve increased attention and alertness (Wilson et al., 2007; Gandal et al., 2010). *Cntnap2* KO mice showed decreased synchronization at the slow timescales assayed by calcium imaging (~4 Hz) in somatosensory cortex, as well as a decrease in the total number of GABAergic interneurons (Peñagarikano et al., 2011). This phenotype, combined with alterations in neuronal migration, a reduction in the total number of inhibitory neurons, and a decrease in excitatory and inhibitory cortical inputs in vitro, is bound to produce alterations in the normal function of local neuronal networks. Understanding how changes in microcircuit connectivity affects brain network dynamics is crucial for revealing the functional consequences of autism. Importantly, this allows for the identification of ASD biomarkers that can easily be used to test the effect of drug treatments or therapeutic interventions (Peñagarikano, 2015; de la Torre-Ubieta et al., 2016).

Therefore, in this chapter I determine whether *Cntnap2* KO mice show a decrease in gamma power at baseline during wakefulness. In order to further expand on these findings, I develop a novel task that will allow for the assessment of brain synchronization changes in a social behavioral context. These experiments hold great promise, as gamma oscillation deficits could be used as a biomarker that can be directly tested for gauging therapeutic treatments that can be translated for human use.

4.3: *In vivo* mPFC network activity

The *in vitro* synaptic pathologies observed in *Cntnap2* KO mice are likely to have significant consequences *in vivo*. Here, I used multi-channel nanosilicon microprobes to record in vivo network activity in the mPFC of *Cntnap2* WT and KO mice (Figure 4.1). This approach allowed for recording of local field potentials (LFPs) in head-fixed, awake-behaving mice. Power spectrum analyses revealed a substantial reduction in LFP power across the entire frequency spectrum in *Cntnap2* KO mice. Such disruptions are indicative of evident perturbations in the ability of the mPFC neuronal network to entrain in synchronous activity and could underlie some of the behavioral impairments observed in our autism mouse model.

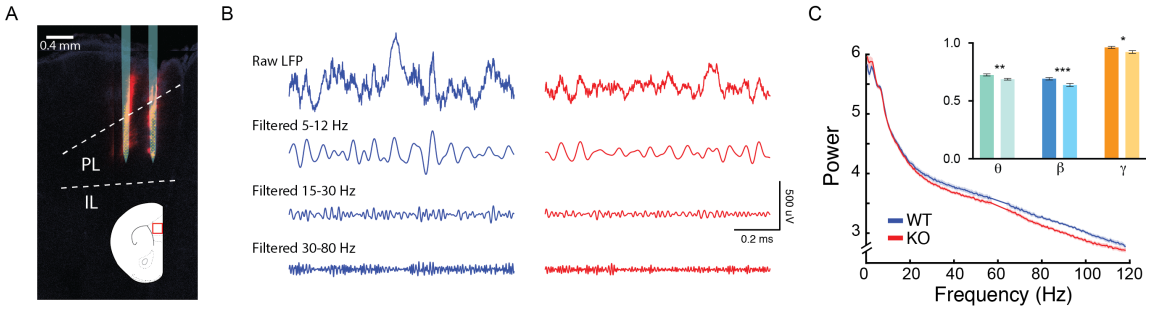

Figure 4.1: *In vivo* brain network activity in *Cntnap2* KO mice and controls. (A) Representative image of multichannel nanosilicon probe placement in mPFC. DiI (red) was used to verify placement in prelimbic (PL) prefrontal cortex. Brain tissue was counterstained with DAPI (Blue). (B) Representative traces of raw (unfiltered) LFP data, and data filtered at different LFP frequency cutoffs (theta 5-12 Hz, beta 15-30 Hz, gamma 30-80 Hz) for WT (blue) and KO (red). (C) Spectrogram of average LFP power along a broad frequency spectrum ranging from 0-200 Hz (WT, blue; KO, red). Inset

demonstrates average power (mean ± SEM) for each of the indicated spectra for WT (theta 0.72 ± 0.01, beta 0.69 ± 0.01, gamma 0.94 ± 0.01; n = 4 mice) and KO (theta 0.69 ± 0.01, beta 0.64 ± 0.01, gamma 0.92 ± 0.01; n = 5 mice). Statistical significance is indicated by ** for $p<0.005$ and *** for $p<0.0005$ for Mann Whitney U-test, and * for $p<0.05$, Unpaired t test.

4.4: A novel social behavior paradigm for in vivo electrophysiology in head-fixed, awake-behaving mice.

The observed in vitro an in vivo physiological pathologies observed in *Cntnap2* KO mice are likely to be implicated in the manifestation of autism-related behavioral deficits, such as social impairments. Moreover, understanding the relationship between disrupted brain network activity during social interactions can be invaluable when gauging the effect of potential therapeutic interventions. Thus, implementation of in vivo electrophysiology in awake-behaving mice is certainly a promising avenue for translational research.

Multichannel nanosilicon probes are an incredible tool that allow for high through-put measurement of brain network activity in vivo (see section 4.3). Nonetheless, these electrodes are limited by the fact that they require experimental mice to be head-fixed for electrophysiological recordings, which further limit our ability to assess brain network dynamics during behavior, especially during social interactions. In order to get around this issue, I designed an experimental paradigm that allows the experimental mouse to come in contact with another mouse, while still head-fixed (Figure 4.2). This new tool consists of a circular platform that has two barred cups on either side. The

platform has a Matlab-driven motor, which rotates the platform and presents either cup at any given interval. In this way, one of the cups can be filled with a live mouse, that can be presented as a social stimulus. The dimensions are such that, once the stimulus mouse is presented, both rodents can come in close contact and interact through sniffing or whisker-touching). Both experimental and stimulus mice can be easily and individually habituated to this context. Preliminary testing of this paradigm has demonstrated feasibility of this approach, which is likely to yield promising information with regards to brain network activity dynamics during these types of social interactions.

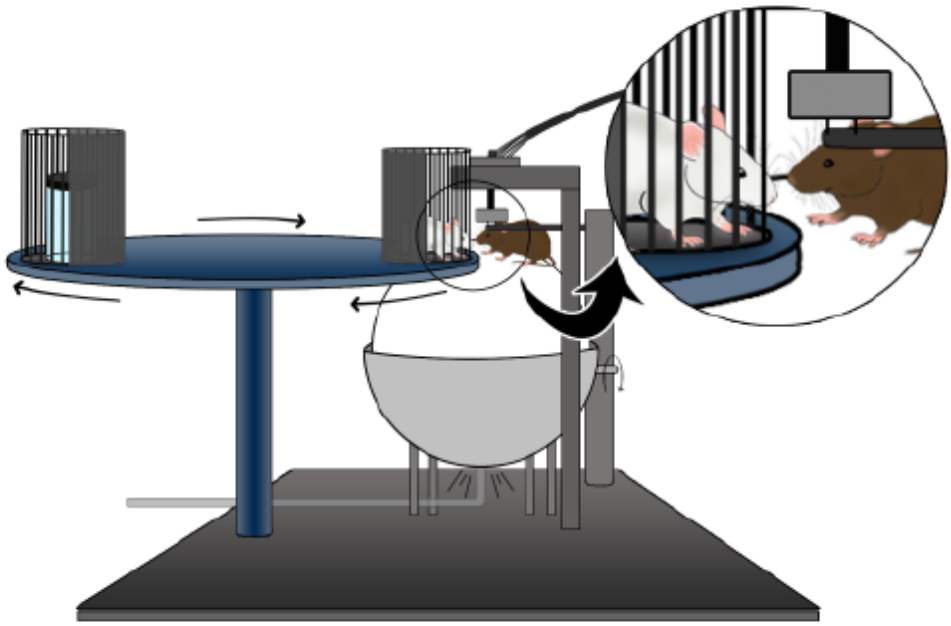

Figure 4.2. Schematic of novel social behavior paradigm for head-fixed mice. *See methods section.*

4.4: Discussion

Here, I observe a decrease in the total band power of LFPs in *Cntnap2* WT and KO mice, which is likely a direct effect of the overall decrease in synaptic inputs within mPFC. The ability of both inhibitory and excitatory cells to fire in a temporally-precise manner is crucial for processing and integration of information, both at the local and long-range circuit level (Chance et al., 2002; Buzsáki and Watson, 2012). Failure to do so often affects psychophysical representations of sensory information and can lead to some of the behavioral disturbances associated with both neurological and psychiatric disorders (Buzsáki and Watson, 2012). Social impairments associated with autism, for example, have often been connected to disturbances in excitatory/inhibitory balance, especially in the medial prefrontal cortex (mPFC) (Nelson and Valakh, 2015). These alterations in E/I ratio can emerge in many ways, including disturbances in tonic GABAergic and glutamatergic neurotransmission, changes in microcircuit connectivity and neural weights, or disruptions in the firing patterns or excitability of excitatory and inhibitory cells (Gogolla et al., 2009; Yizhar et al., 2011; Berg and Geschwind, 2012; D'amour and Froemke, 2015; Nelson and Valakh, 2015). In the future, assessment of behavioral repertoires (such as running, non-running epochs, or grooming periods), should be assessed in order to further correlate brain activity patterns with more specific behavioral states. Moreover, as the magnitude of the observed differences in LFP power was not particularly large (less than 10%), it will be important to replicate these studies and further validate these findings.

From these experiments, I conclude that *Cntnap2* plays an important role in the establishment and function of mPFC microcircuits and that loss of this protein results in

decreased excitatory drive and reduced power of synchronous oscillatory activity. These findings shed light on how functional microcircuit alterations could underlie some of the deficits associated with ASD and provide a starting point for future investigation and interrogation of its direct association to behavioral pathologies and therapy.

4.5: Methods

4.5.a: Surgery, behavioral habituation, and in vivo electrophysiology

Adult male and female *Cntnap2* mutant and wild-type mice (2-5 months old) underwent an initial surgery for implantation of a stainless steel head restraint bar on their skull in preparation for in vivo electrophysiogical recordings. All surgical procedures were performed under isofluorane anesthesia (3–5% induction, 1.5% maintenance) in a stereotaxic apparatus. Mouse body temperature was monitored and kept at 37°C during surgery using a Harvard Apparatus feedback-controlled heating pad and were administered an intracutaneous injection of carprofen (5 mg/kg of body weight) for systemic analgesia. Mice were allowed to recover for 5 days, during which they were given antibiotic treatment (amoxicillin, 0.25 mg/mL in drinking water). After recovery period, mice were habituated for at least three days per each of the following stages: human handling (5 min) headbar attachment (10 min), and head fixation on a spherical treadmill (10 min). The treadmill consisted of an 8-inch Styrofoam ball, tethered with a metal rod which trespassed it through the middle, resting a hollow Styrofoam half-sphere (Graham Sweet). Compressed air was blown, allowing the ball to float and the mouse to spin the ball and run in place and on top of it. After habituation, and one day prior to electrophysiological recordings, the mouse underwent a second surgery (as described above), this time with the objective of drilling a

circular craniotomy (diameter 2 mm) above the medial prefrontal cortex on the right hemisphere (coordinates). The dura above the exposed brain area was carefully removed in order to facilitate electrode insertion. The exposed skull and brain were covered and sealed with a silicone elastomer sealant (Kwik-Cast, WPI). An additional craniotomy was performed over the posterior cerebellum for placement of a silver chloride electrical reference wire, which was glued into place with dental cement. The mouse was allowed to recover overnight. If necessary, mice were given a dose of carprofen on day of recording, to ameliorate any pain associated with the craniotomy surgery.

On the day of the recording, the mouse was head-fixed by attaching the headbar to a post, as had been done during habituation, and placed on the spherical treadmill. The quickseal was removed and cortex buffer (135 mM NaCl, 5 mM KCl, 5 mM HEPES, 1.8 mM $CaCl_2$ and 1 mM $MgCl_2$) was immediately placed on top of the craniotomy in order to keep the exposed brain moist. The mouse skull was then stereotaxically aligned and the silicon microprobe which previously had been previously coated with a fluorescent dye (DiI, Invitrogen), was slowly stereotaxically lowered using a micromanipulator into the mPFC (relative to bregma: anterior 1.8 mm, lateral 0.5 mm, ventral 2.5 mm). This process was monitored using a surgical microscope (Zeiss OPMIpico). The microprobes contained a total of 128 electrode recording sites that were densely distributed (hexagonal array geometry with 25 μm vertical spacing and 16-20 μm horizontal spacing) on two prongs (placed 0.4 μm apart), spanning L2/3 and L5 of the prelimbic (PL) and infralimbic (IL) medial prefrontal cortex. Once inserted, the probe was allowed to settle among the brain tissue for 1 hr. Recording of brain network activity was done for a total duration of 1 hr after that. After the recording session, mice were anaesthetized with isofluorane and

sacrificed. The brain was extracted, sectioned (100 um) on a vibratome (Leica) and mounted on slides with DAPI Fluoromount-G (vendor) mounting media. Confocal tiled images were taken to verify microprobe location (Zeiss LSM 800). Anatomical landmarks were used to determine anterior-posterior coordinates relative to bregma. Each of the128 recording sites was then assigned a coordinate in 3D Cartesian space and classified as belonging to prelimbic (PL) or infralimbic (IL) prefrontal cortex (Allen Brain Atlas). Local field potential power was subsequently quantified for each channel and averaged over a period of 10 min after the recording. Data was analyzed using costum-written Matlab code.

4.5.b: A novel method for social stimulus presentation in head-fixed mice during in vivo electrophysiological recordings

A motorized rotating table was built for the presentation of a mouse inside a cup or an empty cup, very much like a modified "passive" three-chamber social interaction test (Silverman et al., 2010). This allows for the presentation of either stimulus in a precisely time-locked manner, that can be synchronized with electrophysiological data. The installed motor is precisely started and locked to stop for 30 sec every quarter rotation and is driven by custom-written code in Matlab. A sensor, which consists of four bolts hitting a switch, gets triggered at each stimulus presentation, for each one of the quarter rotations, consisting of two "no-stimulus" conditions, empty cup, and cup with mouse inside. As the rotating table reaches each one of the stimulus points, the triggers have been wired to send an electrical signal, indicating when the stimulus has arrived at any given position. This is sent to the data acquisition (DAQ) board and recorded in Matlab, such that it can be synchronized with electrophysiological recording of brain activity in the experimental

mouse. This signal also serves to trigger either a halt in the rotation, or a rotation "go" signal. The two behavior cups are attached to either side for the stimuli, and contain customized barriers that prevent the animal from seeing which stimulus is in the cups before the experience. The rotating platform is placed onto a breadboard that readily attaches to the electrophysiology air table for ease of mounting and dismounting at any given time or for flexibility of use within the experimental setup.

Chapter 5:

Conclusions, limitations, and future directions

Here, I have shown that loss of *Cntnap2* leads to decreased excitatory and, to a lesser degree, inhibitory synaptic inputs in L2/3 pyramidal neurons of the mPFC, concurrent with an overall reduction in the power of neuronal network oscillations *in vivo*. From these findings, I conclude that (1) Caspr2 likely plays a role in the formation and stabilization of excitatory synapses, that (2) this reduction in cortical synapses results in weaker cortical input maps; and that (3) this weakened mPFC microcircuit is associated with a decrease in LFP power in vivo. At a broader scale, I demonstrate how alterations in a single autism-associated gene, *Cntnap2*, can disrupt cortical synapse number, decrease microcircuit connectivity and impair the ability of neuronal populations to engage in synchronous network activity.

Other potentially relevant mechanisms underlying our observations may be secondary to or occurring downstream of disruptions in Cntnap2. Further research is needed in order to assess the interplay between defined genetic etiologies and homeostatic responses of glia at specific developmental time points in the manifestation of ASD. It is possible, for example, that some of the aberrant phenotypes observed in ASD derive from developmental abnormalities or intrinsic changes that affect neuron-glia interactions. The opposite could also be true, whereby disruptions in neuron-glia interactions could result in developmental abnormalities and intrinsic alterations in brain function. Thus, understanding these disruptions from a developmental perspective, such as by assessing changes during embryonic development and in early postnatal periods, could provide incredibly useful mechanistic information. As ASDs are developmental disorders, obtaining a clearer picture of what is occurring in early life periods can likely

yield some of the best options for therapeutic treatments and even provide the possibility for preventative measures.

We also observed a loss of excitatory synapses and cortical inputs in pyramidal neurons of L2/3 of mPFC that is associated with a decrease in LFP power in *Cntnap2* KO mice. In addition to further validating these findings, it will be crucial to understand how a decrease in LFP power affects processing and encoding of relevant information, especially in a behavioral context. Moreover, understanding how discrete neuronal cell types partake in network brain activity changes and how this affects both local and global connections will be crucial for defining a biomarker that can then be used to gauge the effect of therapeutic interventions. However, this in vivo data is consistent with overall lower excitatory and inhibitory drive. In the KO, due to fewer functional excitatory connections. The next step will be to identify how this relates to patients and determine whether this decrease in LFP power is a viable biomarker.

Furthermore, it is important to keep in mind that the physiological alterations that were observed in *Cntnap2* KO mice are representative of a single developmental time point, one at which neuronal circuit maturation is concluding. It will be therefore crucial to test the extent to which these changes manifest at earlier developmental time points. This is particularly important in the context of ASD, given that it is discretely defined as a developmental disorder. Hence, it is possible that assessing these differences early in development will reveal even more robust alterations. Researching and understanding these changes could then provide incredibly useful insights on the molecular and physiological phenomena that prime for alterations observed in young adult mice.

This work should be expanded with the incorporation of novel technologies to further assess how these local changes in mPFC affect long-range connectivity and functional communication with connected brain regions. The novel social task described here could be paired with electrophysiological techniques to simultaneously record the activity of hundreds of neurons and underlying gamma oscillatory activity during a socially-relevant task. With the use of state of the art and innovative techniques that range from in vitro and high throughput in vivo electrophysiology, to biochemistry and genetics, we will be able to dissect key information about how autistic-like social behaviors arise in our model. Furthermore, treating the mice with oxytocin and assessing how it modulates brain activity to rescue social behavior will take us one step closer to developing targeted therapeutic approaches for treating at least some of the core autism symptoms, not only for individuals with *CNTNAP2* mutations, but also for individuals within a broader range of known and unknown autism etiologies.

REFERENCES

Alarcón, M., Abrahams, B. S., Stone, J. L., Duvall, J. A., Perederiy, J. V., Bomar, J. M., … Geschwind, D. H. (2008). Linkage, Association, and Gene-Expression Analyses Identify CNTNAP2 as an Autism-Susceptibility Gene. *American Journal of Human Genetics*, *82*(1), 150–159. https://doi.org/10.1016/j.ajhg.2007.09.005

American Psychiatric Association. (2013). DSM-5 and Diagnoses for Children, *32*, 91–93.

Anderson, G. R., Galfin, T., Xu, W., Aoto, J., Malenka, R. C., & Sudhof, T. C. (2012). Candidate autism gene screen identifies critical role for cell-adhesion molecule CASPR2 in dendritic arborization and spine development. *Proceedings of the National Academy of Sciences*, *109*(44), 18120–18125. https://doi.org/10.1073/pnas.1216398109

Arancibia-Carcamo, I. L., & Attwell, D. (2014). The node of Ranvier in CNS pathology. *Acta Neuropathologica*, *128*(2), 161–175. https://doi.org/10.1007/s00401-014-1305-z

Arons, M. H., Thynne, C. J., Grabrucker, A. M., Li, D., Schoen, M., Cheyne, J. E., … Garner, C. C. (2012). Autism-Associated Mutations in ProSAP2 / Shank3 Impair Synaptic Transmission and Neurexin – Neuroligin-Mediated Transsynaptic Signaling, *32*(43), 14966–14978. https://doi.org/10.1523/JNEUROSCI.2215-12.2012

Austin, C. P., Battey, J. F., Bradley, A., Bucan, M., Capecchi, M., Collins, F. S., … Zambrowicz, B. (2004). The Knockout Mouse Project. *Nature Genetics*, *36*(9), 921–924. https://doi.org/10.1038/ng0904-921

Baker, J. P. (2013). Autism at 70 - Redrawing the Boundaries. *New England Journal of Medicine*, *369*(12), 2013–2015. https://doi.org/10.1056/NEJMp1304681

Banerjee, S., Riordan, M., & Bhat, M. A. (2014). Genetic aspects of autism spectrum disorders: insights from animal models. *Frontiers in Cellular Neuroscience*, *8*(February), 58. https://doi.org/10.3389/fncel.2014.00058

Bateup, H. S., Johnson, C. A., Denefrio, C. L., Saulnier, J. L., Kornacker, K., & Sabatini, B. L. (2013). Excitatory/Inhibitory Synaptic Imbalance Leads to Hippocampal Hyperexcitability in Mouse Models of Tuberous Sclerosis. *Neuron*, *78*(3), 510–522. https://doi.org/10.1016/j.neuron.2013.03.017

Bear, M. F., Huber, K. M., & Warren, S. T. (2004). The mGluR theory of fragile X mental retardation. *Trends in Neurosciences*, *27*(7), 370–377. https://doi.org/10.1016/j.tins.2004.04.009

Bear, M. F., Huber, K. M., & Warren, S. T. (2004). The mGluR theory of fragile X mental retardation. *Trends in Neurosciences*, *27*(7), 370–377. https://doi.org/10.1016/j.tins.2004.04.009

Berg, J. M., & Geschwind, D. H. (2012). Autism genetics: searching for specificity and convergence. *Genome Biology*. https://doi.org/10.1186/gb4034

Berg, J. M., Lee, C., Chen, L., Galvan, L., Cepeda, C., Chen, J. Y., … Geschwind, D. H. (2016). JAKMIP1, a Novel Regulator of Neuronal Translation, Modulates Synaptic Function and Autistic-like Behaviors in Mouse. *Neuron*, *88*(6), 1173–1191. https://doi.org/10.1016/j.neuron.2015.10.031

Berry-Kravis, E., Portes, V. Des, Hagerman, R., Jacquemont, S., Charles, P., Visootsak, J., … Raison, F. Von. (2016). Mavoglurant in fragile X syndrome : Results of two randomized , double-blind , placebo-controlled trials. *Science Translational Medicine*, *8*(321). 10.1126/scitranslmed.aab4109

Blaesse, P., & Schmidt, T. (2015). K-Cl cotransporter KCC2—a moonlighting protein in excitatory and inhibitory synapse development and function. *Pflugers Archiv European Journal of Physiology*, *467*(4), 615–624. https://doi.org/10.1007/s00424-014-1547-6

Bodmer, W., & Bonilla, C. (2008). Common and rare variants in multifactorial susceptibility to common diseases. *Nature Genetics*, *40*(6), 695–701. https://doi.org/10.1038/ng.f.136

Boyden, E. S., Zhang, F., Bamberg, E., Nagel, G., & Deisseroth, K. (2005). Millisecond-timescale, genetically targeted optical control of neural activity. *Nature Neuroscience*, *8*(9), 1263–8. https://doi.org/10.1038/nn1525

Brimberg, L., Mader, S., Jeganathan, V., Berlin, R., Coleman, T. R., Gregersen, P. K., … Diamond, B. (2016). Caspr2-reactive antibody cloned from a mother of an ASD child mediates an ASD-like phenotype in mice. *Molecular Psychiatry*, (August), 1–9. https://doi.org/10.1038/mp.2016.165

Brimberg, L., Sadiq, a, Gregersen, P. K., & Diamond, B. (2013). Brain-reactive IgG correlates with autoimmunity in mothers of a child with an autism spectrum disorder. *Molecular Psychiatry*, *18*(11), 1171–7. https://doi.org/10.1038/mp.2013.101

Burrone, J., O'Byrne, M., & Murthy, V. (2003). Multiple forms of synaptic plasticity. *Nature*, *420*(November), 414–418. https://doi.org/10.1038/nature01179.1.

Buzsáki, G., & Watson, B. O. (2012). Brain rhythms and neural syntax: Implications for efficient coding of cognitive content and neuropsychiatric disease. *Dialogues in*

Clinical Neuroscience, *14*(4), 345–367. https://doi.org/10.1097/ALN.0b013e318212ba87

Callaway, E. M., & Katz, L. C. (1993). Photostimulation using caged glutamate reveals functional circuitry in living brain slices. *Proceedings of the National Academy of Sciences of the United States of America*, *90*(16), 7661–7665. https://doi.org/10.1073/pnas.90.16.7661

Cambiaghi, M., Cursi, M., Magri, L., Castoldi, V., Comi, G., Minicucci, F., … Leocani, L. (2013). Behavioural and EEG effects of chronic rapamycin treatment in a mouse model of Tuberous Sclerosis Complex. *Neuropharmacology*, *67*, 1–7. https://doi.org/10.1016/j.neuropharm.2012.11.003

Casanova, M. F., El-Baz, A. S., Kamat, S. S., Dombroski, B. A., Khalifa, F., Elnakib, A., … Switala, A. E. (2013). Focal cortical dysplasias in autism spectrum disorders. *Acta Neuropathologica Communications*, *1*(1), 67. https://doi.org/10.1186/2051-5960-1-67

Chadman, K. K., Yang, M., & Crawley, J. N. (2009). Criteria for validating mouse models of psychiatric diseases. *American Journal of Medical Genetics, Part B: Neuropsychiatric Genetics*, *150*(1), 1–11. https://doi.org/10.1002/ajmg.b.30777

Chance, F. S., Abbott, L. F., & Reyes, A. D. (2002). Gain modulation from background synaptic input. *Neuron*, *35*(4), 773–782. https://doi.org/10.1016/S0896-6273(02)00820-6

Chen, J. A., Peñagarikano, O., Belgard, T. G., Swarup, V., & Geschwind, D. H. (2015). The Emerging Picture of Autism Spectrum Disorder: Genetics and Pathology. *Annual Review of Pathology: Mechanisms of Disease*, *10*(1), 111–144. https://doi.org/10.1146/annurev-pathol-012414-040405

Chow, D. K., Groszer, M., Pribadi, M., Machniki, M., Carmichael, S. T., Liu, X., & Trachtenberg, J. T. (2009). Laminar and compartmental regulation of dendritic growth in mature cortex. *Nature Neuroscience*, *12*(2), 116–118. https://doi.org/10.1038/nn.2255

Christensen, D. L., Baio, J., Braun, K. V. N., Bilder, D., Charles, J., Constantino, J. N., … Yeargin-Allsopp, M. (2016). Prevalence and Characteristics of Autism Spectrum Disorder Among Children Aged 8 Years - Autism and Developmental Disabilities Monitoring Network, 11 Sites, United States, 2012. *Morbidity and Mortality Weekly Report. Surveillance Summaries*, *65*(3), 1–23. https://doi.org/10.15585/mmwr.ss6503a1

Cobb, S., Guy, J., & Bird, A. (2010). Reversibility of functional deficits in experimental models of Rett syndrome. *Biochem Soc Trans*, *38*(2), 498–506. https://doi.org/10.1042/BST0380498

Cope, E. C., Briones, B. A., Brockett, A. T., Martinez, S., Vigneron, P.-A., Opendak, M., … Gould, E. (2016). Immature neurons and radial glia, but not astrocytes or microglia, are altered in adult Cntnap2 and Shank3 mice, models of autism. *eNeuro*, *3*(October). https://doi.org/10.1523/ENEURO.0196-16.2016

Courchesne, E., Saitoh, O., Townsend, J., Yeung-Courchesne, R., Press, G., Lincoln, A., … Schreibman, L. (1994). Cerebellar hypoplasia and hyperplasia in infantile autism. *The Lancet*, *343*(8888), 63–64. https://doi.org/10.1016/S0140-6736(94)90923-7

D'amour, J. A., & Froemke, R. C. (2015). Inhibitory and excitatory spike-timing-dependent plasticity in the auditory cortex. *Neuron*, *86*(2), 514–528. https://doi.org/10.1016/j.neuron.2015.03.014

Dani, V. S., Chang, Q., Maffei, A., Turrigiano, G. G., Jaenisch, R., & Nelson, S. B. (2005). Reduced cortical activity due to a shift in the balance between excitation and inhibition in a mouse model of Rett syndrome. *Proceedings of the National Academy of Sciences of the United States of America*, *102*(35), 12560–12565. https://doi.org/10.1073/pnas.0506071102

Dantzker, J. L. & Callaway, E. M. (2000) Laminar sources of synaptic input to cortical inhibitory interneurons and pyramidal neurons. *Nature Neuroscience* 3, 701-707, https://doi:10.1038/76656

de la Torre-Ubieta, L., Won, H., Stein, J. L., & Geschwind, D. H. (2016). Advancing the understanding of autism disease mechanisms through genetics. *Nature Medicine*, *22*(4), 345–61. https://doi.org/10.1038/nm.4071

De Rubeis, S., He, X., Goldberg, A. P., Poultney, C. S., Samocha, K., Ercument Cicek, A., … Buxbaum, J. D. (2014). Synaptic, transcriptional and chromatin genes disrupted in autism. *Nature*, *515*(7526), 209–215. https://doi.org/10.1038/nature13772

Debanne, D., Boudkkazi, S., Campanac, E., Cudmore, R. H., Giraud, P., Fronzaroli-Molinieres, L., … Caillard, O. (2008). Paired-recordings from synaptically coupled cortical and hippocampal neurons in acute and cultured brain slices. *Nature Protocols*, *3*(10), 1559–1568. https://doi.org/10.1038/nprot.2008.147

Deisseroth, K. (2015). H I S TO R I C A L C O M M E N TA RY Optogenetics : 10 years of microbial opsins in neuroscience, *18*(9), 1213–1225.

Dickinson, A., Jones, M., & Milne, E. (2016). Measuring neural excitation and inhibition in autism: Different approaches, different findings and different interpretations. *Brain Research*, *1648*, 277–289. https://doi.org/10.1016/j.brainres.2016.07.011

Edmonson, C. A., Ziats, M. N., & Rennert, O. M. (2016). A non-inflammatory role for microglia in autism spectrum disorders. *Frontiers in Neurology*, *7*(FEB), 1–6. https://doi.org/10.3389/fneur.2016.00009

Ehninger, D., Han, S., Shilyansky, C., Zhou, Y., Li, W., & David, J. (2009). Reversal of learning deficits in a Tsc2+/- mouse model of tuberous sclerosis. *Nature Medicine*, *14*(8), 843–848. https://doi.org/10.1038/nm1788.Reversal

Ehninger, D., Li, W., Fox, K., Stryker, M. P., & Silva, A. J. (2008). Reversing Neurodevelopmental Disorders in Adults. *Neuron*, *60*(6), 950–960. https://doi.org/10.1016/j.neuron.2008.12.007

Einstein, M. C., Polack, P.-O., & Golshani, P. (2016). 3-5 Hz membrane potential oscillations decrease the gain of neurons in visual cortex. *bioRxiv*, 69252. https://doi.org/10.1101/069252

Evans, J. a. (2007). Diaphragmatic defects and limb deficiencies - taking sides. *American Journal of Medical Genetics. Part A*, *143A*(18), 2106–2112. https://doi.org/10.1002/ajmg.a

Fatemi, S. H., Halt, A. R., Realmuto, G., Earle, J., Kist, D. A., Thuras, P., & Metz, A. (2002). Purkinje cell size is reduced in cerebellum of patients with autism. *Cellular and Molecular Neurobiology*, *22*(2), 171–175. https://doi.org/10.1023/A:1019861721160

Földy, C., Malenka, R. C., & Südhof, T. C. (2013). Autism-Associated Neuroligin-3 Mutations Commonly Disrupt Tonic Endocannabinoid Signaling. *Neuron*, *78*(3), 498–509. https://doi.org/http://dx.doi.org/10.1016/j.neuron.2013.02.036

Gandal, M. J., Edgar, J. C., Ehrlichman, R. S., Mehta, M., Roberts, T. P. L., & Siegel, S. J. (2010). Validating ?? oscillations and delayed auditory responses as translational biomarkers of autism. *Biological Psychiatry*, *68*(12), 1100–1106. https://doi.org/10.1016/j.biopsych.2010.09.031

Gantois, I., Pop, A. S., de Esch, C. E. F., Buijsen, R. A. M., Pooters, T., Gomez-Mancilla, B., … Willemsen, R. (2013). Chronic administration of AFQ056/Mavoglurant restores social behaviour in Fmr1 knockout mice. *Behavioural Brain Research*, *239*(1), 72–79. https://doi.org/10.1016/j.bbr.2012.10.059

Garcia-Junco-Clemente, P., Chow, D. K., Tring, E., Lazaro, M. T., Trachtenberg, J. T., & Golshani, P. (2013). Overexpression of calcium-activated potassium channels underlies cortical dysfunction in a model of PTEN-associated autism. *Proceedings of the National Academy of Sciences*, *110*(45), 18297–18302. https://doi.org/10.1073/pnas.1309207110

Garcia-Junco-Clemente, P., Chow, D. K., Tring, E., Lazaro, M. T., Trachtenberg, J. T., & Golshani, P. (2013). Overexpression of calcium-activated potassium channels underlies cortical dysfunction in a model of PTEN-associated autism. *Proceedings of the National Academy of Sciences*, *110*(45), 18297–18302. https://doi.org/10.1073/pnas.1309207110

Gauvain, G., Chamma, I., Chevy, Q., Cabezas, C., Irinopoulou, T., Bodrug, N., … Poncer, J. C. (2011). The neuronal K-Cl cotransporter KCC2 influences postsynaptic AMPA receptor content and lateral diffusion in dendritic spines. *Proceedings of the National Academy of Sciences of the United States of America*, *108*(37), 15474–15479. https://doi.org/10.1073/pnas.1107893108

Gdalyahu, A., Lazaro, M., Penagarikano, O., Golshani, P., Trachtenberg, J. T., & Gescwind, D. H. (2015). The autism related protein contactin-associated protein-like 2 (CNTNAP2) stabilizes new spines: An in vivo mouse study. *PLoS ONE*, *10*(5), 1–7. https://doi.org/10.1371/journal.pone.0125633

Gdalyahu, A., Lazaro, M., Penagarikano, O., Golshani, P., Trachtenberg, J. T., & Gescwind, D. H. (2015). The autism related protein contactin-associated protein-like 2 (CNTNAP2) stabilizes new spines: An in vivo mouse study. *PLoS ONE*, *10*(5), 1–7. https://doi.org/10.1371/journal.pone.0125633

Geschwind, D. H. (2008). Autism: Many Genes, Common Pathways? *Cell*, *135*(3), 391–395. https://doi.org/10.1016/j.cell.2008.10.016

Geschwind, D. H. (2009). Advances in autism. *Medicine*, *60*, 367–380. https://doi.org/10.1146/annurev.med.60.053107.121225

Geschwind, D. H. (2011). Genetics of autism spectrum disorders. *Trends in Cognitive Sciences*, *15*(9), 409–16. https://doi.org/10.1016/j.tics.2011.07.003

Gilman, S. R., Iossifov, I., Levy, D., Ronemus, M., Wigler, M., & Vitkup, D. (2011). Rare De Novo Variants Associated with Autism Implicate a Large Functional Network of Genes Involved in Formation and Function of Synapses. *Neuron*, *70*(5), 898–907. https://doi.org/10.1016/j.neuron.2011.05.021

Gogolla, N., LeBlanc, J. J., Quast, K. B., Südhof, T. C., Fagiolini, M., & Hensch, T. K. (2009). Common circuit defect of excitatory-inhibitory balance in mouse models of autism. *Journal of Neurodevelopmental Disorders*, *1*(2), 172–181. https://doi.org/10.1007/s11689-009-9023-x

Gogolla, N., Takesian, A. E., Feng, G., Fagiolini, M., & Hensch, T. K. (2014). Sensory Integration in Mouse Insular Cortex Reflects GABA Circuit Maturation. *Neuron*, *83*(4), 894–905. https://doi.org/10.1016/j.neuron.2014.06.033

Golshani, P., Hutnick, L., Schweizer, F., & Fan, G. (2005). Conditional Dnmt1 deletion in dorsal forebrain disrupts development of somatosensory barrel cortex and thalamocortical long-term potentiation. *Thalamus & Related Systems*, *3*(3), 227–233. https://doi.org/10.1017/S1472928807000222

Gonçalves, J. T., Anstey, J. E., Golshani, P., & Portera-Cailliau, C. (2013). Circuit level defects in the developing neocortex of Fragile X mice. *Nature Neuroscience*, *16*(7), 903–9. https://doi.org/10.1038/nn.3415

Gonzalez-Burgos, G., Kroener, S., Zaitsev, A. V., Povysheva, N. V., Krimer, L. S., Barrionuevo, G., & Lewis, D. A. (2008). Functional maturation of excitatory synapses in layer 3 pyramidal neurons during postnatal development of the primate prefrontal cortex. *Cerebral Cortex*, *18*(3), 626–637. https://doi.org/10.1093/cercor/bhm095

Guy, J., Gan, J., Selfridge, J., Cobb, S., & Bird, A. (2007). Reversal of Neurological Defects in a Mouse Model of Rett Syndrome. *Science Reports*, *315*(February), 1143–1148. https://doi.org/10.1126/science.1229223

Hallmayer, J., Cleveland, S., Torres, A., Phillips, J., Cohen, B., Torigoe, T., … Risch, N. (2015). HHS Public Access, *68*(11), 1095–1102. https://doi.org/10.1001/archgenpsychiatry.2011.76.Genetic

He, Q., Nomura, T., Xu, J., & Contractor, A. (2014). The Developmental Switch in GABA Polarity Is Delayed in Fragile X Mice. *Journal of Neuroscience*, *34*(2), 446–450. https://doi.org/10.1523/JNEUROSCI.4447-13.2014

Hong, W., Kim, D.-W., & Anderson, D. J. (2014). Antagonistic Control of Social versus Repetitive Self-Grooming Behaviors by Separable Amygdala Neuronal Subsets. *Cell*, *158*(6), 1348–1361. https://doi.org/10.1016/j.cell.2014.07.049

Huber, K. M., Gallagher, S. M., Warren, S. T., & Bear, M. F. (2002). Altered synap tic plasticity in a mouse model of fragile X mental retardation. *Proceedings of the National Academy of Sciences of the United States of America*, *99*(11), 7746–7750. https://doi.org/10.1073/pnas.122205699

Hutsler, J. J., & Zhang, H. (2010). Increased dendritic spine densities on cortical projection neurons in autism spectrum disorders. *Brain Research*, *1309*, 83–94. https://doi.org/10.1016/j.brainres.2009.09.120

Ikrar, T., Olivas, N. D., Shi, Y., & Xu, X. (2011). Mapping Inhibitory Neuronal Circuits by Laser Scanning Photostimulation. *Journal of Visualized Experiments*, (56), 5–9. https://doi.org/10.3791/3109

Iossifov, I., O'roak, B. J., Sanders, S. J., Ronemus, M., Krumm, N., Levy, D., … Wigler, M. (2014). The contribution of de novo coding mutations to autism spectrum disorder. *Nature*, *13*(515), 216–221. https://doi.org/10.15154/1149697

Jacquemont, S., Berry-Kravis, E., Hagerman, R., Von Raison, F., Gasparini, F., Apostol, G., … Gomez-Mancilla, B. (2014). The challenges of clinical trials in fragile X syndrome. *Psychopharmacology*, *231*(6), 1237–1250. https://doi.org/10.1007/s00213-013-3289-0

Jeste, S. S., & Geschwind, D. H. (2014). Disentangling the heterogeneity of autism spectrum disorder through genetic findings. *Nat Rev Neurol*, *10*(2), 74–81. http://dx.doi.org/10.1038/nrneurol.2013.278

Jiang, M., Ash, R. T., Baker, S. A., Suter, B., Ferguson, A., Park, J., … Smirnakis, S. M. (2013). Dendritic arborization and spine dynamics are abnormal in the mouse model of MECP2 duplication syndrome. *The Journal of Neuroscience : The Official Journal of the Society for Neuroscience*, *33*(50), 19518–33. https://doi.org/10.1523/JNEUROSCI.1745-13.2013

Jones, W., B., A., Hesselink, J., c. Courchesne, E., b. Duncan, T., b. Matsuda, K., & a. Bellugi, U. (2002). Cerebellar abnormalities in infants and toddlers with Williams syndrome. *Developmental Medicine and Child Neurology*, *44*(10), 688–694. https://doi.org/10.1017/S0012162201002766

Jurgensen, S., & Castillo, P. E. (2015). Selective Dysregulation of Hippocampal Inhibition in the Mouse Lacking Autism Candidate Gene CNTNAP2. *Journal of Neuroscience*, *35*(43), 14681–14687. https://doi.org/10.1523/JNEUROSCI.1666-15.2015

Kanner, L. (1943). Autistic disturbances of affective contact. *Nervous Child*. https://doi.org/10.1105/tpc.11.5.949

Karayannis, T., Au, E., Patel, J. C., Kruglikov, I., Markx, S., Delorme, R., … Fishell, G. (2014). Cntnap4 differentially contributes to GABAergic and dopaminergic synaptic transmission. *Nature*, *511*(7508), 236–40. https://doi.org/10.1038/nature13248

Kas, M. J., Glennon, J. C., Buitelaar, J., Ey, E., Biemans, B., Crawley, J., … Steckler, T. (2014). Assessing behavioural and cognitive domains of autism spectrum disorders in rodents: Current status and future perspectives. *Psychopharmacology*, *231*(6), 1125–1146. https://doi.org/10.1007/s00213-013-3268-5

Krishnan, A., Zhang, R., Yao, V., Theesfeld, C. L., Wong, A. K., Tadych, A., … Troyanskaya, O. G. (2016). Genome-wide prediction and functional characterization of the genetic basis of autism spectrum disorder. *Nature Neuroscience*, (August 2015). https://doi.org/10.1038/nn.4353

Krumm, N., O'Roak, B. J., Shendure, J., & Eichler, E. E. (2014). A de novo convergence of autism genetics and molecular neuroscience. *Trends in Neurosciences*, *37*(2), 95–105. https://doi.org/10.1016/j.tins.2013.11.005

Lázaro, M. T., & Golshani, P. (2015). The utility of rodent models of autism spectrum disorders. *Current Opinion in Neurology*, *28*(2), 103–9. https://doi.org/10.1097/WCO.0000000000000183

Lee, A., Gee, S., Vogt, D., Patel, T., Rubenstein, J., & Sohal, V. (2014). Pyramidal neurons in prefrontal cortex receive subtype-specific forms of excitation and inhibition. *Neuron*, *81*(1), 61–68. https://doi.org/10.1016/j.neuron.2013.10.031

Lee, H. M., Giguere, P. M., & Roth, B. L. (2014). DREADDs: Novel tools for drug discovery and development. *Drug Discovery Today*, *19*(4), 469–473. https://doi.org/10.1016/j.drudis.2013.10.018

Lee, E., Lee, J., & Kim, E. (2016). Excitation/Inhibition Imbalance in Animal Models of Autism Spectrum Disorders. *Biological Psychiatry*, (6), 1–10. https://doi.org/10.1016/j.biopsych.2016.05.011

Lemonnier, E., Degrez, C., Phelep, M., Tyzio, R., Josse, F., Grandgeorge, M., … Ben-Ari, Y. (2012). A randomised controlled trial of bumetanide in the treatment of autism in children. *Translational Psychiatry*, *2*(12), e202. https://doi.org/10.1038/tp.2012.124

Leppa, V. M., Kravitz, S. N., Martin, C. L., Andrieux, J., Le Caignec, C., Martin-Coignard, D., … Geschwind, D. H. (2016). Rare Inherited and De Novo CNVs Reveal Complex Contributions to ASD Risk in Multiplex Families. *American Journal of Human Genetics*, *99*(3), 540–54. https://doi.org/10.1016/j.ajhg.2016.06.036

Li, H., Khirug, S., Cai, C., Ludwig, A., Blaesse, P., Kolikova, J., … Rivera, C. (2007). KCC2 Interacts with the Dendritic Cytoskeleton to Promote Spine Development. *Neuron*, *56*(6), 1019–1033. https://doi.org/10.1016/j.neuron.2007.10.039

Lu, Z., Reddy, M. V. V. V. S., Liu, J., Kalichava, A., Liu, J., Zhang, L., … Rudenko, G. (2016). Molecular Architecture of Contactin-associated Protein-like 2 (CNTNAP2) and its Interaction with Contactin 2 (CNTN2). *Journal of Biological Chemistry*, *2*, jbc.M116.748236. https://doi.org/10.1074/jbc.M116.748236

Luongo, F. J., Horn, M. E., & Sohal, V. S. (2016). Putative microcircuit-level substrates for attention are disrupted in mouse models of autism. *Biological Psychiatry*, *79*(8), 667–675. https://doi.org/10.1016/j.biopsych.2015.04.014

Malinow, R., & Malenka, R. C. (2002). Ampa R Eceptor T Rafficking and S Ynaptic P Lasticity. *Annual Review of Neuroscience*, *25*(1), 103–126. https://doi.org/10.1146/annurev.neuro.25.112701.142758

Mehta, S. Q., & Golshani, P. (2013). Clinical Neurogenetics: Autism Spectrum Disorders. *Neurologic Clinics*, *31*(4), 951–968. https://doi.org/10.1016/j.ncl.2013.04.009

Meng, L., Ward, A. J., Chun, S., Bennett, C. F., Beaudet, A. L., & Rigo, F. (2014). Towards a therapy for Angelman syndrome by targeting a long non-coding RNA. *Nature*, *518*(7539), 409–12. https://doi.org/10.1038/nature13975

Michalon, A., Bruns, A., Risterucci, C., Honer, M., Ballard, T. M., Ozmen, L., … Lindemann, L. (2014). Chronic metabotropic glutamate receptor 5 inhibition corrects local alterations of brain activity and improves cognitive performance in fragile X mice. *Biological Psychiatry*, *75*(3), 189–197. https://doi.org/10.1016/j.biopsych.2013.05.038

Michalon, A., Sidorov, M., Ballard, T. M., Ozmen, L., Spooren, W., Wettstein, J. G., … Lindemann, L. (2012). Chronic Pharmacological mGlu5 Inhibition Corrects Fragile X in Adult Mice. *Neuron*, *74*(1), 49–56. https://doi.org/10.1016/j.neuron.2012.03.009

Miller, J. a, Horvath, S., & Geschwind, D. H. (2010). Divergence of human and mouse brain transcriptome highlights Alzheimer disease pathways. *Proceedings of the National Academy of Sciences of the United States of America*, *107*(28), 12698–12703. https://doi.org/10.1073/pnas.0914257107

Nelson, S. B., & Valakh, V. (2015). Excitatory/Inhibitory Balance and Circuit Homeostasis in Autism Spectrum Disorders. *Neuron*, *87*(4), 684–698. https://doi.org/10.1016/j.neuron.2015.07.033

Nestler, E., & Hyman, S. (2010). Animal models of neuropsychiatric disorders. *Nature Neuroscience*, *13*(10), 1161–1169. https://doi.org/10.1038/nn.2647.Animal

NIMH, T. N. I. of M. H. (2016). Autism Spectrum Disorder, (October), 2012–2013. Retrieved from http://www.nimh.nih.gov/health/topics/autism-spectrum-disorders-asd/index.shtml#part_145441

Nosyreva, E. D., Huber, K. M., Klemmer, P., Meredith, R. M., Holmgren, C. D., Klychnikov, O. I., … Nguyen, P. V. (2006). Metabotropic Receptor-Dependent Long-Term Depression Persists in the Absence of Protein Synthesis in the Mouse Model of Fragile X Syndrome Metabotropic Receptor-Dependent Long-Term Depression Persists in the Absence of Protein Synthesis in the Mouse Model. *Journal of Neurophysiology*, (February 2006), 3291–3295. https://doi.org/10.1152/jn.01316.2005

Oguro-Ando, A., Rosensweig, C., Herman, E., Nishimura, Y., Werling, D., Bill, B. R., … Coppola, G. (2014). Increased CYFIP1 dosage alters cellular and dendritic morphology and dysregulates mTOR. *Molecular Psychiatry*, *20*(9), 1069–1078. https://doi.org/10.1038/mp.2014.124

Olivas, N. D., Quintanar-Zilinskas, V., Nenadic, Z. & Xu, X. Laminar circuit organization and response modulation in mouse visual cortex. *Frontier in Neural Circuits*, 6, 70, doi:10.3389/fncir.2012.00070 (2012).

O'Roak, B. J., Vives, L., Fu, W., Egertson, J. D., Stanaway, I. B., Phelps, I. G., … Shendure, J. (2012). Multiplex Targeted Sequencing Identifies Recurrently Mutated Genes in Autism Spectrum Disorders. *Science*, *338*(6114), 1619 LP-1622. 1 0.1126/science.1227764

Ospina, M. B., Seida, J. K., Clark, B., Karkhaneh, M., Hartling, L., Tjosvold, L., … Smith, V. (2008). Behavioural and developmental interventions for autism spectrum disorder: A clinical systematic review. *PLoS ONE*, *3*(11). https://doi.org/10.1371/journal.pone.0003755

Ozonoff, S., Young, G., Carter, A., Messinger, D., Yirmiya, N., Zwaigenbaum, L., … Hutman, T. (2011). Recurrence risk for autism spectrum disorders: a Baby Siblings Research Consortium study. *Pediatrics*, *128*(3), 488–495. Retrieved from http://pediatrics.aappublications.org/content/128/3/e488.short

Paolicelli, R. C., Bolasco, G., Pagani, F., Maggi, L., Scianni, M., Panzanelli, P., … Gross, C. T. (2011). Synaptic pruning by microglia is necessary for normal brain development. *Science (New York, N.Y.)*, *333*(6048), 1456–8. https://doi.org/10.1126/science.1202529

Paolicelli, R. C., Bisht, K., & Tremblay, M.-È. (2014). Fractalkine regulation of microglial physiology and consequences on the brain and behavior. *Frontiers in Cellular Neuroscience*, *8*(May), 129. https://doi.org/10.3389/fncel.2014.00129

Patel, A. B., Hays, S. A., Bureau, I., Huber, K. M., & Gibson, J. R. (2013). A Target Cell-Specific Role for Presynaptic Fmr1 in Regulating Glutamate Release onto Neocortical Fast-Spiking Inhibitory Neurons. *Journal of Neuroscience*, *33*(6), 2593–2604. https://doi.org/10.1523/JNEUROSCI.2447-12.2013

Peñagarikano, O. (2015). New Therapeutic Options for Autism Spectrum Disorder: Experimental Evidences. *Experimental Neurobiology*, *24*(4), 301–11. https://doi.org/10.5607/en.2015.24.4.301

Peñagarikano, O., Abrahams, B. S., Herman, E. I., Winden, K. D., Gdalyahu, A., Dong, H., … Geschwind, D. H. (2011). Absence of CNTNAP2 leads to epilepsy, neuronal migration abnormalities, and core autism-related deficits. *Cell*, *147*(1), 235–46. https://doi.org/10.1016/j.cell.2011.08.040

Peñagarikano, O., & Geschwind, D. H. (2012). What does CNTNAP2 reveal about autism spectrum disorder? *Trends in Molecular Medicine*, *18*(3), 156–163. https://doi.org/10.1016/j.molmed.2012.01.003

Peter, S., ten Brinke, M. M., Stedehouder, J., Reinelt, C. M., Wu, B., Zhou, H., … De Zeeuw, C. I. (2016). Dysfunctional cerebellar Purkinje cells contribute to autism-like behaviour in Shank2-deficient mice. *Nature Communications*, *7*, 12627. http://dx.doi.org/10.1038/ncomms12627

Pickles, A., Le Couteur, A., Leadbitter, K., Salomone, E., Cole-Fletcher, R., Tobin, H., … Green, J. (2016). Parent-mediated social communication therapy for young children with autism (PACT): long-term follow-up of a randomised controlled trial. *The Lancet*, *6736*(16). https://doi.org/10.1016/S0140-6736(16)31229-6

Pignatelli, M., Piccinin, S., Molinaro, G., Di Menna, L., Riozzi, B., Cannella, M., … Bruno, V. (2014). Changes in mGlu5 receptor-dependent synaptic plasticity and coupling to homer proteins in the hippocampus of Ube3A hemizygous mice modeling angelman syndrome. *The Journal of Neuroscience : The Official Journal of the Society for Neuroscience*, *34*(13), 4558–66. https://doi.org/10.1523/JNEUROSCI.1846-13.2014

Piochon, C., Kloth, A. D., Grasselli, G., Titley, H. K., Nakayama, H., Hashimoto, K., … Hansel, C. (2014). Cerebellar plasticity and motor learning deficits in a copy-number variation mouse model of autism. *Nature Communications*, *5*, 5586. https://doi.org/10.1038/ncomms6586

Piochon, C., Kano, M., & Hansel, C. (2016). LTD-like molecular pathways in developmental synaptic pruning. *Nat Neurosci*, *19*(10), 1299–1310. Retrieved from http://dx.doi.org/10.1038/nn.4389

Platt, R. J., Chen, S., Zhou, Y., Yim, M. J., Swiech, L., Kempton, H. R., … Zhang, F. (2014). CRISPR-Cas9 knockin mice for genome editing and cancer modeling. *Cell*, *159*(2), 440–455. https://doi.org/10.1016/j.cell.2014.09.014

Poliak, S., Gollan, L., Martinez, R., Custer, a, Einheber, S., Salzer, J. L., … Peles, E. (1999). Caspr2, a new member of the neurexin superfamily, is localized at the juxtaparanodes of myelinated axons and associates with K+ channels. *Neuron*, *24*(4), 1037–47. http://dx.doi.org/10.1016/S0896-6273(00)81049-1

Poliak, S., & Peles, E. (2003). The local differentiation of myelinated axons at nodes of Ranvier. *Nature Reviews. Neuroscience*, *4*(12), 968–980. https://doi.org/10.1038/nrn1253

Poliak, S., Salomon, D., Elhanany, H., Sabanay, H., Kiernan, B., Pevny, L., … Peles, E. (2003). Juxtaparanodal clustering of Shaker-like K+ channels in myelinated axons

depends on Caspr2 and TAG-1. *The Journal of Cell Biology*, *162*(6), 1149–60. https://doi.org/10.1083/jcb.200305018

Portmann, T., Yang, M., Mao, R., Panagiotakos, G., Ellegood, J., Dolen, G., … Dolmetsch, R. E. (2014). Behavioral abnormalities and circuit defects in the basal ganglia of a mouse model of 16p11.2 deletion syndrome. *Cell Reports*, *7*(4), 1077–1092. https://doi.org/10.1016/j.celrep.2014.03.036

Prakash, R., Yizhar, O., Grewe, B., Ramakrishnan, C., Wang, N., Goshen, I., … Deisseroth, K. (2012). Two-photon optogenetic toolbox for fast inhibition, excitation and bistable modulation_SI. *Nature Methods*, *9*(12), 1171–9. https://doi.org/10.1038/nmeth.2215

Rabaneda, L. G., Robles-Lanuza, E., Nieto-González, J., & Scholl, F. G. (2014). Neurexin Dysfunction in Adult Neurons Results in Autistic-like Behavior in Mice. *Cell Reports*, *8*(2), 338–346. https://doi.org/10.1016/j.celrep.2014.06.022

Rickgauer, J. P., Deisseroth, K., & Tank, D. W. (2014). Simultaneous cellular-resolution optical perturbation and imaging of place cell firing fields. *Nature Neuroscience*, *17*(12), 1816–24. https://doi.org/10.1038/nn.3866

Roak, B. J. O., Vives, L., Fu, W., Egertson, J. D., Stanaway, I. B., Phelps, I. G., … Shendure, J. (2012). in Autism Spectrum Disorders, *23*(December).

Robinson, L., Guy, J., McKay, L., Brockett, E., Spike, R. C., Selfridge, J., … Cobb, S. R. (2012). Morphological and functional reversal of phenotypes in a mouse model of Rett syndrome. *Brain*, *135*(9), 2699–2710. https://doi.org/10.1093/brain/aws096

Rodenas-Cuadrado, P., Ho, J., & Vernes, S. C. (2014). Shining a light on CNTNAP2: complex functions to complex disorders. *European Journal of Human Genetics : EJHG*, *22*(2), 171–8. https://doi.org/10.1038/ejhg.2013.100

Rosenberg, R. E., Law, J. K., Yenokyan, G., McGready, J., Kaufmann, W. E., & Law, P. a. (2009). Characteristics and concordance of autism spectrum disorders among 277 twin pairs. *Archives of Pediatrics & Adolescent Medicine*, *163*(10), 907–914. https://doi.org/10.1001/archpediatrics.2009.98

Rothwell, P. E., Fuccillo, M. V., Maxeiner, S., Hayton, S. J., Gokce, O., Lim, B. K., … Südhof, T. C. (2014). Autism-associated neuroligin-3 mutations commonly impair striatal circuits to boost repetitive behaviors. *Cell*, *158*(1), 198–212. https://doi.org/10.1016/j.cell.2014.04.045

Sanders, S. J., Murtha, M. T., Gupta, A. R., Murdoch, J. D., Raubeson, M. J., Willsey, A. J., … State, M. W. (2012). De novo mutations revealed by whole-exome sequencing are strongly associated with autism. *Nature*, *485*(7397), 237–241. https://doi.org/10.1038/nature10945

Sato, A., Kasai, S., Kobayashi, T., Takamatsu, Y., Hino, O., Ikeda, K., & Mizuguchi, M. (2012). Rapamycin reverses impaired social interaction in mouse models of tuberous sclerosis complex. *Nat Commun*, *3*, 1292. https://doi.org/10.1038/ncomms2295

Schreibman, L., Dawson, G., Stahmer, A. C., Landa, R., Rogers, S. J., McGee, G. G., … Halladay, A. (2015). Naturalistic Developmental Behavioral Interventions: Empirically Validated Treatments for Autism Spectrum Disorder. *Journal of Autism and Developmental Disorders*, *45*(8), 2411–2428. https://doi.org/10.1007/s10803-015-2407-8

Scott-Van Zeeland, A. A., Abrahams, B. S., Alvarez-Retuerto, A. I., Sonnenblick, L. I., Rudie, J. D., Ghahremani, D., … Bookheimer, S. Y. (2010). Altered functional connectivity in frontal lobe circuits is associated with variation in the autism risk gene CNTNAP2. *Science Translational Medicine*, *2*(56), 56ra80.

Sharma, A., Hoeffer, C. A., Takayasu, Y., Miyawaki, T., McBride, S. M., Klann, E., & Zukin, R. S. (2010). Dysregulation of mTOR signaling in fragile X syndrome. *J Neurosci*, *30*(2), 694–702. https://doi.org/30/2/694 [pii]\r10.1523/JNEUROSCI.3696-09.2010

Shcheglovitov, A., Shcheglovitova, O., Yazawa, M., Portmann, T., Shu, R., Sebastiano, V., … Dolmetsch, R. E. (2013). SHANK3 and IGF1 restore synaptic deficits in neurons from 22q13 deletion syndrome patients. *Nature*, *503*(7475), 267–71. https://doi.org/10.1038/nature12618

Silverman, J. L., Yang, M., Lord, C., & Crawley, J. N. (2010). Behavioural phenotyping assays for mouse models of autism. *Nature Reviews. Neuroscience*, *11*(7), 490–502. https://doi.org/10.1038/nrn2851

Stoner, R., Chow, M. L., Boyle, M. P., Sunkin, S. M., Mouton, P. R., Roy, S., … Courchesne, E. (2014). Patches of disorganization in the neocortex of children with autism. *The New England Journal of Medicine*, *370*(13), 1209–19. https://doi.org/10.1056/NEJMoa1307491

Strauss, K. A., Puffenberger, E. G., Huentelman, M. J., Gottlieb, S., Dobrin, S. E., Parod, J. M., … Morton, D. H. (2006). Recessive symptomatic focal epilepsy and mutant contactin-associated protein-like 2. *The New England Journal of Medicine*, *354*(13), 1370–1377. https://doi.org/354/13/1370 [pii] 10.1056/NEJMoa052773

Strauss, K. A., Puffenberger, E. G., Huentelman, M. J., Gottlieb, S., Dobrin, S. E., Parod, J. M., … Morton, D. H. (2006). Recessive symptomatic focal epilepsy and mutant contactin-associated protein-like 2. *The New England Journal of Medicine*, *354*(13), 1370–1377. https://doi.org/354/13/1370 [pii] 10.1056/NEJMoa052773

Südhof, T. C. (2008). Neuroligins and neurexins link synaptic function to cognitive disease. *Nature*, *455*(7215), 903–11. https://doi.org/10.1038/nature07456

Takeuchi, K., Gertner, M. J., Zhou, J., Parada, L. F., Bennett, M. V. L., & Zukin, R. S. (2013). Dysregulation of synaptic plasticity precedes appearance of morphological defects in a Pten conditional knockout mouse model of autism. *Proceedings of the National Academy of Sciences*, *110*(12), 4738–4743. https://doi.org/10.1073/pnas.1222803110

Tang, G., Gudsnuk, K., Kuo, S. H., Cotrina, M. L., Rosoklija, G., Sosunov, A., … Sulzer, D. (2014). Loss of mTOR-Dependent Macroautophagy Causes Autistic-like Synaptic Pruning Deficits. *Neuron*, *83*(5), 1131–1143. https://doi.org/10.1016/j.neuron.2014.07.040

Tsai, P. T., Hull, C., Chu, Y., Greene-Colozzi, E., Sadowski, A. R., Leech, J. M., … Sahin, M. (2012). Autistic-like behaviour and cerebellar dysfunction in Purkinje cell Tsc1 mutant mice. *Nature*, *488*(7413), 647–51. https://doi.org/10.1038/nature11310

Tyzio, R., Nardou, R., Ferrari, D. C., Tsintsadze, T., Shahrokhi, A., Eftekhari, S., … Ben-Ari, Y. (2014). Oxytocin-Mediated GABA Inhibition During Delivery Attenuates Autism Pathogenesis in Rodent Offspring. *Science*, *343*(6171), 675 LP-679. http://science.sciencemag.org/content/343/6171/675.abstract

U.S. Department of Health and Human Services. (2014). Prevalence of autism spectrum disorder among children aged 8 years - autism and developmental disabilities monitoring network, 11 sites, United States, 2010. *Morbidity and Mortality Weekly Report. Surveillance Summaries (Washington, D.C. : 2002)*, *63*(2), 1–21. https://doi.org/24670961

Varea, O., Martin-de-Saavedra, M. D., Kopeikina, K. J., Schürmann, B., Fleming, H. J., Fawcett-Patel, J. M., … Penzes, P. (2015). Synaptic abnormalities and cytoplasmic glutamate receptor aggregates in contactin associated protein-like 2/Caspr2 knockout neurons. *Proceedings of the National Academy of Sciences of the United States of America*, *112*(19), 6176–81. https://doi.org/10.1073/pnas.1423205112

Voineagu, I., Wang, X., Johnston, P., Lowe, J. K., Tian, Y., Horvath, S., … Geschwind, D. H. (2011). Transcriptomic analysis of autistic brain reveals convergent molecular pathology. *Nature*, *474*(7351), 380–4. https://doi.org/10.1038/nature10110

Wallace, M. L., Burette, A. C., Weinberg, R. J., & Philpot, B. D. (2012). Maternal Loss of Ube3a Produces an Excitatory/Inhibitory Imbalance through Neuron Type-Specific Synaptic Defects. *Neuron*, *74*(5), 793–800. https://doi.org/10.1016/j.neuron.2012.03.036

Wang, J., Tao, Y., Song, F., Sun, Y., Ott, J., & Saffen, D. (2015). Common Regulatory Variants of CYFIP1 Contribute to Susceptibility for Autism Spectrum Disorder (ASD) and Classical Autism. *Annals of Human Genetics*, (15), 329–340. https://doi.org/10.1111/ahg.12121

Wang, H., Pati, S., Pozzo-miller, L., & Doering, L. C. (2015). Targeted pharmacological treatment of autism spectrum disorders : fragile X and Rett syndromes. *Frontiers in Cellular Neuroscience*, *9*(February), 1–23. https://doi.org/10.3389/fncel.2015.00055

Wetmore, D. Z., & Garner, C. C. (2010). Emerging pharmacotherapies for neurodevelopmental disorders. *Journal of Developmental and Behavioral Pediatrics : JDBP*, *31*(7), 564–81. https://doi.org/10.1097/DBP.0b013e3181ee3833

Wilson, T. W., Rojas, D. C., Reite, M. L., Teale, P. D., & Rogers, S. J. (2007). Children and Adolescents with Autism Exhibit Reduced MEG Steady-State Gamma Responses. *Biological Psychiatry*, *62*(3), 192–197. https://doi.org/10.1016/j.biopsych.2006.07.002

Xu, X., Olivas, N. D., Levi, R., Ikrar, T. & Nenadic, Z. High precision and fast functional mapping of cortical circuitry through a combination of voltage sensitive dye imaging and laser scanning photostimulation. *Journal of Neurophysiology*, 103, 2301-2312, doi:00992.2009 [pii]

Xu, X., & Callaway, E. M. (2009). Laminar Specificity of Functional Input to Distinct Types of Inhibitory Cortical Neurons. *Journal of Neuroscience*, *29*(1), 70–85. https://doi.org/10.1523/JNEUROSCI.4104-08.2009

Xu, X., Olivas, N. D., Ikrar, T., Peng, T., Holmes, T. C., Nie, Q., & Shi, Y. (2016). Primary visual cortex shows laminar-specific and balanced circuit organization of excitatory and inhibitory synaptic connectivity. *The Journal of Physiology*, *594*(7), 1891–1910. https://doi.org/10.1113/JP271891

Yizhar, O., Fenno, L. E., Prigge, M., Schneider, F., Davidson, T. J., O'Shea, D. J., … Deisseroth, K. (2011). Neocortical excitation/inhibition balance in information processing and social dysfunction. *Nature*, *477*(7363), 171–178. https://doi.org/10.1038/nature10360

Zhan, Y., Paolicelli, R. C., Sforazzini, F., Weinhard, L., Bolasco, G., Pagani, F., … Gross, C. T. (2014). Deficient neuron-microglia signaling results in impaired functional brain connectivity and social behavior. *Nature Neuroscience*, *17*(3), 400–406. https://doi.org/10.1038/nn.3641

Zhang, Y., Bonnan, A., Bony, G., Ferezou, I., Pietropaolo, S., Ginger, M., … Frick, A. (2014). Dendritic channelopathies contribute to neocortical and sensory hyperexcitability in Fmr1−/y mice. *Nature Neuroscience*, *17*(12), 1701–1709. https://doi.org/10.1038/nn.3864

Zhou, J., Blundell, J., Ogawa, S., Kwon, C.-H., Zhang, W., Sinton, C., … Parada, L. F. (2009). Pharmacological inhibition of mTORC1 suppresses anatomical, cellular, and behavioral abnormalities in neural-specific Pten knock-out mice. *The Journal of*

Neuroscience : The Official Journal of the Society for Neuroscience, *29*(6), 1773–83. https://doi.org/10.1523/JNEUROSCI.5685-08.2009

Ziv, Y., Burns, L. D., Cocker, E. D., Hamel, E. O., Ghosh, K. K., Kitch, L. J., … Schnitzer, M. J. (2013). Long-term dynamics of CA1 hippocampal place codes. *Nature Neuroscience*, *16*(3), 264–6. https://doi.org/10.1038/nn.3329